



Norwegian University of
Science and Technology

Past slope collapse and current unstable slopes along a cliff at Hyllestad Kommune

Vegard Nes

Geology

Submission date: June 2018

Supervisor: Reginald Hermanns, IGP

Co-supervisor: Ivanna Penna, NGU

Norwegian University of Science and Technology
Department of Geoscience and Petroleum

Abstract

With the aim of a complete national database of potential unstable slopes, the Geological Survey of Norway currently carries out systematic geological mapping of rock slopes organized in counties. As part of the survey of Sogn og Fjordane, a hazard and preliminary consequence assessment of a north-facing cliff in Hyllestad municipality has been completed within this thesis.

Two independent inventories were assembled, one on unstable rock slopes along the cliff face, the other on post-glacial rock slope failure deposits. In total 9 unstable slopes were detected, that present a total of 14 failure scenarios. In order to determine the hazard, the Norwegian hazard classification system was used. This comprises in mapping out the limiting structures, defining structural control, and a kinematic feasibility test of failures. In addition, at two sites displacement rates have been measured by dGNSS and extensometers, for the other, these were assessed based on morphological expression of deformation. Rockfall activity was assessed on a 3D photogrammetric model. The resulting hazard classification classified 12 of the scenarios to a medium hazard class, while 2 of the scenarios were classified with low hazard. The preliminary consequence assessment consisted of volume calculations based on delimiting structures and a run-out analysis considering the potential for initiating displacement waves. Of the detected scenarios, 3 have volumes defined that can fail as rock avalanches with excessive travel lengths. A run-out analysis using an empirical relation between volume and “angle of reach” indicate that the failure of all scenarios will reach the fjord.

The inventory of past events was assessed by bathymetric data from the fjord and digital terrain models on the shore. Deposits were interpreted, and volumes were estimated based on the SLBL-method. Frequencies have been analyzed based on the assumption of a constant frequency distribution since last deglaciation. This is supported by data from other fjords. Volume-Frequency distributions suggested a best fit of an inverse power-law model for volumes above a threshold of 0,020Mm³. Resulting frequency of rock slope failures with volumes $\geq 0,020\text{Mm}^3$ was estimated to $1 / 334$ years. The frequency of rock avalanches ($\geq 0,250\text{Mm}^3$) was estimated to $1 / 2879$ years.

Based on the hazard classification of unstable slopes and frequencies of past events, the applicability of quantitative hazard probabilities has been discussed due to the need for quantitative limits for the Norwegian regulations on technical requirements for buildings.

Samandrag

Med formål om ein komplett nasjonal database for potensielle fjellskred, gjennomfører Norges geologiske undersøking ei systematisk geologisk kartlegging av fjellsider inndelt i fylker. Denne avhandlinga gjev ei fare- og konsekvensvurdering av ei nordvendt klippe i Hyllestad kommune, som del i kartlegginga av Sogn og Fjordane.

To uavhengige prosjekt er utført. Det eine omhandlar ustabile fjellparti langs klippa, medan det andre omhandlar tidlegare skredhendingar etter siste istid. Totalt er 9 ustabile fjellparti funne, der totalt 14 ustabile blokker er definert. Ei farevurdering er utført basert på det norske fareklassifiseringssystemet. Dette inneber kartlegging av avgrensande strukturar, definere strukturar som kontrollerar stabilitet, og ei påfølgjande kinematisk analyse av moglege utfallsmekanismar. I tillegg er rørslemålingar utført ved to ustabile fjellparti ved hjelp av dGNSS- og ekstensometermålingar. Der det ikkje er utført rørslemålingar, er rørsle vurdert utifrå morfologiske teikn i fjellpartiet. Steinsprangaktivitet er vurdert ved hjelp av ein fotogrammetrisk modell. Utifrå fareklassifiseringssystemet er 12 blokker vurdert til medium faregrad, medan 2 blokker er vurdert til lav faregrad. Ei førebels konsekvensanalyse inneheld estimering av volum, og ei utløpsanalyse som viser potensialet for ei mogleg flodbølge. Tre av dei kartlagde blokkene er utifrå volumkalkulasjonar definert som fjellskred, med tilhøyrande utløpslengd. Ei vurdering av utløpslengd basert på ein empirisk relasjon mellom siktevinkel og volum viser at alle dei ustabile blokkene vil nå fjorden.

Prosjektet som omhandlar tidlegare skredhendingar er utført ved hjelp av batymetriske data frå fjorden og digitale terrengmodellar frå kystlinja. Avsetjingar er kartlagde og volum er estimert ved hjelp av SLBL-metoden. Skredfrekvens er analysert utifrå ei forventning om konstant distribusjon av skredhendingar etter siste istid. Dette er støtta av funn i andre norske fjordar. Volum-frekvens distribusjonar av skredhendingar følgjer ei invers potenslov for volum over 0,020Mm³. Frekvensen av skredhendingar med volum over 0,020Mm³ er estimert til 1/334 år. Frekvensen av fjellskred ($\geq 0,250\text{Mm}^3$) er estimert til 1/2879 år.

Bruken av kvantitative metodar for estimering av sannsyn er diskutert på bakgrunn av fareklassifikasjonar og frekvens av tidlegare skredhendingar. Dette er grunna bruken av kvantitative faregrenser i forskrifta om tekniske krav til byggverk.

Acknowledgement

These words are the last words written during my Master of Science (M.Sc.) degree in geology at the Department of Geoscience and Petroleum at the Norwegian University of Science and Technology. The thesis is written in collaboration with the Geological Survey of Norway, and the Geohazard and Earth Observation team.

I want to thank my supervisor Reginald Hermanns for the time and concern you have put into this thesis, and my co-supervisor Ivanna Penna for good discussions during the process. I am grateful for the good atmosphere at NGU and the valuable help from the team, especially with technical issues.

I also want to thank my lunch buddies at NTNU for some good years, and a special thanks to my field assistant Jon for the helpful discussions, good dinners, and bad humor.

And, thanks to Marit for keeping up with my long days.

Trondheim, June 2018

Vegard Nes

Table of contents

Abstract	III
Samandrag	V
Acknowledgement.....	VII
Table of contents	IX
Abbreviations	XIII
1 Introduction	1
1.1 The hazard of rock slope failures in Norway	1
1.2 Aims for the study	2
1.3 Available data	2
1.4 Location	3
1.5 Geological settings	4
1.5.1 Regional geology.....	4
1.5.2 Glacial history	6
1.6 Historic events	7
2 Theory	11
2.1 Landslides	11
2.1.1 Classification.....	11
2.1.2 Type of movement	12
2.1.3 Controlling factors.....	13
2.1.4 Deposition	14
2.1.5 Post-glacial frequency models	15
2.2 Secondary effects.....	16
2.2.1 Displacement waves	17
2.3 Remote sensing.....	18
2.3.1 LiDAR scanning.....	19
2.3.2 Photogrammetry	19
2.3.3 Bathymetry data	19
2.4 NGU mapping approach.....	20
2.5 Hazard assessment developed at NGU	22
2.5.1 Hazard classification	22
2.5.2 Consequence assessment.....	24
2.5.3 Risk analysis.....	26
3 Methods.....	29
3.1 Geological mapping.....	29

3.1.1	Subaerial interpretation	29
3.1.2	Field work	30
3.1.3	Subaquatic interpretation.....	31
3.2	Structural analysis.....	31
3.2.1	Field measurements	31
3.2.2	Regional lineaments	32
3.3	Application of the hazard classification system	33
3.3.1	Kinematic analysis	33
3.3.2	Displacement measurements	34
3.4	Application of the consequence assessment	35
3.4.1	Volume estimation	35
3.4.2	Run-out analysis	37
3.5	Frequency analysis	38
3.6	Quantification of hazard	39
3.6.1	Norwegian conversion method.....	40
3.6.2	Empirical analysis	40
4	Results	41
4.1	Results from structural analysis.....	41
4.1.1	Field measurements.....	41
4.1.2	Regional lineaments	45
4.2	Results from kinematic analysis	47
4.3	Results from field investigation.....	52
4.3.1	Bedding	52
4.3.2	Joint sets	53
4.4	Assessment of unstable slopes.....	58
4.4.1	Distribution.....	58
4.4.2	Delimiting structures	59
4.4.3	Calculated volumes	80
4.4.4	Run-out.....	81
4.4.5	Hazard classification	81
4.5	Assessment of past events	85
4.5.1	Distribution.....	85
4.5.2	Volume estimation	89
4.5.3	Frequency analysis	90
5	Discussion	93
5.1	Comparing the structural analyses.....	93
5.1.1	Western domain.....	93

5.1.2	Mid domain	93
5.1.3	Eastern domain	94
5.1.4	Implications for the analyses	94
5.2	Structures controlling the unstable slopes	96
5.2.1	Back scarp	96
5.2.2	Lateral limits	96
5.2.3	Toe lines	97
5.3	Reduction of uncertainties of the hazard classification	98
5.4	Frequency analysis	101
5.4.1	Applicability of post-glacial distribution model	101
5.4.2	Uncertainties and adjustments done to the used dataset	102
5.5	Quantification of hazard	104
5.5.1	Norwegian conversion method.....	104
5.5.2	Empirical analysis	106
5.5.3	Applicability of the quantification methods.....	107
5.6	Differing volume sizes of the assessed inventories	108
6	Conclusion.....	111
6.1	Controlling structures and hazard classification.....	111
6.2	Inventory of past events and conducted frequencies	112
6.3	Further investigations	112
	Bibliography.....	I
	Appendix	VII

Abbreviations

NTNU	Norwegian University of Science and Technology
NGU	Geological Survey of Norway
NVE	Norwegian Water Resources and Energy Directorate
NGI	Norwegian Geotechnical Institute
TEK17	Norwegian regulations on technical requirements for structures
SLBL	Sloping Local Base Level
LiDAR	Light Detection And Ranging
DEM	Digital Elevation Model
InSAR	Interferometric Synthetic Aperture Radar
GIS	Geographic Information System
dGNSS	differential Global Navigation Satellite System

1 Introduction

1.1 The hazard of rock slope failures in Norway

The country of Norway is lying along the remains of the Caledonian mountain range, created 395 million years ago (Tucker, *et al.*, 1987). After this time, multiple glaciations have carved the landscape. Present Norway is characterized by deeply incised valleys and fjords. The extreme relief of these valleys are a threat for multiple potential natural disasters. One of these disasters are landslides. The last 100 years, as many as 170 persons have been killed as a result of landslides. (Blikra, *et al.*, 2006b)

The primary effect is the rock mass itself, but as deadly are the secondary effects that can cause damming of rivers and displacement waves (Hermanns, 2013, Harbitz, *et al.*, 2014). The fjords of Norway stretching into the mountainous regions with a dense population along the shore line facilitates for disastrous displacement waves responsible for most of the damage after catastrophic failures (Harbitz, *et al.*, 1993). Due to later years increase of tourism in the fjords, a future failure might cost even higher fatalities, unless mitigation measures are considered (Harbitz, *et al.*, 2014).

Due to a considerable hazard of rock slope failures in Norway, the Geological Survey of Norway started a systematic mapping approach with a goal to detect all potential rock slope failures with considered catastrophic consequences (Hermanns, *et al.*, 2014a). Since the start in 2005, over 300 potential failures have been identified and gathered in a database developed by NGU (NGU, 2017). Identified unstable slopes are assessed following a hazard and risk classification defining the hazard and attached consequences of a failure from the slope (Hermanns, *et al.*, 2013b).

In 1992 there was a rock slope failure at the cliff of Lifjellet causing a displacement wave with considerable run-up along the shore of Aafjorden. The municipality of Hyllestad started an investigation of the area, consulted by Harbitz and Domaas from NGI. The investigation showed a highly fractured area of 40 000 m³ with potentially catastrophic consequences. In 2007, this slope was included in the NGU database, followed by another slope from the same cliff in 2011 (Böhme, *et al.*, 2011). Periodic displacement monitoring was started and is still active.

1.2 Aims for the study

The aim for this thesis is to investigate the north-facing cliff of Lifjellet, trying to detect other unstable slopes than the already monitored locations, and to define the hazard and risk they pose to society. This is supplemented with a frequency analyses of both unstable slopes and rock slope failure deposits on the fjord floor. Investigations include:

- Mapping of geomorphological structures connected to deformation of a slope such as cracks and depressions, through subaerial interpretation and field observations.
- Structural measuring of discontinuities, and a structural analysis of significant structures and their spatial variability. Dividing the area based on structural control and assess a kinematic analysis of the defined domains.
- Mapping and analysis of regional lineaments based on a digital elevation model(DEM)
- Detection of unstable slopes and define their controlling structures and feasibility for failure. Assess the hazard for each scenario based on a hazard assessment developed at NGU.
- Volume calculation of unstable slopes using a three-dimensional manual construction of back scarp and release surfaces (CloudCompare), and evaluation of their potential for initiating displacement waves
- Mapping of deposits and estimation of their volumes using the Sloping Local Base Level (SLBL) method.
- Frequency analysis of past failures from the cliff of Lifjellet based on deglaciation history and the assessment of deposits.

1.3 Available data

The work in this thesis is mainly based on data collected during a detailed geological mapping of the area done by the author and his field assistant, Jon Runar Drotninghaug. The collecting was carried out during a period of two weeks in June and August 2017.

The following list shows data available during the assessment (Table 1-1).

Table 1-1: Available data

Data	Source
DEM (LiDAR) – 1x1m resolution	NGU
Orthophotos	Statens kartverk
Topographic data	Statens kartverk
Bathymetric data	NGU
Photogrammetric point cloud model	NGU
Extensometer measurements	NGU/Hyllestad kommune
dGNSS-measurements	NGU

1.4 Location

Lifjellet is a mountain plateau located at the west coast of Norway, in Hyllestad municipality. It is also known under names as Lihesten and Gygrekjeften. The mountain plateau is surrounded by steep cliffs falling into the fjords Lifjorden and Aafjorden. The cliff of interest is 6 km long, oriented to the northeast, and with heights of 400-700 m.a.s.l. dipping steep into Aafjorden.

Aafjorden is a short fjord arm ending in the town Hyllestad. The north side of the fjord is closely inhabited, with both private housings and industry. At the south side of the fjord, at the foot of the location, there is no infrastructure.

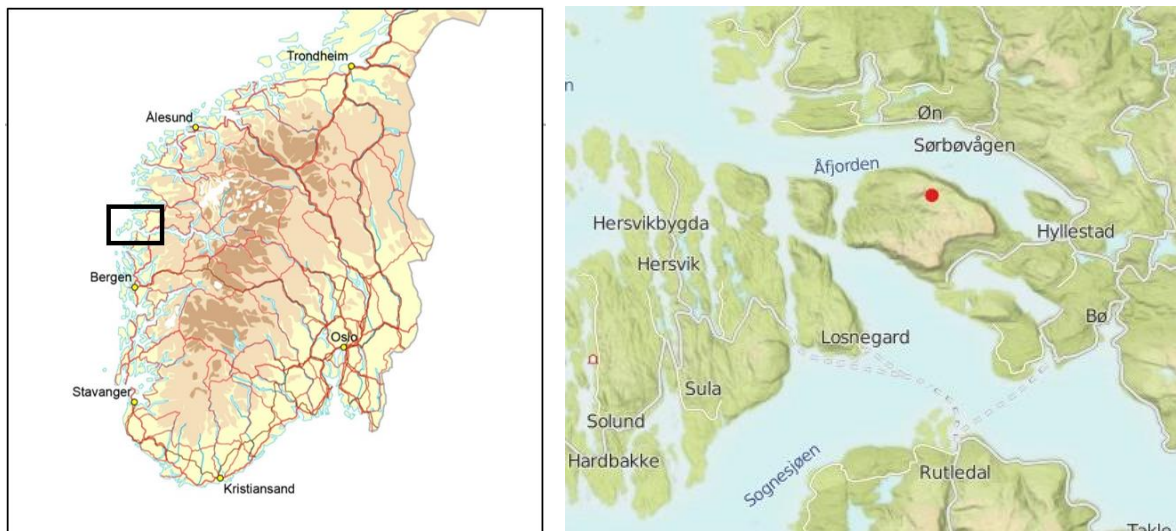


Figure 1.1: Figures showing the location of Lifjellet in the western part of Southern Norway. The cliff of Lifjellet is oriented to the north, towards the fjord Aafjorden.

1.5 Geological settings

1.5.1 Regional geology

The geology of the area is built up by three distinct nappes. The upper unit, which includes Lifjellet, is a sedimentary rock, consisting of Devonian conglomerates. The layer is part of the Solund Devonian basin, an intramountainous basin created through a period of stretching of the Caledonian orogeny (Fossen, *et al.*, 2008a). The Solund Devonian basin is lying above the Solund fault, a low-angle normal fault dipping towards NW (Hacker, *et al.*, 2003).

East of Lifjellet there is a low angle shear zone called the Nordfjord-Sogn shear zone. It consists of more than a kilometer thick layer of Mylonites created by extensive stretching of both bedrock and Paleozoic rock types. (Fossen, *et al.*, 2008a)

Further east, the bedrock consists of autochthonous Precambrian rock types, mostly granitic and dioritic gneisses, but some places migmatitic. These rocks are part of the western gneiss region, stretching all the way from Sogn to Trøndelag. (Austrheim, *et al.*, 2003)

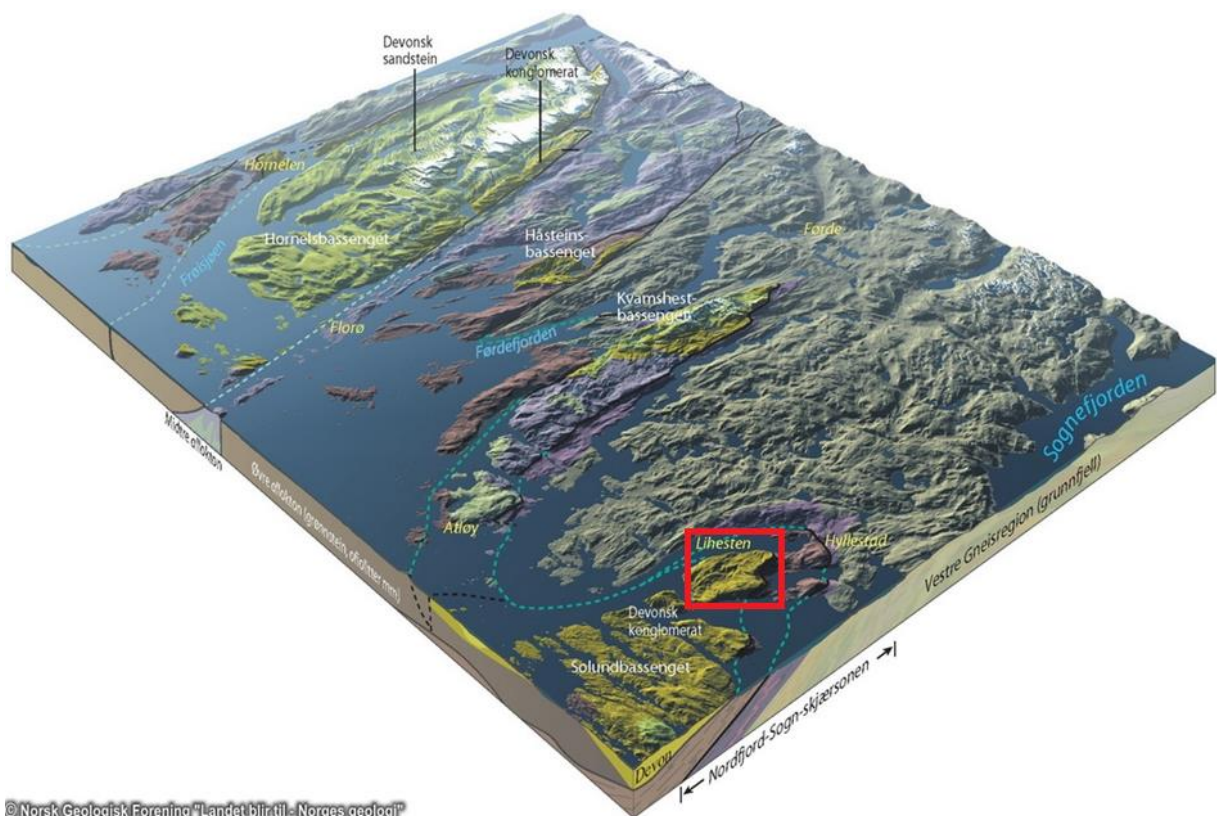


Figure 1.2: Figure showing the layering structure of the regional rock types. Purple and brown is part of the Nordfjord-Sogn shear zone. Yellow is Devonian sedimentary rocks, while grey is the Western Gneiss region. Field area is marked with the red square. Modified after Ramberg, *et al.* (2006)

The Western Gneiss region is part of the Baltic shield (Austrheim, *et al.*, 2003). It went through a high to medium grade metamorphic event around 395 Million years ago, during the Caledonian orogeny (Tucker, *et al.*, 1987). At this time the Baltic shield was pushed under the Laurentic plate, and the Caledonian mountain range with heights of today's Himalayas were built (Fossen, *et al.*, 2008b).

The Caledonian orogeny ended in the lower Devonian, followed by extensive stretching of the landscape in the western direction. The stretching created large extensional faults and shear zones. The mountains east of the stretching kept their height because of uplift of the inner parts when the stretching and mass movement continued west. One of those extensional shear zones created at this time is the Nordfjord-Sogn shear zone. The difference in metamorphism of the under- and overlying rocks, suggests a movement along the shear zone of 50-100 km, one of the largest extensional shear zones in the world. (Fossen, *et al.*, 2008a)

During the stretching of the landscape, in lower Devonian, the new mountain range was going through multiple weathering processes. The erosional products at the western side of the mountains ended up in intramountainous basins, such as the Solund Devonian basin. The inner stratigraphy of these Devonian basins reveals a more than 10km thick package of layers. The only reasonable explanation for this extensive layering is a western-dipping rotational fault, sliding because of the sediment loading of the basin, rotating the layers to an easterly dip as seen in Figure 1.3. These basins have later been uplifted to today's vertical layering. (Fossen, *et al.*, 2008a)

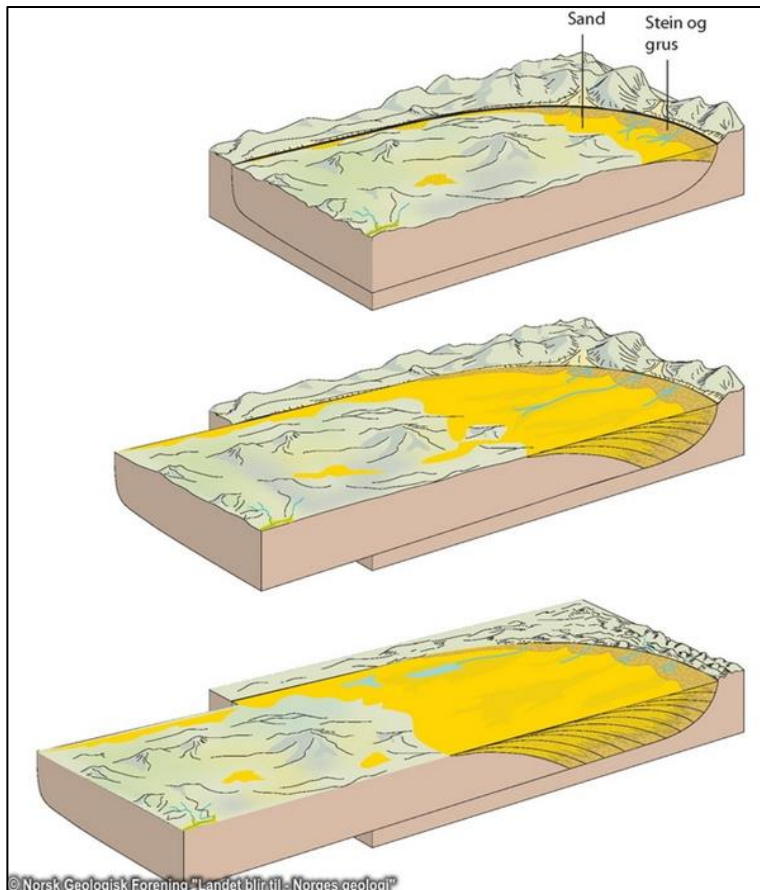


Figure 1.3: Model of the stratigraphic layering process in the sedimentary basins. (Ramberg, et al., 2006)

After the deposition of the sedimentary basins and the movement of the Nordfjord-Sogn shear zone, the whole package has been folded into east-west folds by compressional forces in the north-south direction. The compression most likely lasted into the Carboniferous period.

(Fossen, *et al.*, 2008a)

1.5.2 Glacial history

The plateau of Lifjellet reveals signs of glacial striae. Scandinavia was covered by the Fennoscandic ice sheet in Weichsel, the last glacial era (Vorren & Mangerud, 2008). The era had a glacial maximum 25000-18000 years BP. The first deglaciation of Lifjellet is predicted to around 15 500 BP, in the end of the glacial interstadial Bølling. A glacial re-advance in Younger Dryas is widely described in literature. It is defined by the Younger Dryas moraine detected 10km west of Lifjellet (Aarseth & Mangerud, 1974). The calibrated age of the Younger Dryas moraine is 11500 BP. The last deglaciation of the region was a fast retreat, in a period of 1000 years in Preboreal the glaciers retreated to the inner fjords of Sognefjorden and Hardangerfjorden (Hughes, *et al.*, 2016).

Glacial terraces in the region reveals a sea level 27 meters higher than present sea level (Aa, 1985). This is a consequence of the weight of ice on the crust, in combination with the melting of ice sheets causing a higher sea level. Glacial striae from both younger dryas and older glacial stadials show a glacial movement to the west. (Aa, 1985)

1.6 Historic events

In a period of 6 years in the 1990s, in total five historic events took place around Aafjorden. Two rock slope failures with substantial volumes fell into the fjord, in addition to three periods of heavy rock fall activity (Harbitz, 1999). The 1992-event, a failure of rock mass from Bukkenova at the seacliff of Lifjellet, happened the 15. of February (NVE, 2018). The source area is described as Lifjellet Øst in the reports from Harbitz, *et al.* (2001) and Böhme, *et al.* (2011), and seen as “Skred A” in Figure 1.4.

The rock slope failure in 1992 was calculated to a size of 25000-35000m³, reaching the fjord in a speed of 45m/s, calculated from a film clip of the landslide (Harbitz, 1999). The failure released in three separate events, and was sliding along a gradual slope with an irregular topography before reaching the water (Kveldsvik, 1998). These factors lowered the kinetic energy transferred to the water body, causing a displacement wave of only one meter. Displacement waves damaged boats and boat houses at the other side of the fjord. Again, in the winter of 1998, there was substantial rockfall activity from the same slope as the event of 1992, which increased the inhabitant’s fear of a new displacement wave. (Harbitz, *et al.*, 2001)

In 1998, the 19. of March, another rock slope failure released in the same fjord, at Katlenova (Skred B in Figure 1.4). The landslide had a volume of 20-30 000m³, and the total volume fell straight into the fjord. The slide created displacement waves with 6 meters run-up at the north side of the fjord causing material damage on boats, boathouses, and roads. In the fall of 1998, two more events occurred from Katlenova, the last causing waves with a run-up of 1,5-2 meters up on shore. (Harbitz, *et al.*, 2001)

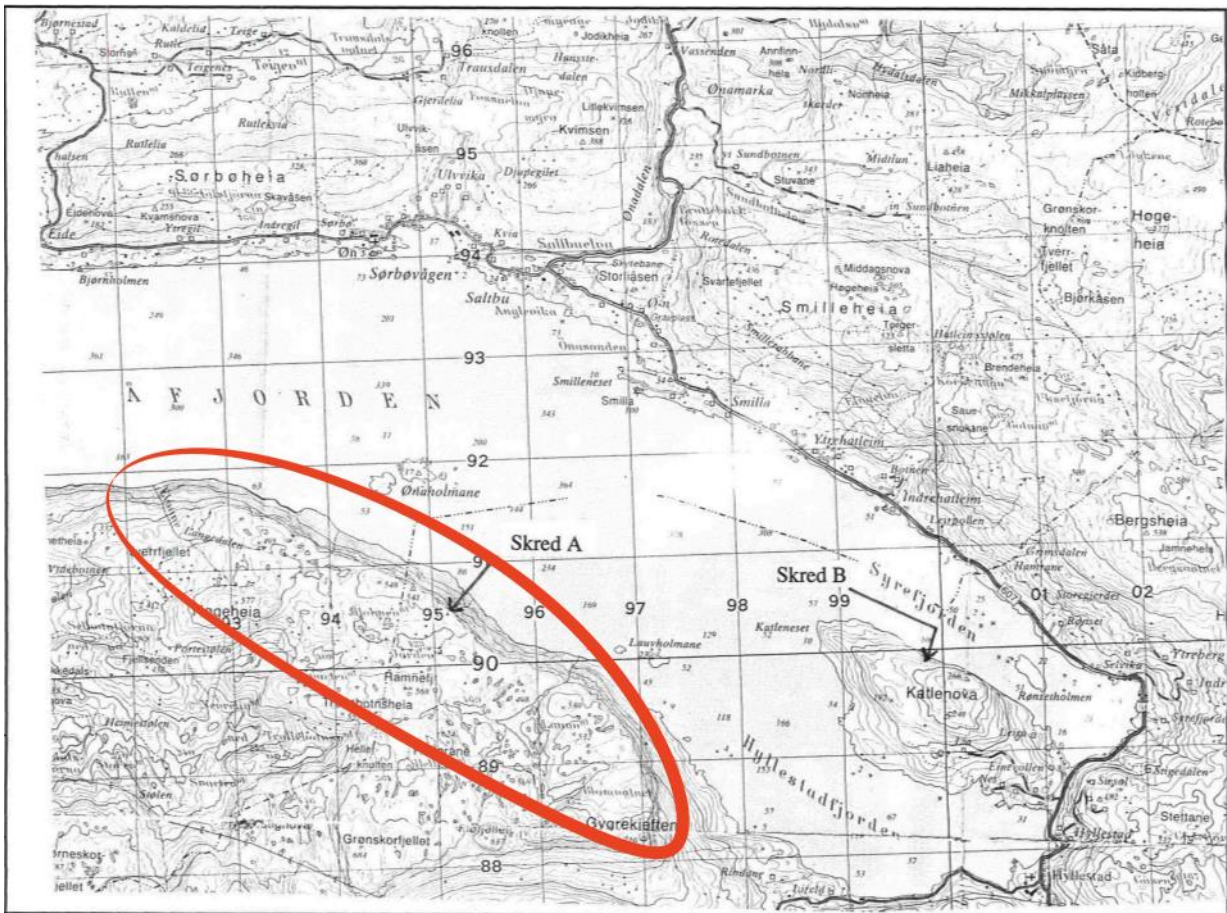


Figure 1.4: Overview map of Aafjorden, with the two slope failures in the 1990s highlighted. Bukkenova mapped as “Skred A” and Katlenova as “Skred B”. The field area of this thesis is marked with red. Modified after Kveldsvik (1998).

Through this short time period, the only factors varying is the weather and earthquakes. For a landslide to be triggered, there is needed an earthquake of magnitude 4 (Keefer, 1984). Based on seismicity rates over the 20th century, typical recurrence rates for magnitude 5 earthquakes is 10 years, and for M 7 earthquakes is 1100 years (Bungum, *et al.*, 2005). No seismic events above M4.5 were detected in the 1990s (Bungum, *et al.*, 2005), which eliminates earthquake activity as the main triggering factor for the six-year period.

More likely is the weather, in form of precipitation and temperature. Failure of a slope requires failure of rock bridges along the sliding plane (Stead & Eberhardt, 2013). Increase in pore water pressure both increases the driving forces and decreases the resisting forces in a slope (Picarelli, *et al.*, 2012). Temperature is a factor both affecting the type of precipitation, and introduce an important damage mechanism, the freeze-thaw cycle.

When considering precipitation in the months prior to the events, the amount is compared to a 30-year normal period, 1961-1990. It is also compared to extreme values of the same normal

period. These data are retrieved from the meteorological station Hovlandsdal, positioned at 85 m.a.s.l. 13 km northeast of Lifjellet.

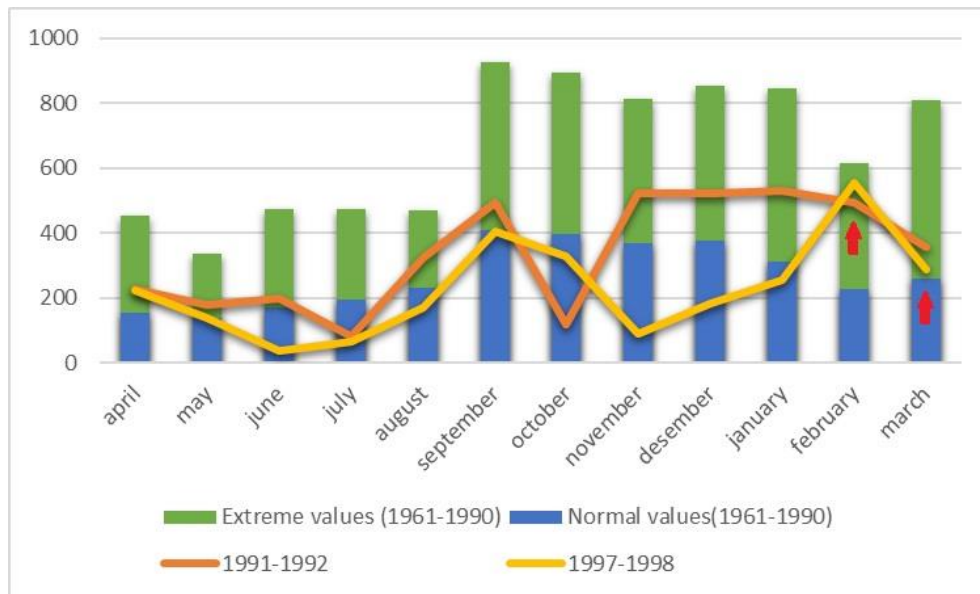


Figure 1.5: Change in precipitation (mm) the months prior to the events in February 1992 and March 1998, compared with normal values and extreme values in the period 1961-1990. (Norwegian Meteorological Institute, 2018)

The winter of 1992 shows precipitation of 500mm/month for four months prior to the event. It shows more than twice the normal amount in February, and close to the extreme values for the month. Before the 1998 event, also the month of February was close to the extreme values. The precipitation amount was well above 500mm. But in March, the precipitation amount was normalized before the event of 1998.

The temperature the month before the 1998-event shows multiple possible freeze-thaw cycles with temperatures varying between -4 and 4 degrees Celsius. (Norwegian Meteorological Institute, 2018)

2 Theory

2.1 Landslides

“A landslide is the failure and movement of a mass of rock, sediment, or artificial fill under the influence of gravity” (Clague, 2013). These landslides can occur all over the landscape with the right conditions in place. This is because of the wide range of controlling factors and triggering mechanisms (Highland & Bobrowsky, 2008). The variety of landslides is connected to the variation in material content, movement type and the environment they occur.

2.1.1 Classification

By assessing their type of movement and material content, we can classify the landslides.

Hungr, *et al.* (2014) presents a classification based on the former Varnes classification (Varnes, 1978), dividing the landslides due to their type of movement and source material.

(Table 2-1)

Table 2-1: Classification of landslides by their type of movement and material content. (Hungr, *et al.*, 2014)

Type of movement	Rock	Soil
Fall	Rock/ice fall ^a	Boulder/debris/silt fall ^a
Topple	Rock block topple ^a Rock flexural topple	Gravel/sand/silt topple ^a
Slide	Rock rotational slide Rock planar slide ^a Rock wedge slide ^a Rock compound slide Rock irregular slide ^a	Clay/silt rotational slide Clay/silt planar slide Gravel/sand/debris slide ^a Clay/silt compound slide
Spread	Rock slope spread	Sand/silt liquefaction spread ^a Sensitive clay spread ^a
Flow	Rock/ice avalanche ^a	Sand/silt/debris dry flow Sand/silt/debris flowslide ^a Sensitive clay flowslide ^a Debris flow ^a Mud flow ^a Debris flood Debris avalanche ^a Earth/peat flow
Slope deformation	Mountain slope deformation Rock slope deformation	Soil slope deformation Soil creep Solifluction

^a: Movement types that usually reach extremely rapid velocities as defined by Cruden and Varnes (1996). The other landslide types are most often (but not always) extremely slow to very rapid.

2.1.2 Type of movement

Landslides are classified by their type of movement. Within the classification of rock as the material content, the difference between a flow movement and other movement types is the excessive travel lengths (Hungri, *et al.*, 2014). Excessive travel lengths are defined by the Scheidegger curve. This is a direct relation between failure volumes and a height/length ratio proposed by Scheidegger (1973). At a certain volume threshold the deposit volumes deviate from the relation (Corominas, 1996). This cut-off is set to a volume threshold of 250 000 m³, where smaller volumes follow a truncation with “angle of reach” of 31 degrees (Figure 2.1).

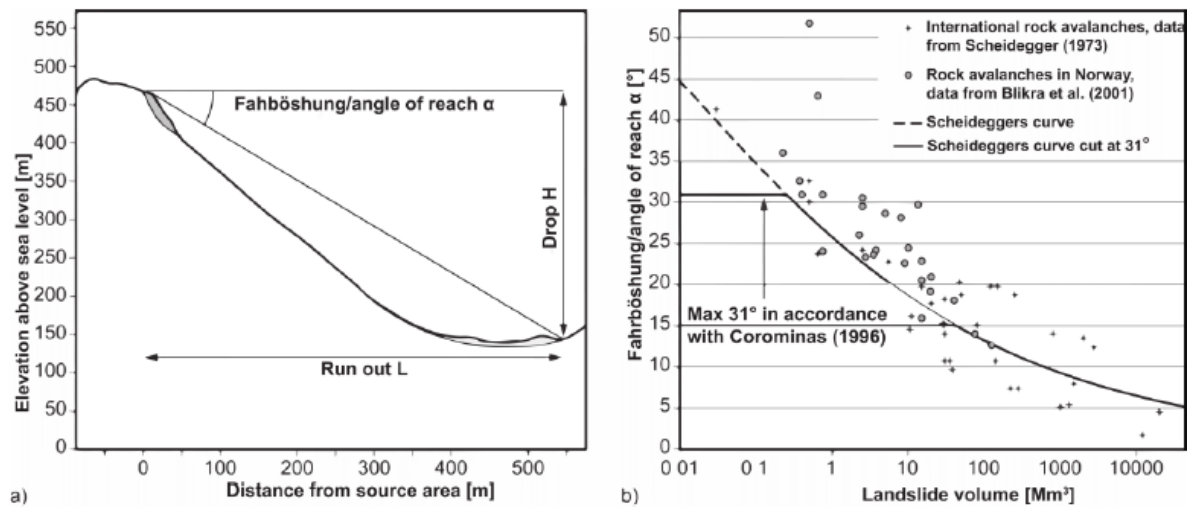


Figure 2.1: Empirical relation of the “angle of reach” of rock avalanches. a) Profile of a rock avalanche. b) empirical relation between “angle of reach” and failure volumes, based on international rock avalanches (Scheidegger, 1973). Scheidegger cut-off is shown as the truncated line with a constant “angle of reach” below a certain volume threshold (Corominas, 1996). Rock avalanches from Norway is plotted, showing in general a higher “angle of reach” than the Scheidegger curve (Blikra, *et al.*, 2001). Figure modified after Oppikofer, *et al.* (2016).

Landslides with main material content of rock following the Scheidegger curve is due to their flow movement classified as rock avalanches. Landslides of rock material with volumes below the Scheidegger cut-off is not considered a flow movement. These landslides are classified as fall, topple, slide or spread based on their kinematic failure (Hungri, *et al.*, 2014). Rock slopes with slow movement is classified as mountain slope deformations and rock slope deformation in Hungri, *et al.* (2014).

In this thesis the landslides consisting of rock is classified as:

- Rock slope failures
- Rock avalanches
- Rock slope deformation

2.1.3 Controlling factors

Stability of a rock slope is often connected to driving forces against resisting forces along a plane calculated with a limit equilibrium analysis (Wyllie, *et al.*, 2004). Due to the complexity of landslides consisting of rock, stability is connected to the number of rock bridges that must break along one or several failure planes, connecting the controlling structures of the unstable slope. A slope failure occurs when the number of rock bridges is reduced to a critical threshold, where the rock mass can't resist the gravitational forces. This process of reducing rock bridges occurs due to (Stead & Eberhardt, 2013):

- Tectonics - folds, faults, uplift, deformation phases
- Geologic processes associated with rock genesis (intrusion, metamorphism, alteration)
- Geomorphic processes – glacial erosion, glacial rebound, fluvial down-cutting
- Earthquakes
- Precipitation and snowmelt events
- Long-term creep

The damage of the rock slope is influenced by the morphology of the failure surface. Varying failure surface geometries induces different damage processes. Planar sliding along bedding planes induces less damage than a multiplanar slide where rock bridges between different structures must break. Complex failure surface geometries with associated damage processes are shown in Figure 2.2.

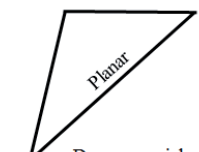
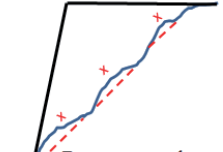
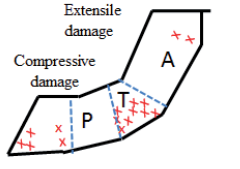
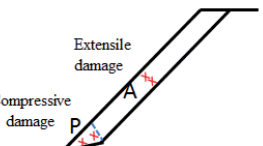
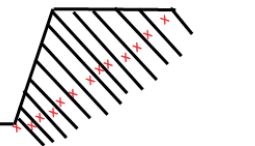
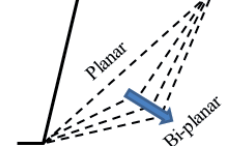
<p>a) Planar</p>  <p>Damage mainly limited to shearing of roughness or intact rock bridges between joints.</p>	<p>b) Undulating</p>  <p>Damage as rock mass rides over undulations. Some shearing of undulations.</p>	<p>c) Multi-planar</p>  <p>Damage at changes in failure surface gradient and in active (A), passive (P) and Prandtl prism transition zone (T).</p>
<p>d) Active-passive footwall</p>  <p>Compression induced brittle fracture damage. Extensile damage in upper slope (+/- buckling or ploughing).</p>	<p>e) Flexural toppling</p>  <p>Internal toppling root zone damage. Compression induced damage at toe.</p>	<p>f) Damage shape factor</p>  <p>Increased probability of internal slope damage with failure depth (planar → bi-planar).</p>

Figure 2.2: Examples of failure surface geometries with associated damage processes. Retrieved from Stead and Eberhardt (2013)

2.1.4 Deposition

A rock avalanche deposit consists of morphological features defining the spread of the collapse. The toe is defined as the longest run-out of the slide. It consists of coarse material in a lobate shape, characterized by sharp and steep bulging fronts. At the rims of the deposit, often lateral levees are deposited parallel to the direction of movement (Abele, 1974, von Poschinger, 2002). The internal structure of a rock avalanche deposit consists of a slight upwards coarsening of material with no matrix content. The spatial deposition also shows an upwards coarsening towards the central part of the deposit (Crosta, *et al.*, 2017).

Multiple failures from the same source area can produce an overlapping morphology of deposits. To determine if the deposit consists of multiple rock avalanche events, some main criteria must be set. These includes the vertical superposition, run out distance, presence of lobes within the spread of a deposit, and movement direction of slides conditioned by already deposited events (Crosta, *et al.*, 2017). The run-out distance can be assessed due to the direct relation between landslide volumes and the height/length ratio proposed by Scheidegger (1973). A well-established model later confirmed by researchers within both rock and debris avalanche studies. The study shows that the H/L ratio decreases systematically with volume increase, which means that if two failures occur from the same source area, the largest volume will reach the longest run-out. The superposition of events can be discovered by a vertical profile within the deposit (Schleier, *et al.*, 2017). A distinct layering of different events can be seen. A method of defining rock avalanche events in a cluster by remote sensing, is assessing the criteria of presence of lobes within the spread of a deposit. The theory of spatial upwards fining of material towards the source area can reveal if repetitional sequences of upwards fining exists. The method also gives the opportunity to do a relative dating if multiple events are overlapping.

Deposition of rock slope failures can vary from intact rock to highly fragmented rock mass depending on the volume and velocity, and rock strength and elastic properties (Frattini, *et al.*, 2012). The depositional zone for rock slope failures start where the slope angle is below 38 degrees, with deposition of the finest material first from a rock fall event (Hung & Evans, 1989). The deposit surface is a chaotic blocky carapace with a lobate shape. Clasts are angular and up to a few meters large. Inconsistent with rock avalanches, smaller rock slope failures have no grading in the vertical direction and no lateral levees. (Wieczorek, *et al.*, 2000)

When rock avalanches fail, they fragment in the process of gaining excessive travel lengths. In this process the initial volume will increase. The increase is assessed in literature with

volume increases varying from 7% to 26%. These estimates require that both the volume of the source area and the deposit is calculated accurately, which is rarely possible. Another estimate is retrieved from measurements of the porosity of well-graded crushed rock, which gives a typical increase of 18%-35%. The estimate of porosity in crushed rock also includes rock slope failures without a flowing movement. It also eliminates the factor of entrainment of the run-out area and highlights the fragmentation increase only. (Hung & Evans, 2004)

2.1.5 Post-glacial frequency models

The frequency distribution of landslides after the last deglaciation is widely discussed in literature, and different models have been proposed. The four suggested models for changing frequency is shown in Figure 2.3.

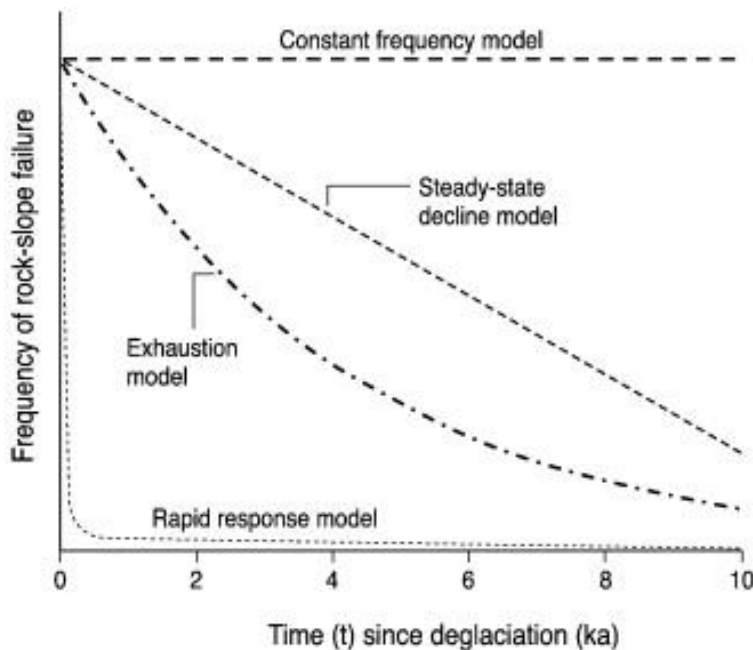


Figure 2.3: Models suggested for the distribution of rock slope failures over time. Modified from Ballantyne and Stone (2013).

The exhaustion model developed by Cruden and Hu (1993) is a model based on a failure rate declining exponential as potential source areas of failure will be used up. The model is based on slope failures along bedding surfaces, which exhausts hazardous sites and creates stable dip-slope landforms. If the failure eliminates an over dipping slope, there is no risk of another failure. A criterion for the model is that no erosion of the toe exists, and the slope is thus abandoned.

The steady state decline model proposed by Thorn and Loewenherz (1987), and Ballantyne and Stone (2013) introduces the possibility of a linearly declining frequency over time from deglaciation.

The constant frequency model suggests a constant frequency from deglaciation until now (Evans & Gardner, 1989). The model assumes a large population of hazardous slopes and the failure conditions are not changed with time or of past events. The frequency of rock slides after deglaciation is calculated by dividing the past failures by the years after deglaciation. Blikra, *et al.* (2006a) suggests this model based on resulting distributions suggesting higher frequencies the last 5000years BP.

The rapid response model suggests that nearly all failures occur the first centuries after deglaciation, while there are very infrequent failures after this rapid response (Evans & Clague, 1994). The combination of this model with a constant frequency model after the first centuries have been proposed by Church and Ryder (1972), suggesting a maximum sediment yield during and directly after deglaciation, followed by rapidly declining rates towards the geological norm (constant frequency). This combination is also the findings of Böhme, *et al.* (2015) from the Storfjord area of Western Norway, which highlights the presence of the largest total failure volumes directly after deglaciation. Ballantyne and Stone (2013) points out the removing of glacially-induced confining stresses as the reason for high failure frequencies directly after deglaciation, followed by a lower constant frequency of failures.

2.2 Secondary effects

Subsequent effects following a landslide are called secondary effects. The consequences of such effects have caused devastating damage and a large amount of fatalities through the Norwegian history (Hermanns, *et al.*, 2012a). The two types of hazard that can follow a landslide is:

- Displacement waves
- Landslide damming

“Displacement waves are waves triggered by subaerial mass movements” (Hermanns, *et al.*, 2013a). An example is a landslide hitting a water body. These events have caused most of the fatalities by secondary effects in Norway. The last 100 years, three events have caused 174 fatalities (Harbitz, *et al.*, 2014).

Landslide damming is created by a landslide deposit blocking a water course, leading to the formation of a natural reservoir. The danger of landslide damming is attached to the failure of the dam, causing a flood of water and sediments downstream. (Hermanns, 2013)

2.2.1 Displacement waves

This type of secondary effect can occur in a wide range of environments, like continental margins, ocean islands, fjords, natural and artificial dams and rivers (Hermanns, *et al.*, 2013a). The common triggers in Norway are snow avalanches, rock avalanches, rock falls, quick clay slides and debris flows (Hermanns, *et al.*, 2014b). The main reason for the high concentration of landslide-triggered displacement waves in Norway is the deeply incised valleys and fjords. A high relief created by multiple glacial cycles, in addition to the Holocene isostatic rebound layering sensitive marine sediments have made the coast line of Norway exposed (Hermanns, *et al.*, 2014b).

The displacement waves can occur in different ways depending on the landslide material, origin, and velocity. Landslides originating subaerially hits the water body with high velocity. If the landslide volume is larger or equal to the volume of the water body, it initiates a “push wave” (Figure 2.4). This is often the case in reservoirs and valley lakes. If the volume of the water body is larger than the landslide volume, a “body wave” is initiated. This type of wave is the case for the displacement waves initiated in the fjords of Norway. Failures of mixed subaerial-subaqueous landslides can also occur, where either the slide starts under water with a substantial volume above the water, or the slide starts under water and propagates retrogressively to the subaerial mountain side (Figure 2.4). In some cases, a cliff failures onto a tidal flat, where only parts of the deposit get submerged. (De Blasio, 2011)

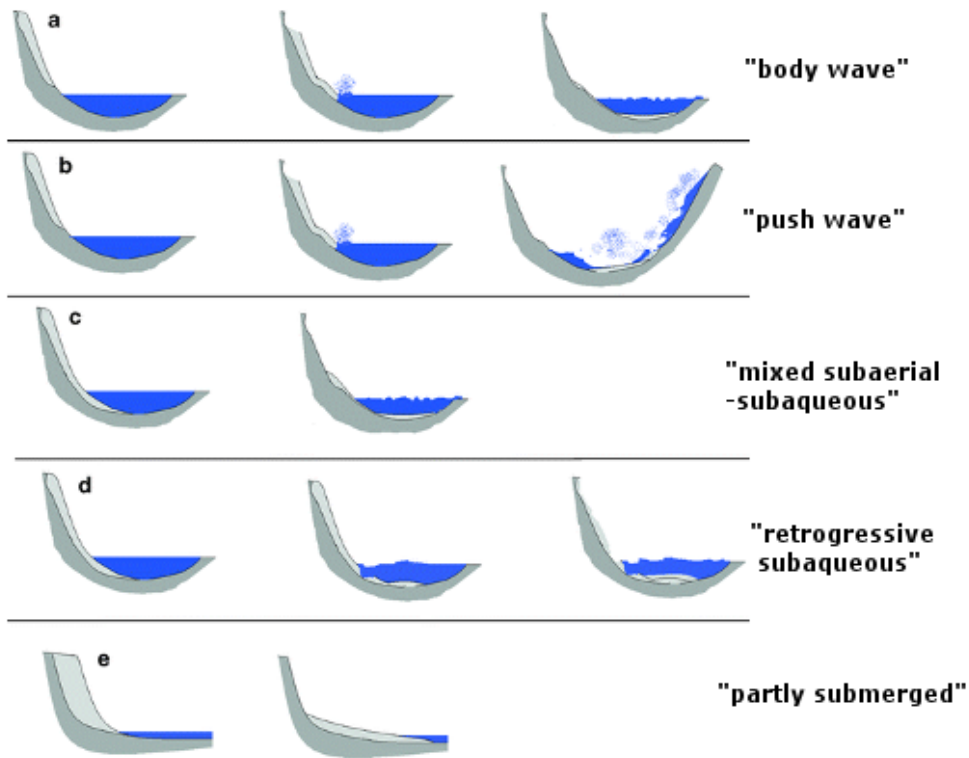


Figure 2.4: Potential situations for landslide failures into water basins of various size. (De Blasio, 2011)

Displacement waves in fjords can cause oscillations creating multiple waves. These waves can vary in size and continue for hours. The highest run-up heights are obtained where the impact of the waves is perpendicular to the shore. This is often on the opposite side of a fjord or reservoir. High run-up can also occur in the head of fjords, where the fjord is narrowing and get shallower than where the displacement wave initiated. These factors concentrate the wave energy and amplifies the height, despite the increasing distance from the source area. (Harbitz, *et al.*, 2014, Oppikofer, *et al.*, 2018)

2.3 Remote sensing

The last decades, remote sensing techniques have developed to be a key component of landslide investigation. With new techniques, both identification, classification, characterization, mapping and monitoring can be carried out remotely. (Petley, *et al.*, 2012)

2.3.1 LiDAR scanning

LiDAR stands for Light Detection And Ranging, and is a technique assessed by a laser scan either ground-based or from an airplane. The scan obtains a dense cloud of points with a known distance from the scanner, together with a dip and azimuth. The point cloud from aerial laser scanning can be georeferenced and used as a Digital Elevation Model with resolution of 1 meter. LiDAR is a remote sensing technique often used when an area is vegetated or inaccessible due to steepness. The possibility of processing the point cloud, gives the opportunity to cut out the signals created by vegetation, often the first return pulses of the scan. This technique enables to distinguish morphological structures on the ground.

(Jaboyedoff, *et al.*, 2012)

2.3.2 Photogrammetry

Photogrammetry techniques have existed for a long time, all the way back to when aerial photos were examined through stereoscopes (Petley, *et al.*, 2012). Along the development of digital technology, there was also made digital photogrammetry software converging photos into 3D models. The method can be used both aerial and terrestrial, by overlapping two photographs taken from different positions (Michoud, *et al.*, 2010). The Agisoft Photoscan software aligns pictures taken from any angle and height. The only conditions are corresponding points between two adjacent pictures of the slope that is aligned, and that the point where the photos are taken from is registered (Li, *et al.*, 2016). The model can be georeferenced, either with fixed points, or aligned with the Digital Elevation Model retrieved from the LiDAR scan. The photogrammetric model can be combined with other point clouds.

2.3.3 Bathymetry data

Multibeam bathymetric data is a remote sensing technique used to map large submerged areas effectively. The data is retrieved from a multibeam sonar at a boat. This high-resolution bathymetric data can be rapidly surveyed with a decimetric accuracy (Quinn, *et al.*, 2008). The bathymetric data can be supplied as digital elevation model with a grid down to 1m resolution and assessed in the software ArcGIS (Westley, *et al.*, 2011). The data can also be combined with other DEMs assuring a full aerial/aquatic assessment of a fjord site.

2.4 NGU mapping approach

Systematic geological mapping is carried out to detect potential unstable rock slopes that can collapse catastrophically and involve substantial run-out larger than that of a rock fall.

Smaller rock slope failures are included if secondary effects can be initiated (Hermanns, *et al.*, 2012b). This work has been conducted in Norway since 2005, now financed by NVE. The mapping approach is provided to guarantee the same amount of geological information for all unstable slopes with the same risk level (Hermanns, *et al.*, 2014a).

The mapping approach is divided into six main steps:

Step 1: Detection of unstable rock slopes

Step 2: Reconnaissance

Step 3: Preliminary consequence analysis

Step 4: Geological mapping

Step 5: Periodic displacement measuring

Step 6: Establish scenarios

Detection of unstable rock slopes is assessed through remote sensing techniques such as aerial photos, Digital Elevation Models (DEM) and satellite-based radar interferometry (InSAR).

The aim is to detect morphological features connected to instability such as opening of cracks, displacement of blocks and high fracture density of bedrock, or by mapping deformation velocities of the unstable slope.

Reconnaissance is carried out to secure that the detection is assessed on the right premises.

Both old tectonic structures and displacement due to solifluction can be mistaken as signs of rock slope deformation. The reconnaissance process is conducted by either easy access to the unstable area or from a helicopter. Sites with no signs of deformation of large volumes will be categorized as the following: A) too small to cause a catastrophic failure, B) no structural or lithological conditions, or C) structural or lithological conditions, but no sign of displacement or deformation. The last category still must be assessed in the future for potential changes of activity, as the slope might become active.

A preliminary consequence analyses will be carried out after the reconnaissance stage. The aim is to divide sites with no evident consequences into low-risk sites. Volume calculations

and run-out analyses will be carried out to assess potential consequences. The sites with evident consequences within the run-out area, as buildings, life lines or water bodies, will be further investigated.

The simple geological mapping focuses on criteria needed for the further hazard classification developed at NGU (Hermanns, *et al.*, 2013b). Geological information of both morphological and structural development, and signs of activity is assessed for the following criteria:

1. Development of a back scarp
2. Potential failure surfaces
3. Development of lateral release surfaces
4. Kinematic feasibility
5. Morphologic expression of a basal rupture surface
6. Displacement rates
7. Acceleration of displacement
8. Increase in rockfall activity on the unstable slope
9. Presence of post-glacial events along the affected slope and its vicinity

If the geological conditions through this simple geological mapping are well understood, periodic displacement measurements are carried out to reduce uncertainties. If the simple geological mapping could not assess the geological criteria, a more detailed mapping is necessary.

Periodic displacement measuring is assessed to reduce the uncertainties attached to the criteria considering displacement rates and the acceleration of displacement. Different monitoring techniques can be used like extensometers, differential GPS-systems, satellite and ground-based InSAR, laser scanning or photogrammetry.

The establishment of scenarios is the last mapping stage building on the other approaches. Both varying geological conditions and slope activity within the same slope can cause various failure scenarios each with a different hazard. The establishment of scenarios should be conducted for all slopes with a combination of: 1) different deformation rates, 2) varying structural conditions, or 3) internal scarps, cracks and depressions which dissect the unstable slope (Hermanns, *et al.*, 2013b). All scenarios are mapped as a standalone risk object for the hazard classification. For the consequence analysis, volume and run-out is estimated for the defined scenario.

2.5 Hazard assessment developed at NGU

The hazard assessment of Norwegian unstable rock slopes is based on a qualitative classification system developed by a group of both Norwegian and international experts (Hermanns, *et al.*, 2013b). It classifies the hazard of catastrophic failures, which is defined as rock slope failures with fragmentation of rock mass and substantial run-out of high velocities that can impact larger areas than rockfall events (Hermanns & Longva, 2012).

A preliminary quantitative assessment is assessed based on the results from hazard classification of 22 unstable slopes in Norway. This is due to the need for quantitative probabilities for the Norwegian regulations on technical requirements for structures. (Blikra, *et al.*, 2016)

The hazard assessment is focusing on aseismic failures. The reason for that is a study of 32 historic events showing that no catastrophic failures occurs after an earthquake without any pre-failure slope deformation (Hermanns, *et al.*, 2012b). However, seismic events with a magnitude of 7,0 can occur every 1100 years (Bungum, *et al.*, 2005), and thus play an important role in the quantitative assessment of hazard.

2.5.1 Hazard classification

The hazard classification system is based on the findings in the NGU mapping approach, described in chapter 2.4. Each criterion has two or more conditions with a given score to each condition from 0 to 1, except for the criterion assessing displacement where the score ranges from 0 to 5. The total hazard score can thus vary from 0 to 12 where 12 is the highest hazard obtained for a scenario. A high hazard score can be reached in many ways, combining high scores from different criteria. The most important criteria, which gives scores from 0 to 5 is the displacement rate, 0 for no movement and 5 for above 10cm/year. If the displacement in such short period of time as cm/year is high, it is an important sign of a sudden failure. The criteria and attached conditions are seen in Figure 2.5.

1. Back-scarp	Score
Not developed	0
Partly open over width of slide body (few cm to m)	0.5
Fully open over width of slide body (few cm to m)	1
2. Potential sliding structures	Score
No penetrative structures dip out of the slope	0
Penetrative structures dip on average < 20 degree or steeper than the slope	0.5
Penetrative structures dip on average > 20 degree and daylight with the slope	1
3. Lateral release surfaces	Score
Not developed	0
Partly developed on 1 side	0.25
Fully developed or free slope on 1 side or partly developed on 2 sides	0.5
Fully developed or free slope on 1 side and partly developed on 1 side	0.75
Fully developed or free slope on 2 sides	1
4. Kinematic feasibility test	Score
Kinematic feasibility test does not allow for planar sliding, wedge sliding or toppling	0
Failure is partly kinematically possible (movement direction is more than $\pm 30^\circ$ to slope orientation)	0.5
Failure is kinematically possible (movement direction is less than $\pm 30^\circ$ to slope orientation)	0.75
Failure is partly kinematically possible on persistent discontinuities (movement direction is more than $\pm 30^\circ$ to slope orientation)	0.75
Failure is kinematically possible on persistent discontinuities (movement direction is less than $\pm 30^\circ$ to slope orientation)	1
5. Morphologic expression of the rupture surface	Score
No indication on slope morphology	0
Slope morphology suggests formation of a rupture surface (bulging, concavity-convexity, springs)	0.5
Continuous rupture surface is suggested by slope morphology and can be mapped out	1
6. Displacement rates	Score
No significant movement	0
0.2 - 0.5 cm/year	1
0.5 - 1 cm/year	2
1 - 4 cm/year	3
4 - 10 cm/year	4
> 10 cm/year	5
7. Acceleration (if velocity is >0.5 cm/yr and <10 cm/yr)	Score
No acceleration or change in displacement rates	0
Increase in displacement rates	1
8. Increase of rock fall activity	Score
No increase of rock fall activity	0
Increase of rock fall activity	1
9. Past events	Score
No post-glacial events of similar size	0
One or several events older than 5000 years of similar size	0.5
One or several events younger than 5000 years of similar size	1

Figure 2.5: Nine criteria describing the present state of the slope: For each criterion a condition must be chosen with a score varying from 0 to 1. The score for the displacement criterion varies from 0 to 5. (Hermanns, *et al.*, 2013b)

Total hazard scores are divided into five hazard classes, from very low to very high, with equal intervals. The reason for that is effective communication and understanding of the hazard. Early in the mapping process, with only a few criteria mapped, it can be found out if the hazard score can reach the medium or high hazard class. If only a low hazard class can be reached, it may not be necessary to execute a more detailed mapping, and displacement

monitoring will not be necessary. If criteria of the simple mapping are estimated to a medium hazard score, there will be an important measure to define the displacement rates.

For the Norwegian regulations on technical requirements for structures (TEK 17), hazard probabilities are used to assess the safety demands. Building requirements are divided into three safety classes (S1, S2 and S3), each with a required minimum probability threshold, dependent of the consequence of a hazard reaching the building. Schools and hospitals (S3) are considered a probability threshold at 1/5000, houses (S2) at 1/1000, sheds and garages (S1) at 1/100. This quantitative classification requires a conversion of the qualitative hazard scores to annual probabilities, assessed by Blikra, *et al.* (2016) with the following considerations:

1. Historical data shows an average of 2-3 fatal rock avalanches each century. Based on the national database for potential large rock slope failures, there is three scenarios with a hazard score above 9,6 (NGU, 2017). This fits well to the average failures expected with annual frequencies of 1/100.
2. Risk matrices are built up by logarithmic scales both in hazard and consequence. This is also used for the annual probabilities, with an increase of 10 for each hazard class. The annual probability of 1/5000 is placed logarithmic within the medium hazard class.
3. Slopes with no displacement rate should be plotted with a lower probability than 1/5000, due to the consequences for urban planning.

The resulting thresholds for the safety classes S1, S2 and S3 is set to hazard scores of 9,6; 7,2 and 5,5 due to the considerations of Blikra, *et al.* (2016).

2.5.2 Consequence assessment

When assessing the consequences of a failure, the focus is on loss of lives. Fatalities can occur by the effect of rock mass itself, or from secondary effects like displacement waves or bursting of landslide dams. The assessment focuses on 5 main steps (Oppikofer, *et al.*, 2016):

1. Volume estimation
2. Run-out analysis
3. Assessment of displacement waves
4. Assessment of landslide damming
5. Element at risk analysis

Volume estimation is an important step to obtain in the consequence analyses as the results are used in step 2,3 and 4. An overestimation of the volume can cause economic losses in high monitoring costs, but an underestimation can cause severe damage of property and loss of lives if the resulting hazard zones are mapped too small. A volume estimation can be obtained with different methods according to the degree of details needed. Sloping Local Base Level is a method used in the preliminary consequence assessment, while a three-dimensional construction of back scarp and release surfaces are obtained in a detailed consequence assessment. (Oppikofer, *et al.*, 2016)

Run-out analysis is a calculation of the longest potential run-out of the estimated volume. There is an empirical relation between angle of reach and the volume, giving a first estimation of run-out (Scheidegger, 1973, Corominas, 1996). This relationship is experienced by a continuous reduction of the angle of reach, the angle from the source area to the toe of the deposit, when the volume increases (Corominas, 1996). A more detailed analysis can be conducted in the software Flow-R, basing their software on the angle of reach in a digital terrain model. Numerical run-out modelling is computed if there is a medium or high-risk site. This is a 2D or 3D model where the rock mass is controlled by simple rheological conditions. (Oppikofer, *et al.*, 2016)

Displacement waves can be assessed in three different ways, also here depending on the accuracy needed. A) an empirical relation between run-up, volume and distance, B) the VAW-model, or C) three-dimensional numerical modelling of displacement waves and run-up. The empirical relation is based on linking run-up to their distance to initiation point, and their volumes, for 254 registered events (Oppikofer, *et al.*, 2018). The VAW-model is based on modelling of slide-initiated displacement waves in 2D and 3D, used for a more detailed assessment of displacement waves if the hazard classification shows medium or high hazard (Oppikofer, *et al.*, 2016). The three-dimensional numerical modelling of displacement waves is assessed by expert knowledge modelling in the software GloBouss and DpWaves (Harbitz, *et al.*, 2014). Parameters from the run-out assessments and findings from the less detailed displacement wave assessments are implemented.

Assessment of landslide damming is assessed in three different ways. An empirical relation can be obtained between dam height, dam volume and the dam area. A detailed modelling of the dam height is considered if the hazard is considered medium or high. An empirical assessment of the dam stability is useful to estimate the probability of dam failure. A blocking index is calculated by the volume and height of the dam, and the drainage area upstream from

the dam. A last assessment is modelling of the potential flooding area downstream from the damming in case of dam breaching. This can be modelled in the software FLO-2D and RiverFlow2D. (Oppikofer, *et al.*, 2016)

The element at risk analysis is first assessed as a preliminary analysis, where all inhabitants affected by the hazard is considered as fatalities. In this assessment, national database of buildings is used to estimate the number of inhabitants in each building based on the building type. For private houses, other statistics are available to estimate the exact number of persons living in each house. A detailed analysis implements the exposure time and vulnerability of all inhabitants for the expected hazard type.

2.5.3 Risk analysis

A risk analysis consists of the qualitative hazard assessment and a quantitative consequence analysis. Risk is calculated by the risk equation (Fell, *et al.*, 2005):

$$R = P_F \times P_P \times P_E \times V \times E$$

where P_F = probability of failure, P_P = probability of propagation, P_E = probability of presence of the element in risk, V = vulnerability of the element in risk, and E = element at risk (number of people affected). When assessing a preliminary risk analysis, the consequence is set to a worst-case scenario. All inhabitants (E) affected by either run-out of the failure or secondary effects (P_P) are counted as fatalities ($V=1$). That means that the factors P_P , P_E , and V are set to 1, and the number of potential fatalities is equal to E .

A detailed consequence analysis is needed if the preliminary risk analysis assesses medium or high-risk objects. Detailed mapping gives a detailed run-out assessment, and numerical displacement wave simulations are computed. Building types can roughly be evaluated, and affect the parameter P_E , while the vulnerability will be assessed for each inhabitant dependent on the hit by primary or secondary effects of the landslide. The survival rate of a direct hit by a landslide is close to zero, while the survival rate when hit by a displacement wave is 30% (Blikra, *et al.*, 2006a).

The result of the hazard assessment and consequence analysis is shown in a risk matrix. The purpose is to define the degree of follow-up needed. The follow-up can consist of monitoring, more detailed field investigations and mitigation measures. As seen in Figure 2.6, a low-risk

site can be either a site with a very low probability of hazard, but with consequences of up to 1000 fatalities, or a site with a high hazard score but the consequence of a failure is the loss of one life. The sites within this blue area of the risk matrix does not need further follow-up. Sites placed within medium risk has a low hazard class but connected to large consequences. Medium to high risk sites are sites with a high hazard score but lower consequences than the medium risk sites. For all sites within the medium, medium to high, and high risk in the matrix a follow-up is needed.

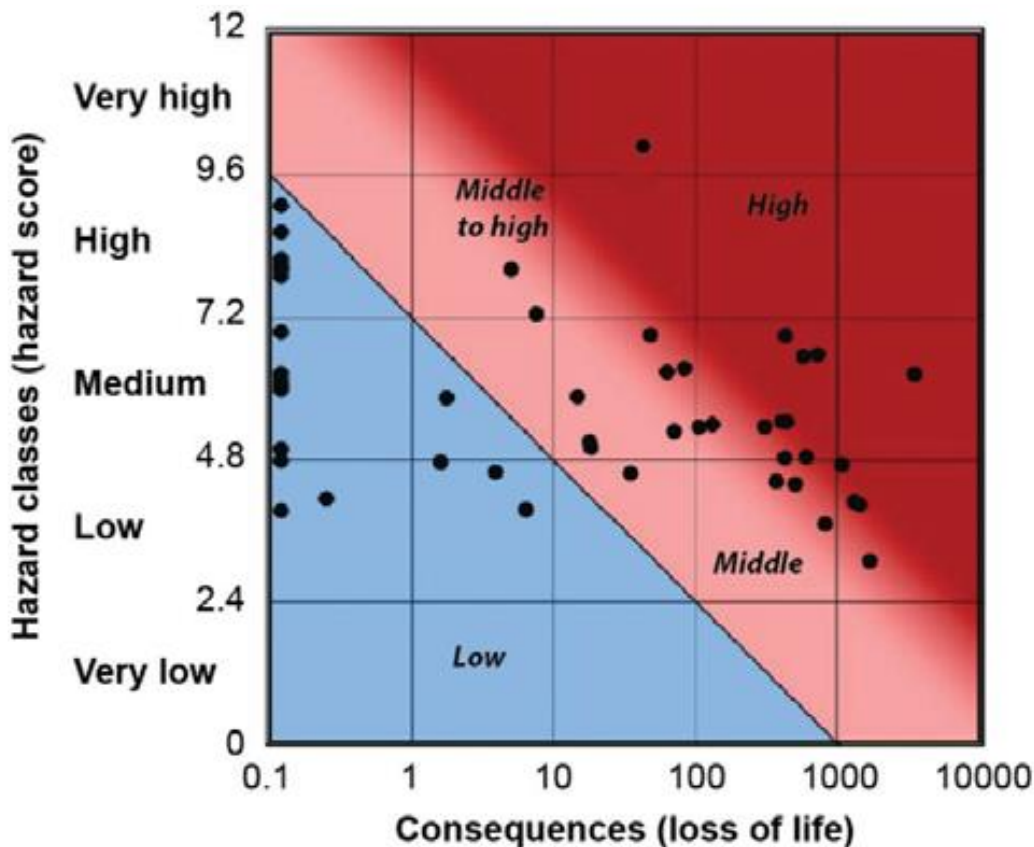


Figure 2.6: Risk classification matrix divided into four levels of risk, Low, Middle, Middle to high, and High. For unstable slopes plotted in the blue area, there is no need for further follow-up. For slopes plotted in the red area there is need for a more detailed assessment. The follow-up needed is in terms of monitoring and further investigations. (Hermanns, *et al.*, 2016)

The Norwegian hazard and consequence analyses also gives the possibility to add uncertainties to the risk classification. The consequences are plotted as a mean value, with uncertainties from minimum to maximum values of fatalities. The uncertainties of the hazard are plotted statistically as the 5% and 95% percentiles of the hazard score. (Hermanns, *et al.*, 2013b)

3 Methods

3.1 Geological mapping

Geological mapping is assessed both subaerial and subaquatic. In the subaerial assessment both remote sensing techniques and field work have been used. Of remote sensing techniques, digital terrain models, orthophotos and photogrammetric models of the vertical cliff have been assessed. In the subaquatic assessment, a high resolution bathymetric terrain model is used.

3.1.1 Subaerial interpretation

Aerial survey

The area of interest in this thesis is a 6 km long sea cliff with change in topography, vegetation, and accessibility. The need for interpretation of aerial photos and Digital Elevation Models was crucial, due to the limited time of field work, long walking distances and tough weather conditions. Interpretation of possible unstable slopes, cracks, and lineaments laid the foundation for further geological mapping.

The interpretation was carried out through orthophotos (Statens Kartverk, *et al.*, 2017), and a digital elevation model of 1m resolution conducted through LiDAR scanning. The mapping have been assessed in ArcGIS, using the tool Hillshade (ESRI, 2017). The tool is highlighting the morphology of an area by shading the DEM with a hypothetical light source from a given azimuth and sun altitude (angle above the horizon). The positioning of the light source can be changed, shading the morphology in a different direction.

The first step of the mapping process was to follow the edge of the cliff, looking for delimiting structures such as opening of cracks and depressions as a first sign of unstable slopes. The structures were mapped, and GPS-positions were stored for the field work. Large-scale structures were mapped, both for the structural analysis of regional lineaments and because of the difficulty of detecting such structures in the field with varying topography.

An interpretation of the deposits seen along the toe of the cliff have been assessed with the hillshade-tool and verified by orthophotos. A mapping of deposits, interpretation of main characteristics, and a separation of overlapping deposits have been conducted.

Terrestrial survey

As mentioned in the previous chapter, a 1m resolution DEM is available for the area obtained through aerial LiDAR-scanning. The challenge of assessing steep cliffs as the cliff of Lifjellet is that aerial scans will have a reduced number of points in the point cloud for steep terrain. For overhanging cliffs, there will be black holes in the point cloud. This problem addressed the need for a terrestrial survey. A three-dimensional photogrammetric model based on 906 high-quality photos taken from numerous angles covering the whole cliff face of Lifjellet were constructed. Photos were taken with a DSLR-camera from a boat and aligned in the software Agisoft Photoscan. The photogrammetric model was converted as a point cloud to the program Polyworks, where the model was georeferenced by aligning it with the DEM.

The photogrammetric model has been used for the interpretation of morphologic expressions, possible sliding structures, past events, and rockfall activity using the software CloudCompare (CloudCompare, 2018). Displaying the point cloud in CloudCompare gives a realistic 3D model with high resolution and natural colors extracted from the original photos. The CloudCompare plugin Ransac was used to automatically detect structural planes on the cliff face, by sorting all points with neighboring points of the same direction. Through this method, the dip and dip direction of back scarps and release surfaces could be assessed, and limits for the volume calculations obtained.

3.1.2 Field work

The field work consisted of two main tasks. The first was to detect and document unstable slopes along the cliff. This was assessed by handheld maps, a GPS, a Harbin geological compass, Canon Digital single lens reflex camera, measuring tape, and pen and paper. This process have been executed according to the simple geological mapping in the NGU mapping approach (Hermanns, *et al.*, 2014a). The goal was to assess the criteria needed for a preliminary hazard classification. Orientation and persistence of back scarps and lateral release surfaces were mapped. Potential sliding structures were evaluated, and any signs of recent activity were noted. Unstable slopes with varying structural conditions, internal scarps or depressions were divided into standalone scenarios.

The second task was to collect field measurements for the structural analysis detailed in chapter 3.2.1. The measurements were focusing on the dip direction and dip of structures, and all structures within a radius of 50m from each measuring station were applied. In total 1752 measurements were taken, at 43 different measuring stations spatially distributed over the area. The GPS-positions attached to each station is seen in Appendix A.

3.1.3 Subaquatic interpretation

The interpretation of deposits in the fjord are assessed in ArcGIS with a subaquatic DEM of 1m resolution conducted by the remote sensing technique described in chapter 2.3.3. The tool Hillshade has been used to highlight the morphology of the area (ESRI, 2017). The interpretation of deposits was assessed following the principles of deposition of rock avalanches and smaller rock slope failures explained in chapter 2.1.4. Their main characteristics have been verified, a separation of overlapping deposits have been mapped and a relative dating of the overlapping deposits based on the interpretation of a chronological order have been suggested.

3.2 Structural analysis

A structural analysis was performed to establish mean orientations of structures within the field area. The analysis evaluates the structural control of the unstable slopes and shows importance for the kinematic feasibility of failure. The spatial variation of structures is the basis for dividing the field area into structural domains.

3.2.1 Field measurements

All structural measurements collected in the field are plotted in the software Dips 7.0 (Rocscience, 2017a). The stereographic projection is plotted in lower hemisphere, equal area, Fisher distribution, with dip/dip direction settings. The measurements are imported as excel-files into dips, creating a contour of the structural poles. Here, the contour is preset to a scale of 0 to 10, where 10 shows a dark color and 0 shows a light color. To present the mean planes of a discontinuity, the poles are chosen from a cluster analysis of all poles in a maximum range of 25 degrees. Each cluster is showing a variability cone with a radius of 1 standard deviation of the presented poles. When choosing what planes are statistically robust, there is used a rule of thumb, saying that a cluster with density concentration above 6% is very significant, 4-6% is marginally significant, and density concentrations below 4% should be considered not significant unless the measurement quantity is very high (Rocscience, 2017b).

One stereographic plot has been produced for each measurement station. This is done to detect the spatial variation of structures throughout the area. All stereographic plots have been plotted according to their GPS-coordinates on the overview-photo exported from ArcGIS,

seen in Appendix A). The aim is to assess the spatial variation of significant structures in the area.

If there are spatial variability of significant structures, the area is divided into structural domains with the same significant structures. Within each domain all structures measured have been re-analyzed, and the mean orientation of the significant structures are found. This is the basis for the kinematic analysis computed for the hazard classification of unstable slopes (chapter 2.5.1).

3.2.2 Regional lineaments

The sparse vegetation and thin bedrock cover by soil and quaternary deposits at Lifjellet is allowing a regional assessment of lineaments within the field area. DEM's and orthophotos are used in the software ArcGIS to interpret and map lineaments. Mostly, the lineaments have been interpreted with the ArcGIS-tool Hillshade, but also the tool Aspect were used. The Aspect-tool highlights the aspect of structures by coloring the planes of similar orientation. The aspects are divided into 10 different colors, each color representing an orientation of 36 degrees. The tool makes it easier to detect less dominant structures, such as depressions (Charrière, *et al.*, 2015).

The orientation of all lineaments are measured and plotted into a rosette plot in the software Dips (Rocscience, 2017a). The analysis is based on defining the most prominent orientations of the lineaments. The rosette plot is divided into bin widths of 10 degrees, and the plot shows 6 planes per circle increment. The same procedure has been used after dividing the area into domains, based on the structural analysis of the field measurements. All lineaments inside a domain have been plotted in the rosette. The analysis can then assess the spatial variation of significant lineament orientations between the different structural domains.

3.3 Application of the hazard classification system

The hazard classification system has been applied to all unstable slopes along the cliff of Lifjellet following the methodology of Hermanns, *et al.* (2013b), described in chapter 2.5. Criteria not yet assessed for all locations such as displacement rates and acceleration have been set to standard values with high uncertainties generated through method testing at NGU.

3.3.1 Kinematic analysis

The criteria of kinematic feasibility is assessing the different failure mechanisms of a rock slope, classified by Hungr, *et al.* (2014) in chapter 2.1.1. The three failure mechanisms assessed are planar sliding, wedge failure and block toppling. The analysis is based on significant structures within each domain, with respect to the slope orientation. The assessment is carried out in the software Dips 7.0 (Rocscience, 2017a), following the recommendations of Hermanns, *et al.* (2012b).

Standard engineering geological criteria for kinematic analyses have been applied for the three failure mechanisms (Hoek & Bray, 1981, Wyllie, *et al.*, 2004). However, due to the complexity of large unstable slopes, higher lateral tolerance both for planar and wedge sliding have been suggested. Failure is partly possible if the angle between slope aspect and the failure direction is above 30degrees, and possible if the angle is below 30 degrees (Hermanns, *et al.*, 2012b). For the toppling analysis, direct toppling has been assessed with lateral tolerance of 30 degrees, which means that the intersection between the two delimiting planes must be plotted within 30 degrees from the slope aspect for failure to be possible. A plane with dip below the friction angle of the rock mass must also plot within the lateral tolerance. If it plots outside the lateral tolerance, oblique toppling is possible, addressed as partly possible in the feasibility test.

In the resulting kinematic analysis, the considerations of slope orientation are important. Oppikofer, *et al.* (2015) highlights the importance of the steepest scarps in the area for the estimation of slope dip, due to the risk of underestimating the possibilities for failure. Slope aspect is considered as the average orientation of the cliff within each structural domain. A friction angle of 20 degrees is set based on the conservative recommendations for all rock types by Hermanns, *et al.* (2012b). All considerations are implemented to reduce the chance of underestimating the possibility of failure.

3.3.2 Displacement measurements

The chapter describes the methodology of the Differential Global Navigation Satellite System and Extensometer-measurements.

Differential Global Navigation Satellite System (dGNSS)

dGNSS- measurements are obtained through variation in distance between a fixed point and a rover point. The fixed point is set in a position where there is no movement of the slope, while the rover point is placed at the unstable block. The measuring technique is based on statistical measuring of vectors with an interval of 5 seconds over a period of one hour. The coordinates of each GNSS-point are calculated by a least squares adjustment (Böhme, *et al.*, 2016). The change in position of the rover point is interpreted as displacement. The significance of displacement is calculated by 3 standard deviations of the vectors, often better than 1mm in the horizontal direction and 2mm in the vertical direction. These significance levels are often found to be too low, and the actual precision is normally 2-3 times higher than estimated values (Böhme, *et al.*, 2016).

When analyzing the cumulative displacement over a time series, linear regression is used to calculate average yearly displacement. A continuous trend of displacement in a certain direction is a good indication of gravitational displacement (Böhme, *et al.*, 2013).

Extensometer

Extensometer-measurements are obtained by measuring distance between two eyebolts. The method is easy to use and lightweight, consisting of a measuring-tape. Positions of measuring is often across back scarps or other internal cracks of an unstable slope. The measurements obtains displacement in one direction, a straight line between the measuring bolts. (Oppikofer, *et al.*, 2013)

The measuring tool used by NGU is a Digital Tape Extensometer, a 20m long tape consisting of stainless steel with a tensioning device reading accuracies down to 0,01mm. Repeatability tests executed by NGU suggests a standard deviation between 0,04 and 0,19mm. (Oppikofer, *et al.*, 2013)

3.4 Application of the consequence assessment

Of the five main steps described in chapter 2.5.2, two of the steps have been assessed in this thesis. Volume estimations have been assessed due to the evaluation of consequences for a potential failure, and due to the assessment of frequencies of past events. The run-out analysis tests the potential for a failure of a distinct volume to hit the water body. The assessment of displacement waves and the element at risk analysis is left out of this thesis to focus on geological conditions. These steps will be carried out by NGU for the final risk assessment.

3.4.1 Volume estimation

For the different estimations of volume, two methods have been used both described in the methodology of Oppikofer, *et al.* (2016). The method used for unstable slopes is a three-dimensional construction of failure surfaces (Jaboyedoff, *et al.*, 2015). For the estimation of deposits, the method Sloping Local Base Level is used (Jaboyedoff, *et al.*, 2005).

Unstable slopes

A three-dimensional manual construction of back scarp and release surfaces assume that structures follow the same orientation and dip with depth of the rock mass, which highlights the importance of the significance and persistence of structures. The method fits best for small unstable blocks, where the slope is controlled by geological structures (Oppikofer, *et al.*, 2016). The construction is assessed in the software CloudCompare (CloudCompare, 2018).

The construction of the unstable block is assessed combining point clouds obtained by two different remote sensing techniques. The Digital Elevation Model is covering the horizontal area, computed by aerial LiDAR-scans. The steeper part is assessed through a photogrammetric model. Both techniques are described in chapter 2.3. Planes delimiting the block are fitted into the point cloud until the block is fully detached on all sides. Planes are manually fit to follow the orientation of significant structures from field measurements, or they can be oriented by significant structures along the cliff detected in the 3D-model.

Volume is computed by a calculation-plugin in CloudCompare calculating the volume based on the georeferenced metric size of the block. This gives the calculation of the volume a high accuracy.

Deposits

The SLBL-method is an ArcGIS tool developed at NGU to estimate either deposits sticking up from the original topography or estimate volumes of large-scale unstable slopes. For the use in this thesis when estimating deposit volumes, the underlying limit is drawn by a tolerance value of 0. This means that the topography prior to the event is constructed as a straight line between points on each side of the deposit, without any curvature exceeding the thickness of the deposit. To assess if the construction of the lower limit is good, a hillshade of the constructed topography is compared to the surrounding topography not covered by deposits.

A combined DEM of the subaerial and the bathymetric DEM is used for the estimation. A grid size of 5m is set to reduce the calculation time. This change of grid size has been tested, finding minor effects on the computed volume (Oppikofer, *et al.*, 2016). When combining the two DEM's, there are areas along the shoreline with no elevation data. This is due to the difficulty of collecting data in shallow water. These “holes” are estimated by multiplying the area of the deposit with no elevation data with the average thickness of the deposit calculated by the bathymetric data.

Upper limits for the calculated deposits have been set to a slope angle of 38 degrees. This is defined as the start of the depositional zone for rock fall activity by Hungr and Evans (1989) described in chapter 2.1.4. This limit is computed with the tool “Slope” in ArcGIS, where change in slope angle is displayed with changing colors.

The interpretation of a chronological order of overlapping deposits have been used for the calibration of volume sizes. The reason for the calibration is due to the estimation method used in SLBL. The volume computed for an underlying deposit will be increased by the total volume of the overlying deposits. Where overlying deposits are situated with its whole volume above the underlying deposit, a simple reduction of the total volume is done. Where overlying deposits are partly covering the underlying volume, a simple estimation of area times average thickness of overlying deposit is calculated. Several methods are suggested for the calibration, but due the limited time of assessing classified bathymetry data and the already high uncertainties, the simple estimation was used.

When correlating the estimated volumes of deposits with the calculated volumes of unstable slopes, the fragmentation process must be considered. This is because fragmentation of the initiated failure volume will fragment to an increased volume, described in chapter 2.1.4. For

the volume estimation of rockslide deposits both the deposited volume and the initial volume will be computed. The initial volume will be calculated by a fragmentation rate of 25%, a value at the center of the range of porosities measured of well-graded crushed rock (Hungar & Evans, 2004).

3.4.2 Run-out analysis

In this thesis there are no consequences attached to direct impacts of a failure. The aim for the run-out analysis is to confirm if the potential failure can initiate a displacement wave. This allows for a low accuracy run-out estimation assessed following the empirical relationship developed by Scheidegger (1973). The run-out length L is assessed as a function of the failure volume V and the fall height H . Empirical relations between the “angle of reach” for a landslide and the volume of the slide is best fit to a power law equation:

$$\tan \alpha = \frac{H}{L} = 10^{0.62419} \cdot V^{-0.15666}$$

The equation is used for the calculation of “angle of reach” for scenarios classified with a flow movement, described in chapter 2.1.2. The scenarios with failure volumes below the Scheidegger cut-off is given standard values based on Corominas (1996). The calculations are based on the volume estimations of unstable slopes and the height estimations retrieved from GPS-points for each unstable slope in the field. A comparison of “angle of reach” and the angle to the water body is assessed to evaluate if the potential failure can initiate a displacement wave. If the “angle of reach” is lower than the angle to the water body, the potential failure will reach the water body.

3.5 Frequency analysis

A frequency analysis is based on interpretations of past events for a complete inventory limited to a regional area (Böhme, *et al.*, 2015). The aim is to assess a frequency of events occurring in a given period. The result can be analyzed based on their failure volumes and an annual frequency above a certain volume threshold can be estimated. Results are used for a semi-quantitative assessment of hazard within the limited area. Workflow for the frequency analysis is presented in Figure 3.1.

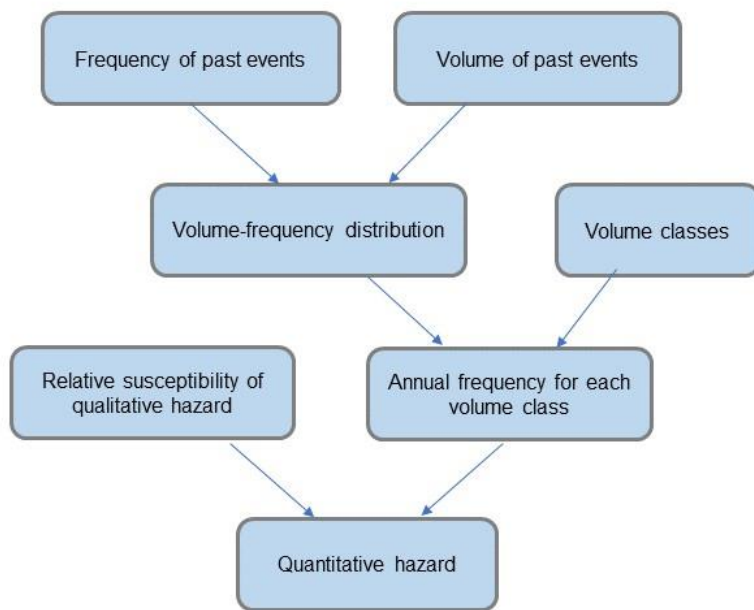


Figure 3.1: Workflow for the frequency analysis assessing frequencies of past events, volume-frequency of certain deposit volumes, and the workflow to define quantitative hazard based on past events.

The frequency of past events is estimated by the number of events deposited and the period of deposition in years. The period is obtained using deglaciation inventories assessed after last glaciation (Hughes, *et al.*, 2016). The number of events deposited is based on the subaquatic mapping of deposits described in chapter 3.1.3.

When the number of deposits and the period of deposition have been estimated, the distribution of deposition through time must be analyzed. Post-glacial frequency models have been suggested in literature, described in chapter 2.1.5. Distribution can be assessed based on absolute dating of deposits. Due to the lack of absolute dating for this inventory, a constant frequency model has been assessed for the following frequency analysis.

A volume-frequency distribution is analyzed in a log-log plot of cumulated past failures and their estimated volumes. Volumes of past failures are derived from estimations with the SLBL-method, described in chapter 3.4.1. Literature validates different models for the distribution, such as double Pareto distributions (Stark & Hovius, 2001), inverse Gamma distribution (Malamud, *et al.*, 2004), Weibull distribution (Crosta, *et al.*, 2007), Lognormal distribution (Ten Brink, *et al.*, 2009, Haas, *et al.*, 2012) and an inverse power-law model (Santana, *et al.*, 2012). The inverse power-law model is most commonly fitted to the volume-cumulated frequency, suggesting a linear distribution above a certain threshold. The equation is:

$$F(V \geq x) = ax^{-b}$$

where $f(V \geq x)$ is the cumulative number of past failures exceeding a given volume x . The model best fitting the volume-frequency distribution is chosen for the further estimation of annual frequencies for certain volume classes.

An estimation of annual frequencies for volumes above volume thresholds can be retrieved. The volume thresholds are set due to the definition of rock avalanches and rock slope failures for this thesis, described in chapter 2.1.2. The estimation is based on the calculation of a certain volume threshold with the equation of the best fit distribution model, and the frequency of past failures estimated by the constant frequency model, following the equation:

$$f(V \geq x, t) = f(V \geq x) * f(t)$$

3.6 Quantification of hazard

A quantification of hazard is needed to consider the results against the quantitative probability thresholds for the building requirements in TEK17, described in chapter 2.5.1. The quantification is assessed based on two methods. Blikra, *et al.* (2016) suggests a quantification based on qualitative hazard scores from 22 large slope failures in Norway. Böhme, *et al.* (2015) suggests the use of regional frequencies of past failures to assess a semi-quantitative assessment correlated by relative susceptibilities of the qualitative hazard scores of scenarios within the same volume class.

The importance for this thesis is to find the total probability of failure along the cliff. When considering the spatial distribution of potential failures, a correction for possible failure of

multiple scenarios from each location is of importance. If the largest scenario of a location fails, the smaller scenarios of the same location cannot fail. Considering this correction, the quantitative hazard will be assessed by the scenario of each location with the highest hazard score from the qualitative assessment.

3.6.1 Norwegian conversion method

The conversion is based on the considerations assessed by Blikra, *et al.* (2016), described in chapter 2.5.1. The hazard scores from each scenario is converted to an annual probability, following a logarithmic scale. The conversion is calculated by the equation:

$$f(x) = 10^{0,414x-5,98}$$

where x is the hazard score, and exponents are retrieved from the linear distribution combining hazard scores and logarithmic annual probabilities based on the thresholds set by (Blikra, *et al.*, 2016).

The annual probability of failure for the whole cliff face is estimated by adding the annual probabilities of all scenarios.

3.6.2 Empirical analysis

A semi-quantitative annual hazard H for each scenario can be estimated under the assumption that the regional inventory of unstable slopes is complete (Böhme, *et al.*, 2015). The calculation is based on the susceptibility of qualitative hazard scores and the annual frequencies retrieved for a certain volume class $x_1 \leq V \leq x_2$.

The results of the qualitative hazard assessment are giving hazard scores from 0 to 12. These rankings r_i are used to calculate the susceptibility for a certain scenario within a certain volume class:

$$S_i = \frac{r_i}{\sum_{i=1}^n r_i}$$

where n is the number of scenarios of the volume class. The annual frequencies for a certain volume class is obtained from the frequency analysis described in chapter 3.5 and estimated within a certain volume class instead of above a volume threshold.

The resulting annual hazard for each scenario is calculated by multiplying the annual frequency of the volume class by the susceptibility for the certain scenario to fail.

$$H = f(x_1 \leq V \leq x_2) \times S_i$$

4 Results

4.1 Results from structural analysis

4.1.1 Field measurements

Stereoplots of 44 measurement stations distributed along the north cliff of Lifjellet are analyzed to be able to assess a change in structural controls of the area. Through this assessment, the focus has been on joint sets with varying density concentrations through the area. In appendix B, the 44 stereoplots are aligned with the measurement stations, creating the basis for the assessment. The assessment of the stereoplots showed a spatial variability in the appearance of some joint sets, creating a natural border between domains. Precautions considering cliff orientation were needed when assessing the domains, considering that the cliff orientation along all domains had to fit within the lateral tolerance of 30 degrees from the average slope orientation for each domain. After the domains were set, new stereoplots were made assessing all structural measurements inside each domain. The domains, and the resulting stereoplots with mean planes of the measured structures are seen in Figure 4.1.

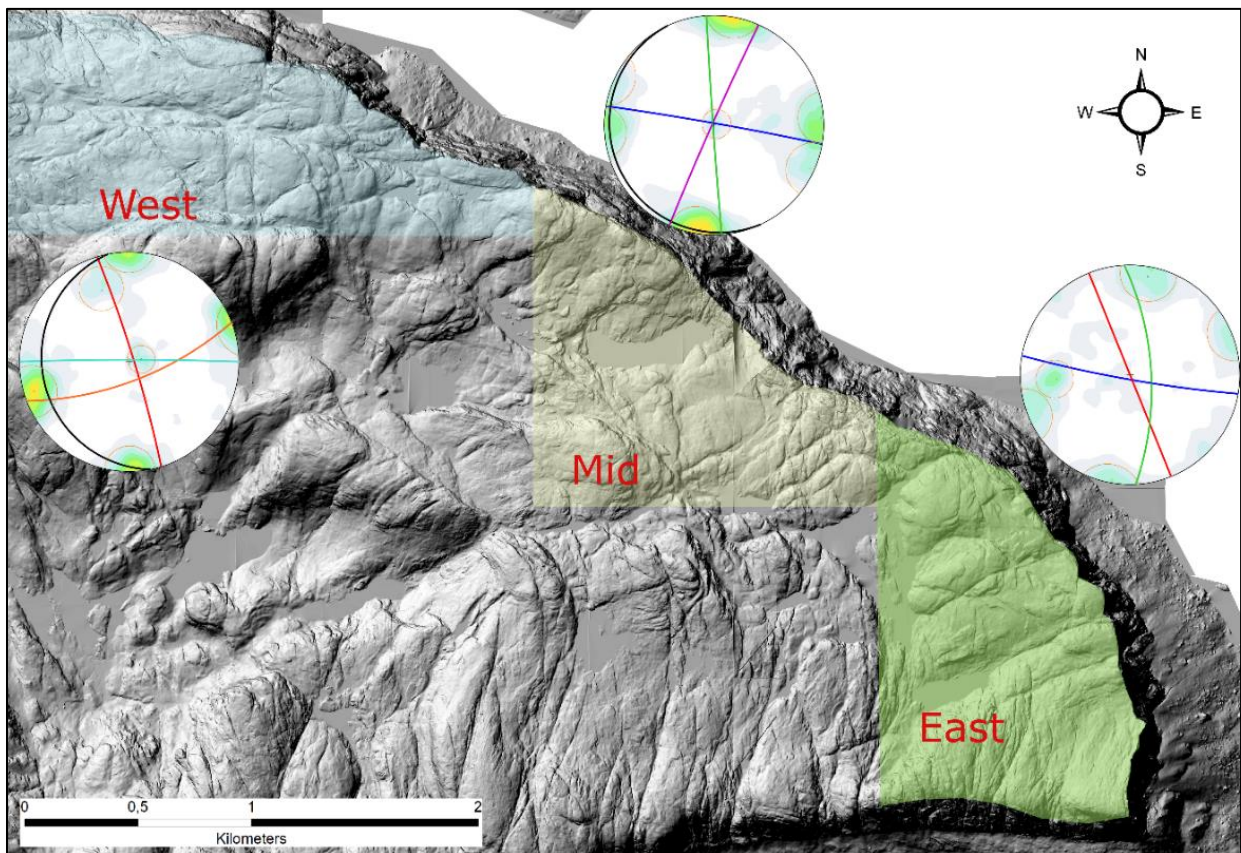


Figure 4.1: Structural domains, each showing the stereonet of the structural measurements taken inside their domain highlighted by their mean planes.

Western domain

In the western domain of Lifjellet, two joint sets are statistically significant structures. This is J3 and J6. Two more structures are not statistically significant but detected in the field. This is J5 and the bedding of the sedimentary rock.

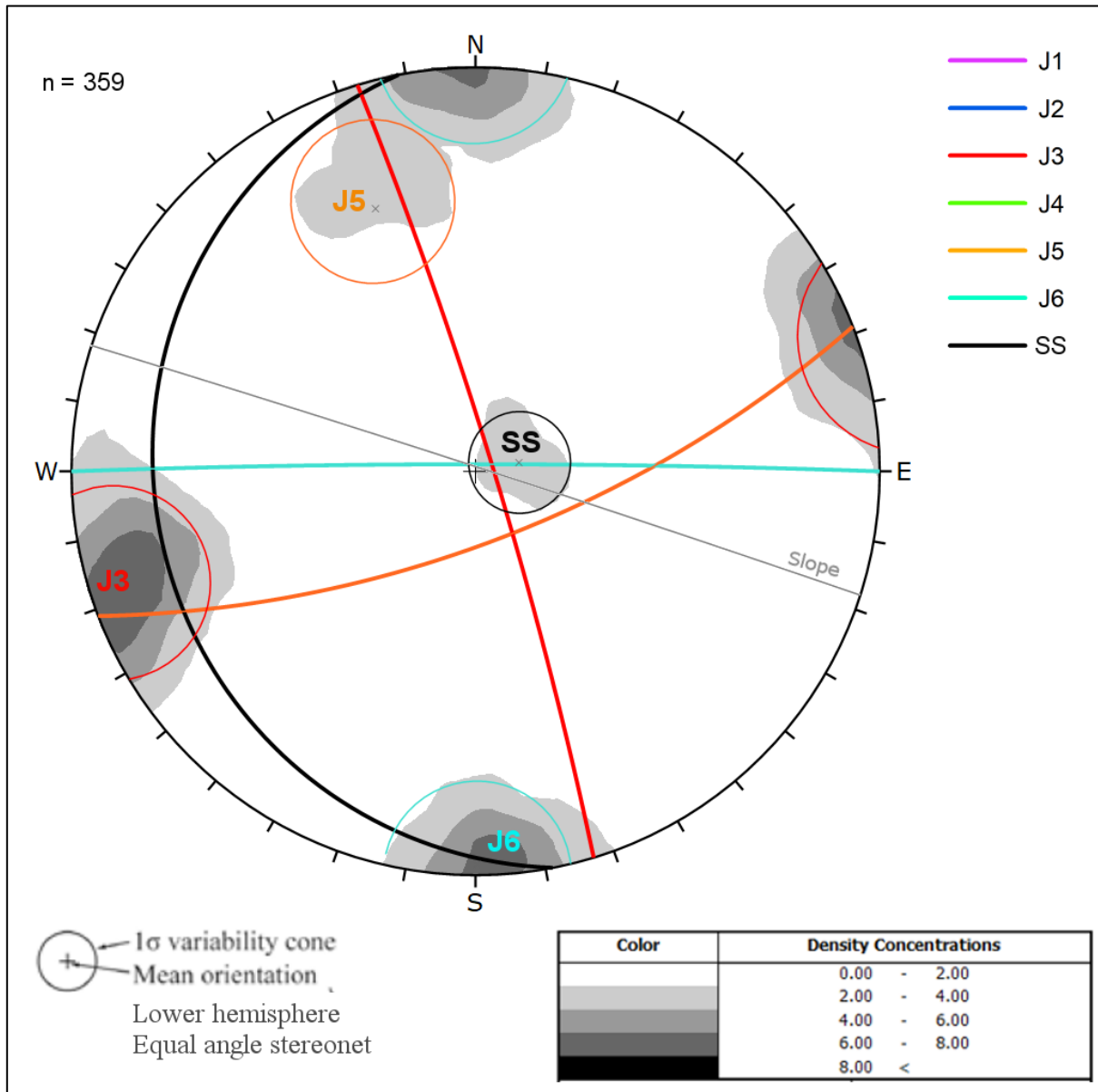


Figure 4.2: Stereonet of structural measurements in the western domain. J3 (red), J5 (brown), J6 (turquoise) and the bedding plane (black) is shown. J3 and J6 is showing a density concentration above 6%. J5 and the bedding shows a density concentration below 4%.

Mid domain

In the mid domain, there is two structures statistically significant. This is J2 that is very significant, and J4 that is marginally significant. Two more joint sets are not significant, but well documented in the field. This is J1 and the flat joint set created by the bedding.

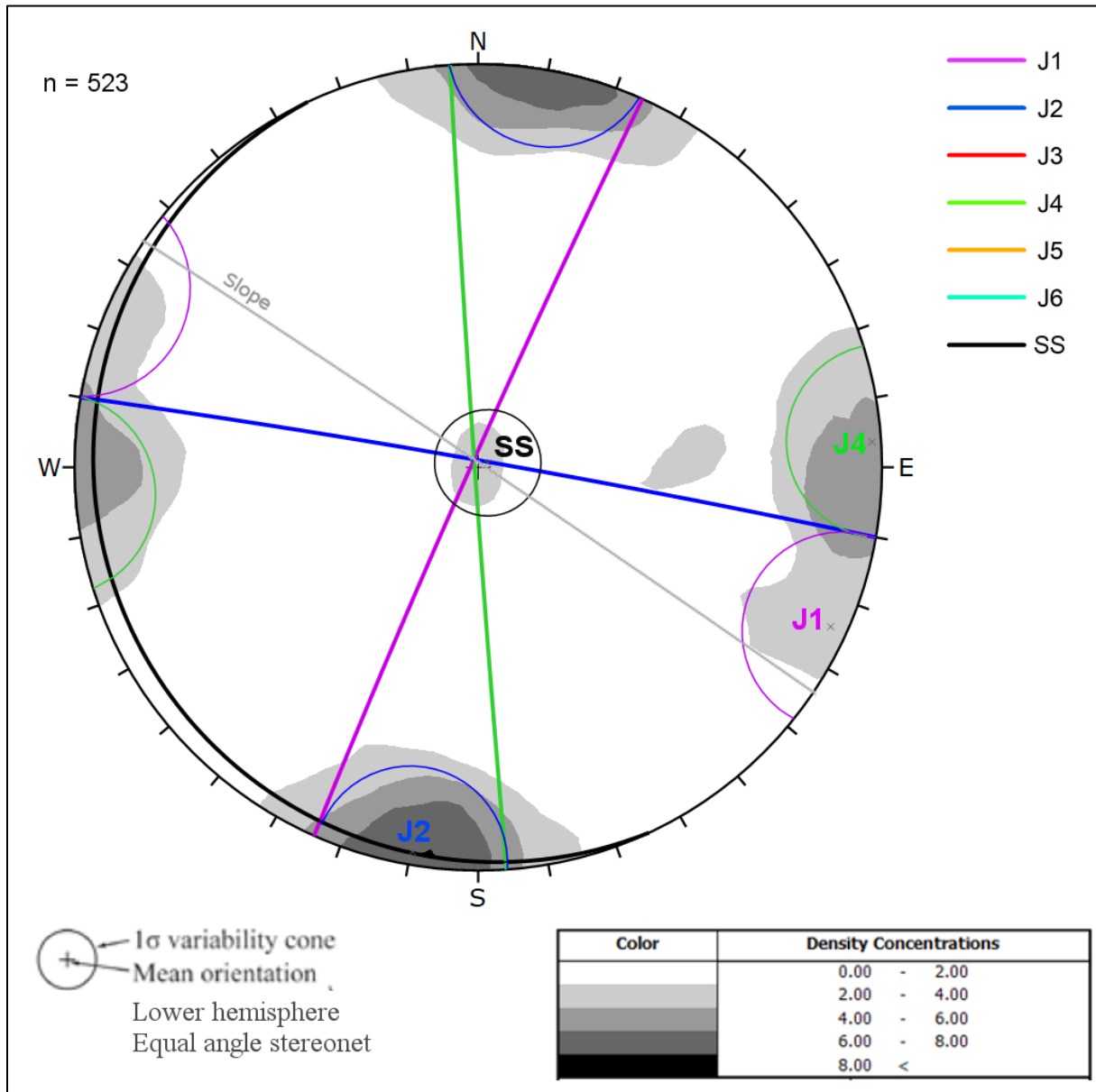


Figure 4.3: Stereoplot of structural measurements in the mid domain. J1 (purple), J2 (blue), J4 (green) and the bedding plane is shown in the plot. J2 is showing a density concentration above 6%. J4 is showing a concentration above 4%, which is marginally significant. J1 and the bedding is showing a density concentration below 4%.

Eastern domain

In the eastern domain, there is three joint sets just marginally significant. This domain is the area with the largest amount of structural measurements and is also the most widespread domain. The significant joint sets are J2, J3 and J4. J2 and J3 is showing an orientation within the uncertainty limits of what is seen in the other domains, while J4 has a slacker dip in the eastern domain than seen in the rest of the area. The bedding in this domain is not statistically significant.

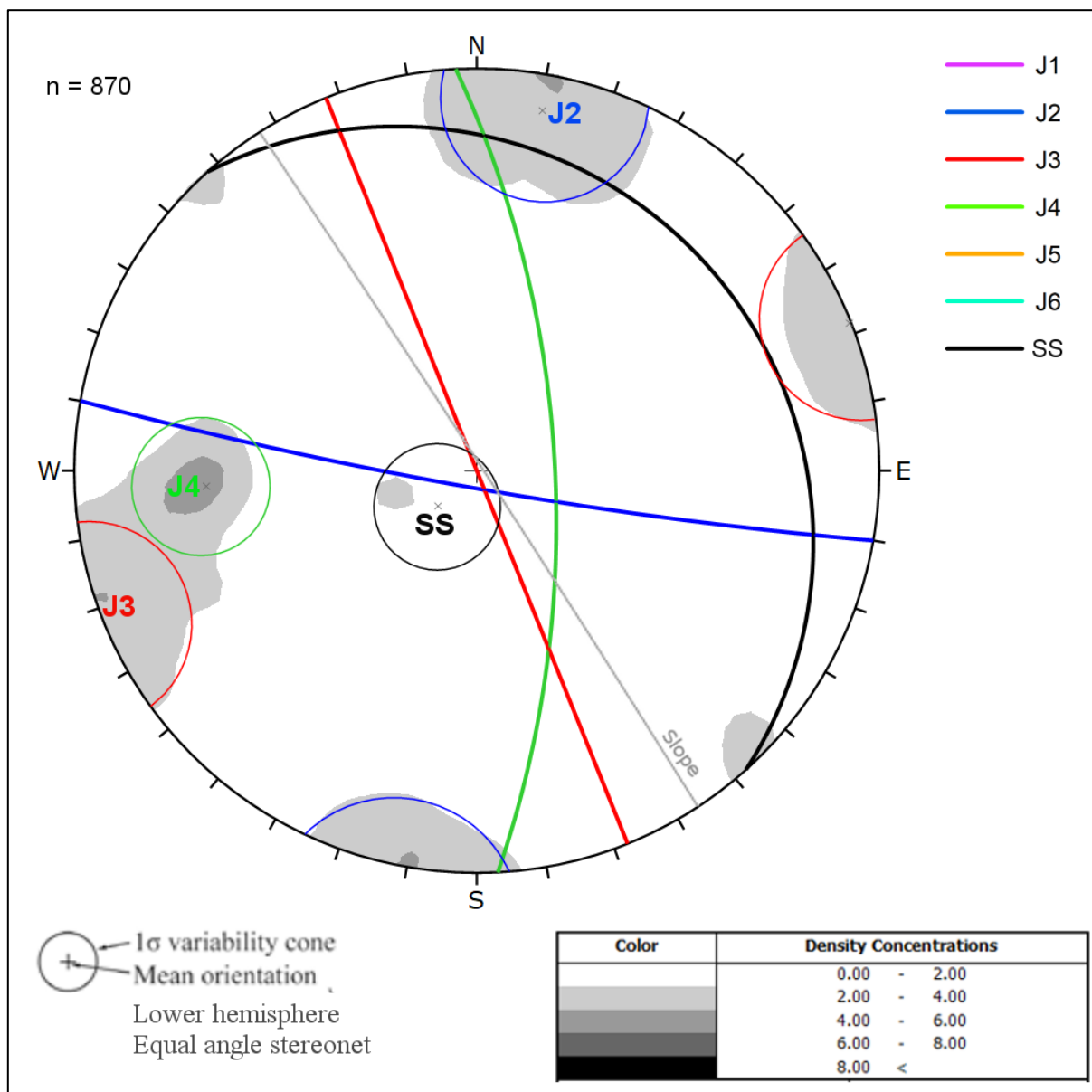


Figure 4.4: Stereoplot of structural measurements in the eastern domain. J2 (blue), J3 (red) and J4 (green) shows a density concentration above 4%. The bedding has a density concentration below 4%.

4.1.2 Regional lineaments

The results of the regional lineament analysis described in chapter 3.2.2 is shown in Figure 4.5. As described in the methodology, the area is divided into domains based on the distribution of joint sets assessed in the structural analysis. The resulting regional lineaments are used to validate these domains. It also reveals the persistence of the joint sets dominating the domain. The mapped lineaments are shown in Appendix C.

The structural analysis of regional lineaments clearly shows a variation between the divided domains. Lineaments with 6 different orientations are traced, with only the middle domain showing them all in the rosette plot.

The western domain shows three dominating lineaments, J3, J5 and J6. These lineaments have the same orientation as the three main joint sets in the structural analysis of the western domain. This means that the most dominant structures when assessing field measurements are the same as the dominant lineament orientations. In the assessment of regional lineaments, a larger deviation between J2 and J6 is seen than in the analysis of field measurements.

The mid domain shows dominant structures in J2, J4 and J5, with J4 as the most dominant structure. Compared to the structural analysis, the biggest deviation is that J5 is not a significant structure in the analysis of field measurements.

The eastern domain shows significant lineaments in the orientations of J1, J3 and J4. Field measurements do not show a significant amount of measurements for J1. As seen in Appendix C, J1 is dominating in the southern part of the eastern domain, a part where no structural measurements are taken. At the other side, J2 that is a significant structure in the eastern domain, is not appearing as a dominating structure in the regional lineament analysis.

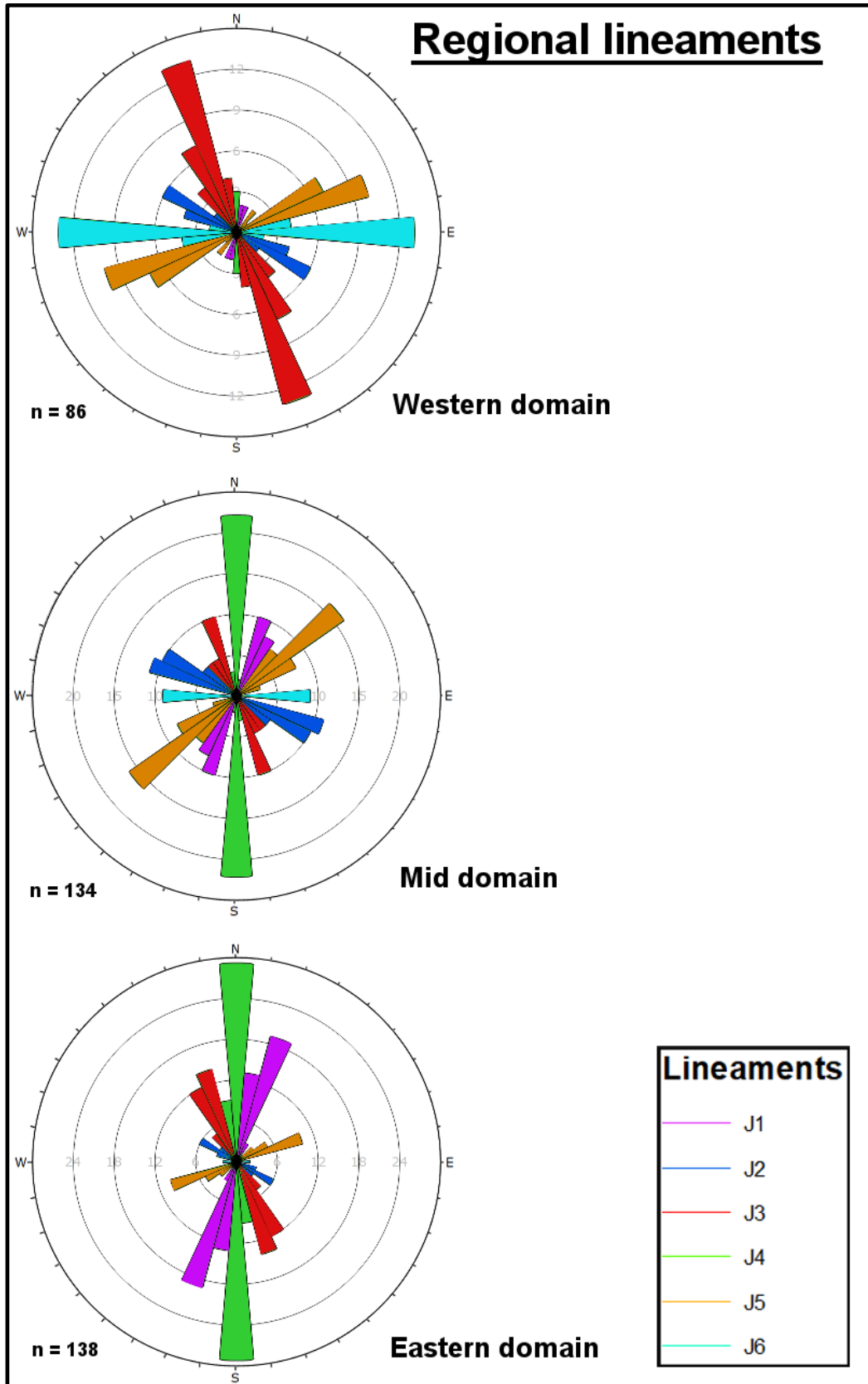


Figure 4.5: Resulting rosette plots from the structural analysis of regional lineaments for each domain.

4.2 Results from kinematic analysis

The chapter presents the result of the kinematic analysis described in chapter 3.3.1. The kinematics of the three structural domains highlighted are assessed. Due to unstable slopes hanging along the cliff with a vertical slope dip in all domains, a maximum dip angle of 89 degrees were used when assessing the kinematic feasibility. The slope orientation was estimated from the average slope orientation of each domain, assured that the local slope orientation fits within the lateral tolerance of the analysis. The analysis is assessed with a lateral tolerance of 30 degrees according to the “Recommended hazard and risk classification” by Hermanns, *et al.* (2012b). This is due to more complex failure morphologies involved in large-scale rock slope failures. When assessing toppling failure, direct toppling is evaluated due to the rock type assessed not favoring flexural toppling.

The friction angle for the test is set to 20 degrees due to the conservative recommendations for all rock types stated in Hermanns, *et al.* (2012b). When assessing the kinematic feasibility of an unstable slope, a hazard score should increase by 0,25 if the persistence of delimiting structures is very high relative to the unstable mass (>20m for smaller unstable masses).

Table 4-1: Input values to the kinematic analysis of structural domains.

Domain	Slope orientation		Friction angle
	Dip direction	Dip	
West	18°	89°	20°
Mid	34°	89°	20°
East	57°	89°	20°

In the kinematic analysis, we separate between areas where failure is possible (pink), and areas where failure is partly possible (green). The evaluation of oblique toppling is considered as partly possible in this assessment. The “partly possible” area is giving a lower hazard score than “possible” for the criteria of kinematic feasibility. The white color shows the area where failure is not possible. Joint sets are presented as poles for the planar sliding, while presented as planes in the wedge analysis. This is due to the importance of intersections between two planes in the wedge analysis. In the assessment of direct toppling, both poles and planes are presented due to the importance of both intersections of two planes within the pink area and a pole within the friction cone. Where joint sets are plotted with poles, a variability cone is also

presented, showing the uncertainty of the pole of one standard deviation. The slope orientation, lateral tolerance and friction angle is presented with grey lines.

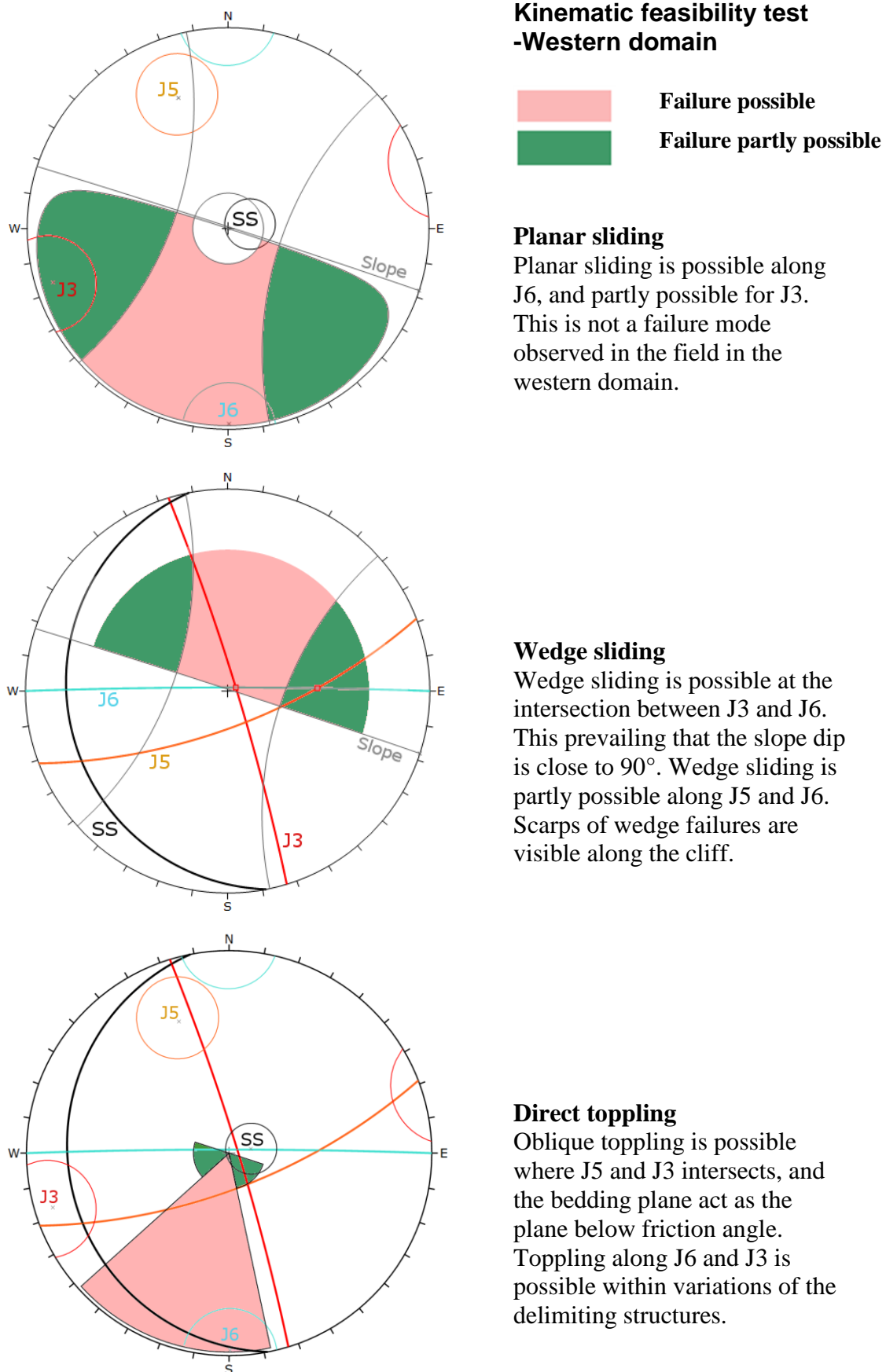


Figure 4.6: Kinematic feasibility test for the western domain. Planar sliding, wedge sliding, and oblique toppling is possible.

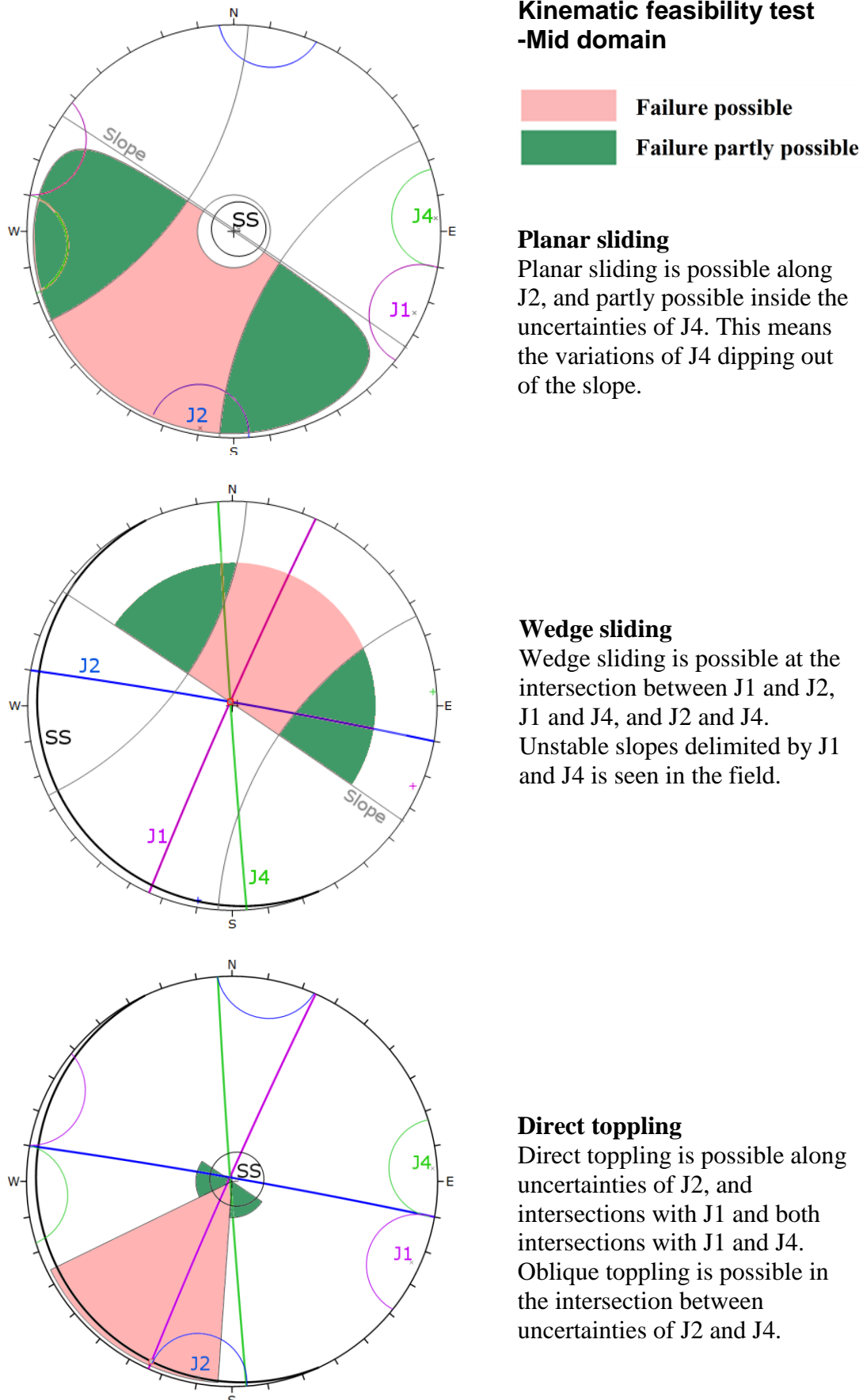
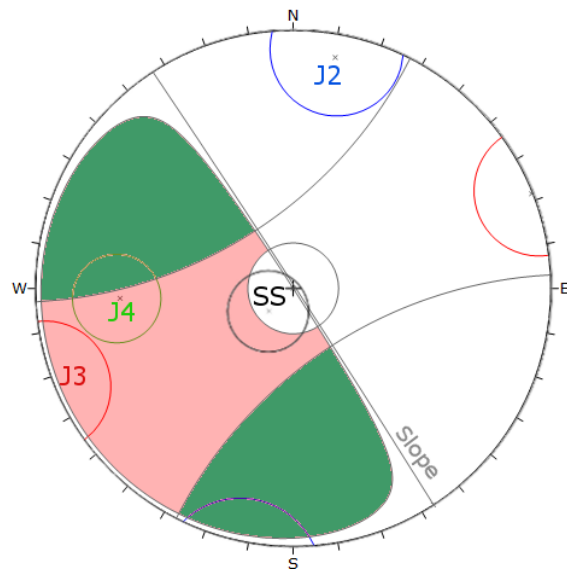


Figure 4.7: Kinematic feasibility test for the mid domain. Planar sliding, wedge sliding and direct toppling is possible.

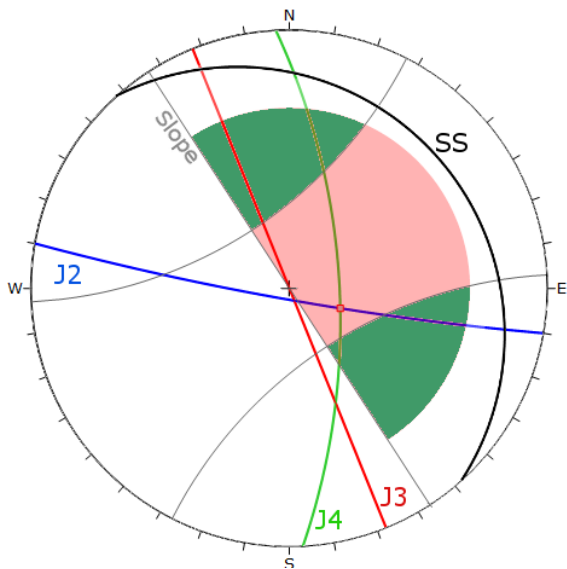


Kinematic feasibility test -Eastern domain

- Failure possible
- Failure partly possible

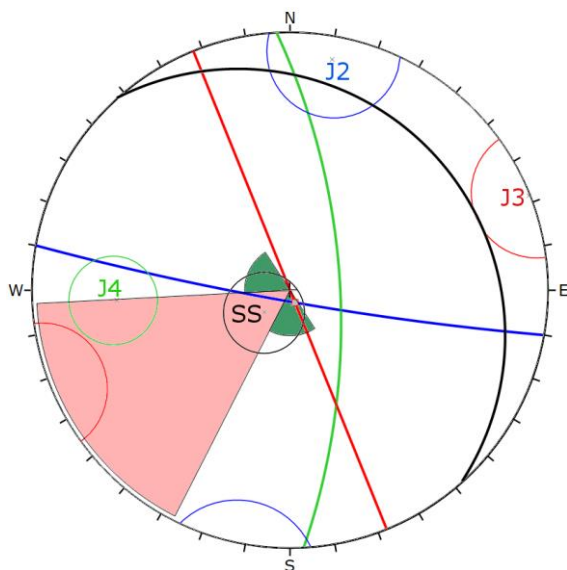
Planar sliding

Planar sliding is possible along J3 and J4. Failure along J3 prevails that the slope dip is vertical or overhanging for the sliding plane to daylight.



Wedge sliding

Wedge sliding is possible at the intersection between J2 and J4. It is also possible within the uncertainties of the intersection between J2 and J3.



Direct toppling

Oblique toppling failure is possible along J2 and J3, where the bedding plane acts as a plane below friction angle. Bedding is not significant in the eastern domain but is detected in field.

Figure 4.8: Kinematic feasibility test for the eastern domain. Planar sliding, wedge sliding and oblique toppling is possible.

4.3 Results from field investigation

The orientation of geological structures in this thesis is given in degrees as dip direction/dip. Variabilities of the structures are given as one standard deviation, shown with \pm degrees.

4.3.1 Bedding

Given the lithology of the area, a distinct orientation of the bedding is difficult to obtain. The bedding has been observed and measured at two places in the eastern domain, while the bedding has been interpreted as a flat-lying plane in the mid domain. In the western domain, the lithology makes the rock more massive, which makes it difficult to interpret the bedding.

Table 4-2: Orientation and dip of the bedding observed in the different domains highlighted in Figure 4.1.

Domain	DipDir/Dip
West	259/13 \pm 15
Mid	245/03 \pm 15
East	048/15 \pm 18

According to the structural analysis, bedding planes are not statistical significant in either of the three domains. The bedding is observed a few places along the cliff, but it can be assumed that due to the flat dip of the bedding, glacial scouring might be a reason for the lack of exposed bedding planes. The bedding is best seen in outcrops where overhanging rocks are sticking out of the cliff. The structure has a close spacing and smooth surface, as seen in Figure 4.9. The structure is seen as a potential structural control that is breaking off blocks, obviously being a weakness in the rock mass.

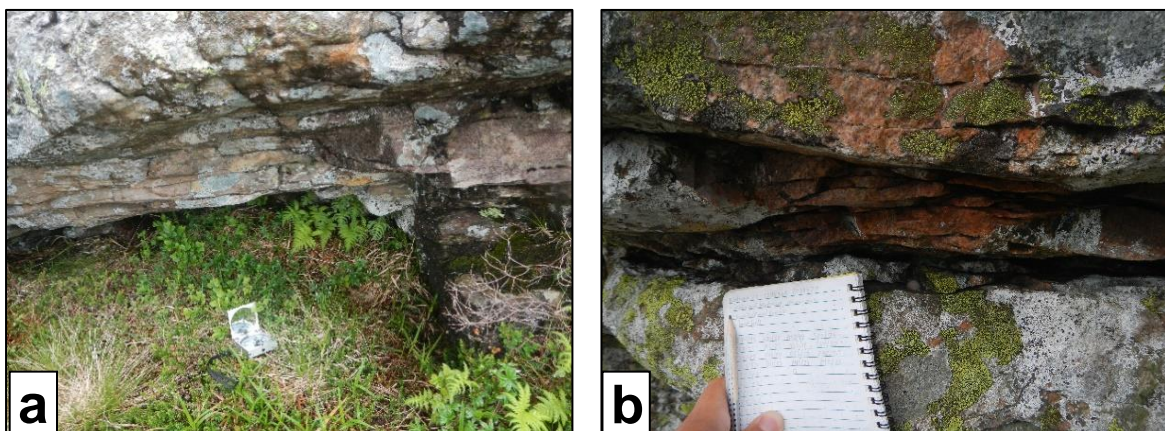


Figure 4.9: Bedding planes shown under overhanging cliffs. The bedding planes are almost flat. The bedding is seen over the whole area, but is best seen in the eastern domain, where these pictures are taken.

4.3.2 Joint sets

Field observations of the area highlights six joint sets, which is presented in the following subchapters. Four of the joint sets are statistically significant in the structural analysis of field measurements (chapter 4.1.1). The joint sets not statistically significant is both dominating structures in the analysis of regional lineaments (chapter 4.1.2). The joint sets are described by orientation and dip, persistence, and surface roughness.

Table 4-3: Overview of joint orientations within the different structural domains. The orientations outlined is not statistically significant structures based on the analysis of structural measurements.

Domain	J1	J2	J3	J4	J5	J6
West	-	-	073/85±15	-	159/70±16	360/88±14
Mid	294/88±15	010/88±14	-	266/89±14	-	-
East	-	190/85±16	248/90±15	087/68±14	-	-

Spacing and persistence of the joint sets are varying spatially between domains, and also within each domain. The results presented in Table 4-4 are therefore estimated values, based on field observations in the domains where the structures are represented and subaerial interpretation.

Table 4-4: Spacing and persistence of the joint sets based on field observations and subaerial interpretation.

Structure	Spacing	Persistence
Bedding	<1cm	-
Joint set 1	1m-25m	>100m
Joint set 2	10cm-5m	>30m
Joint set 3	30cm-15m	>100m
Joint set 4	20cm-1m	>100m
Joint set 5	20m-50m	>100m
Joint set 6	1m-5m	>10m

Joint set 1

J1 is a joint set found to be sub-vertical and striking NE–SW. The structure is seen as a controlling structure of the unstable slope at location 5, shown in Figure 4.26. Mostly, the structure is seen as a depression. Where the plane is visible, it has a smooth surface with close spacing. The structure is found in the mid domain, where it also is a statistically significant joint set. The persistence is interpreted as >100m because the depressions following the orientation of J1 is tracked over long distances.

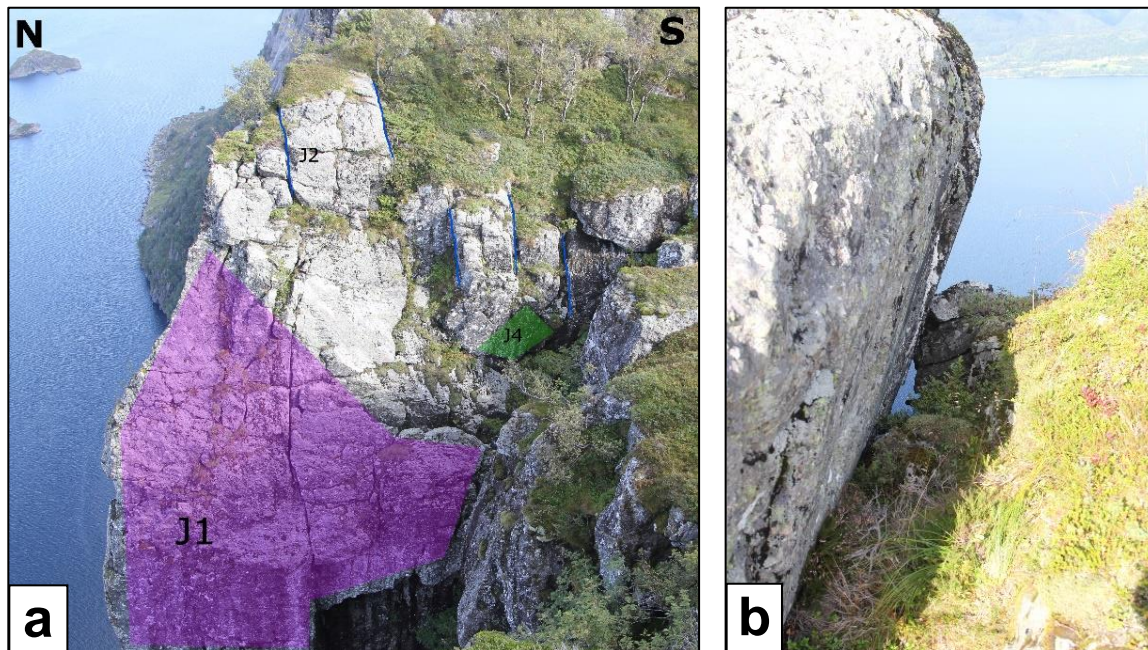


Figure 4.10: Pictures show structures following J1, seen as the purple plane in picture a taken from the west side of location 5 (chapter 4.4.2). The plane is sub-vertical and has a smooth surface. At this location, the joint set is seen with a spacing of 1m. Picture b shows a close-up of a structure at the same location with a variation of dip of 15degrees.

Joint set 2

J2 is also a sub-vertical joint set, but with varying dip of up to 14 degrees measured in the field. The structure is often seen as open cracks along the cliff. The structure is the delimiting structure of both location 5 and location 6, seen respectively in picture *b* and *a* of Figure 4.11. A specific structure of J2 is showing the persistence of the joint set with depth, an estimated depth of 100m. It shows a 30cm opening, with the lake outrun going into the crack. The joint set is found over the whole field area, being statistical significant in the mid and eastern domain. The surface is smooth, and there is a close spacing, as seen in picture c of Figure 4.11.

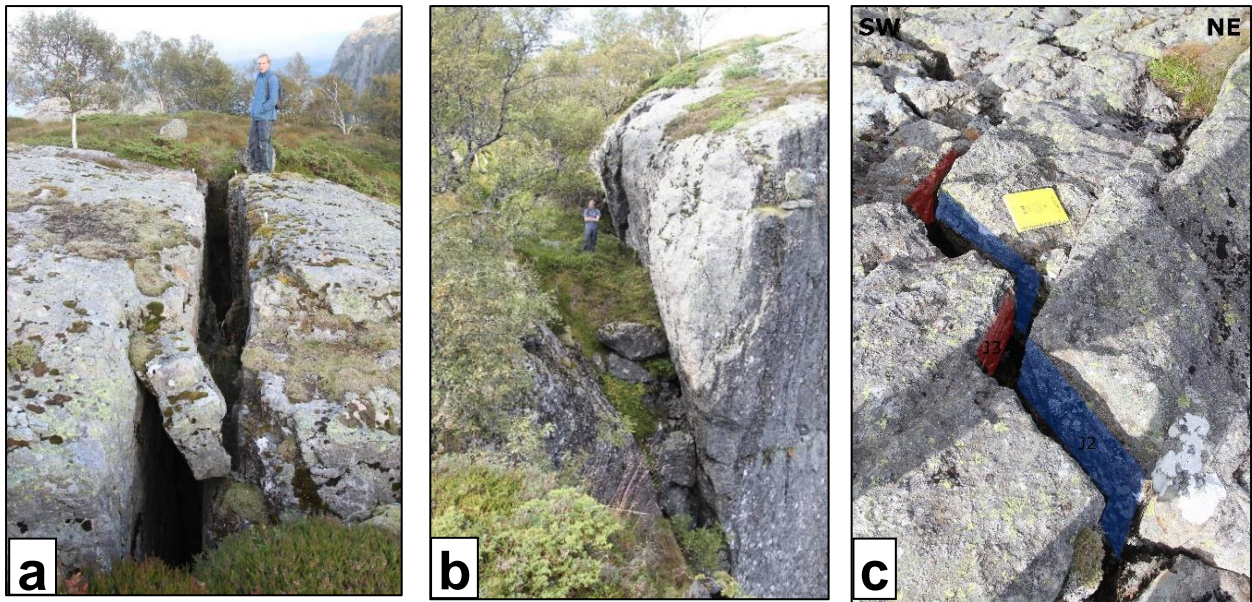


Figure 4.11: The structure has a smooth surface, and a very consistent persistence. As seen in picture b, variations in dip of the joint set up to 14 degrees is detected. As the joint set in the picture is measured to 75 degrees, this dip is barely inside the variability cone of the structural measurements. Picture c shows a stepwise structure, where the crack jumps between J2 and J3.

Joint set 3

J3 is a statistically significant structure seen in both the eastern and western domain. The joint set shows a spacing of 30cm-15m, with the discontinuities showing a smooth surface. This almost vertical joint set is the most persistent joint set through the area. The joint set creates persistent lineaments easily detectable on the hillshade-map. The surface and spacing is seen in Figure 4.12.

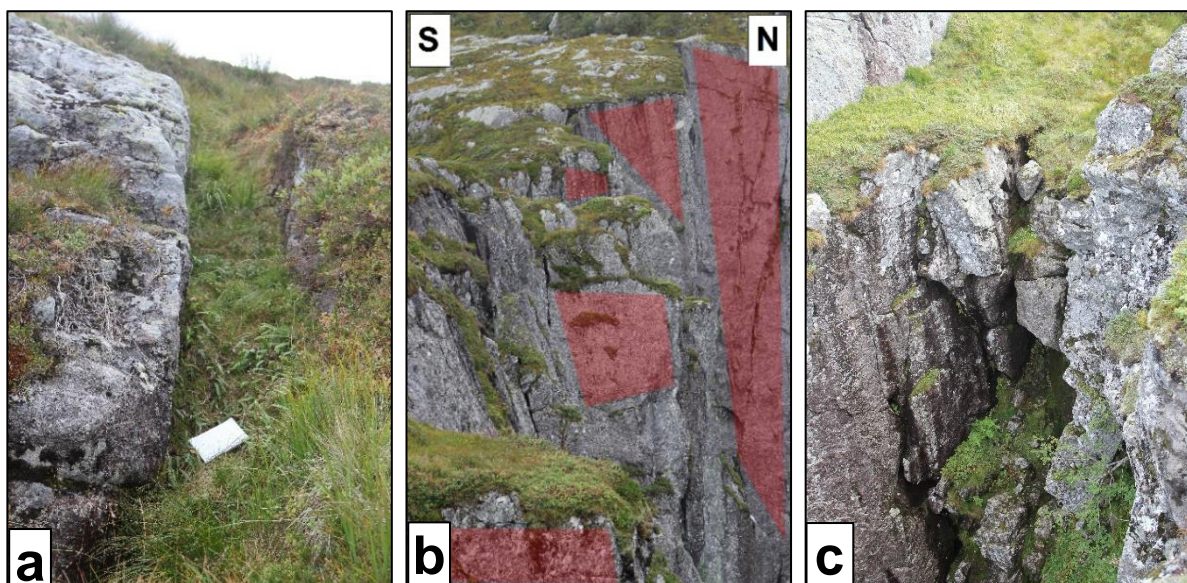


Figure 4.12: Pictures taken of structures following the orientation of J3. Surfaces are smooth, with opening of up to 50cm. Spacing is seen as close spacing in picture c, and spacing of $\approx 15\text{m}$ in picture b.

Joint set 4

J4 is a significant structure observed in the mid and eastern domain. The structure is sub-vertical in the mid domain, while the structure is dipping towards east in the eastern domain favoring planar sliding failures. The joint set is seen as structural control of unstable slopes in both the mid and east domain, as shown in Figure 4.13. The joint set is seen as large-scale lineaments on the hillshade-map, and the persistence is estimated to >100m. The joint set has a close spacing causing multiple potential back scarp structures as seen in picture c (Figure 4.13).

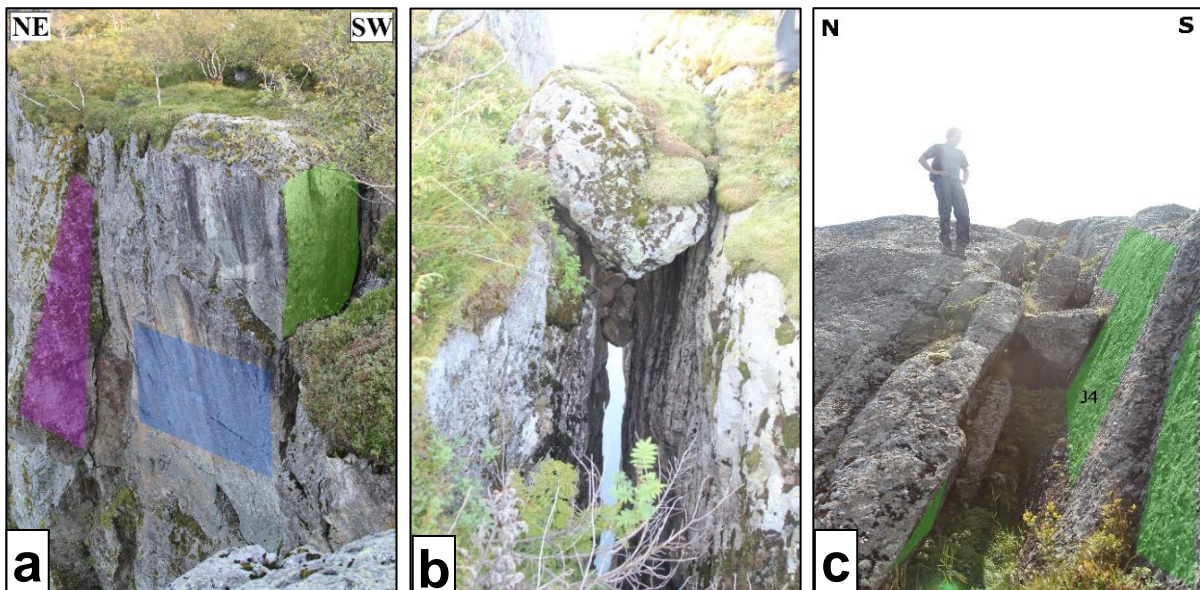


Figure 4.13: In picture *a*, J4 is the lateral limit of the unstable slope at location 6 (4.4.2). Picture *b* shows the same structure, a persistent structure with opening of 50cm. Picture *c* shows the smooth surface and close spacing of J4, dipping to the east at location 1 in the eastern domain (chapter 4.4.2).

Joint set 5

J5 has an irregular surface, mostly visible as a large-scale structure. The joint is dipping 70 degrees towards the south-east. The plane is not statistically significant but is contributing as one of the controlling structures at location 8 in the western domain (chapter 4.4.2). The structure is also seen as a controlling structure at location 3 in the eastern domain, but not a dominating structure.

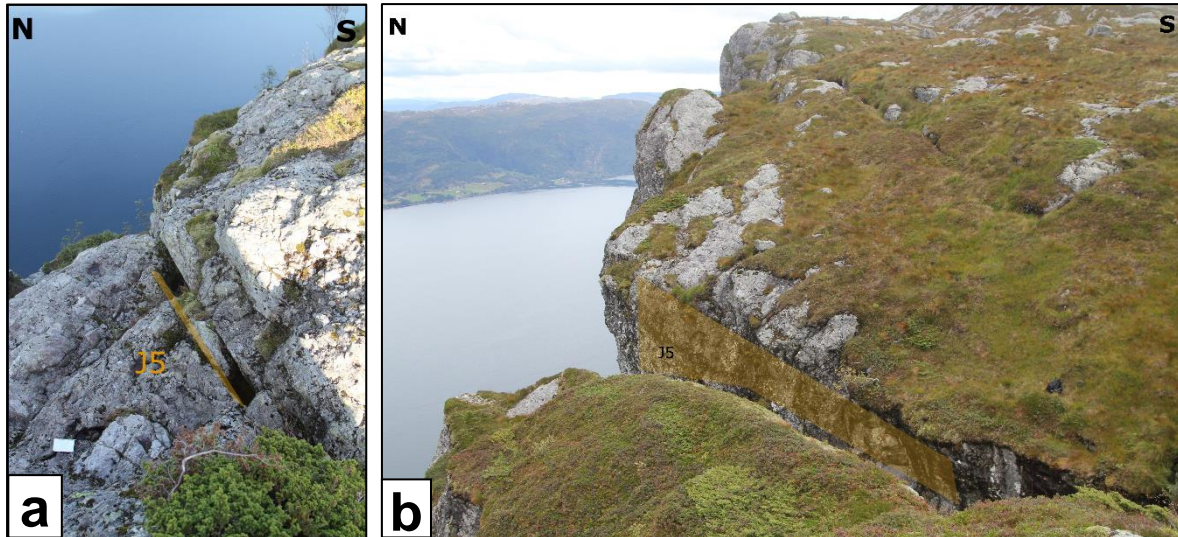


Figure 4.14: Picture *a* is taken at location 3 (chapter 4.4.2), where J5 is a water-bearing structure creating a lateral structure dividing the scenarios. Picture *b* is taken at location 8 (chapter 4.4.2), where J5 creates a backscarp with an opening of 2 meters. The irregular surface is seen at the back wall. The persistence of the crack is 20m, but the crack continues as a depression for 60m.

Joint set 6

J6 is a significant structure in the analysis of both field measurements and regional lineaments in the western domain. In the rest of the field area, the structure is difficult to detect. The joint set has a rough surface and is often seen in combination with other structures, as in picture *c* (Figure 4.15). The spacing is varying spatially, but picture *c* shows a spacing of 1meter. J6 is a controlling structure in location 7 and location 8, described in chapter 4.4.2.

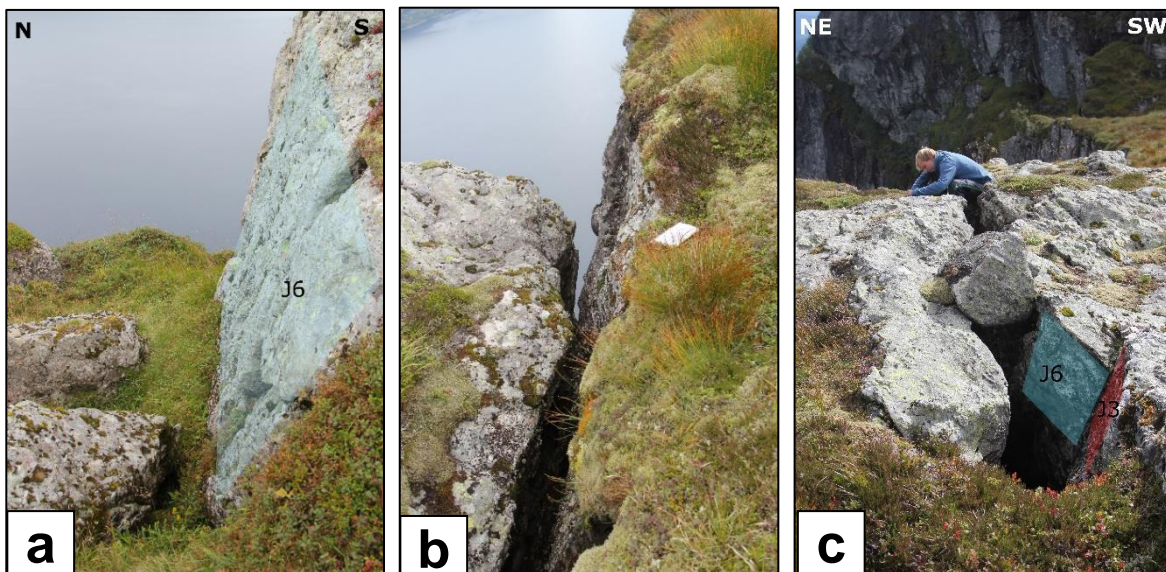


Figure 4.15: Picture *a* shows the irregular surface of J6. Picture *b* shows the back scarp of location 8(chapter 4.4.2), with an opening of 10 cm. Picture *c* shows a stepwise structure between J6 and J3, with a spacing of approximately 1m.

4.4 Assessment of unstable slopes

The assessment of unstable slopes considers the distribution of detected unstable slopes, geomorphological mapping, structural analysis, volume calculation and a final hazard classification.

Unstable slopes are detected following the NGU mapping approach described in chapter 2.4, by detecting morphological features connected to instability such as opening of cracks, development of depressions, high fracture density and displacement of blocks. The unstable slopes have been located through interpretation of orthophotos and DEM's in ArcGIS and through field work.

4.4.1 Distribution

Unstable slopes are detected in all structural domains, distributed along the 6km long cliff of Lifjellet as seen in Figure 4.16. Four slopes located in the eastern domain, two in the mid domain and three slopes in the western domain.

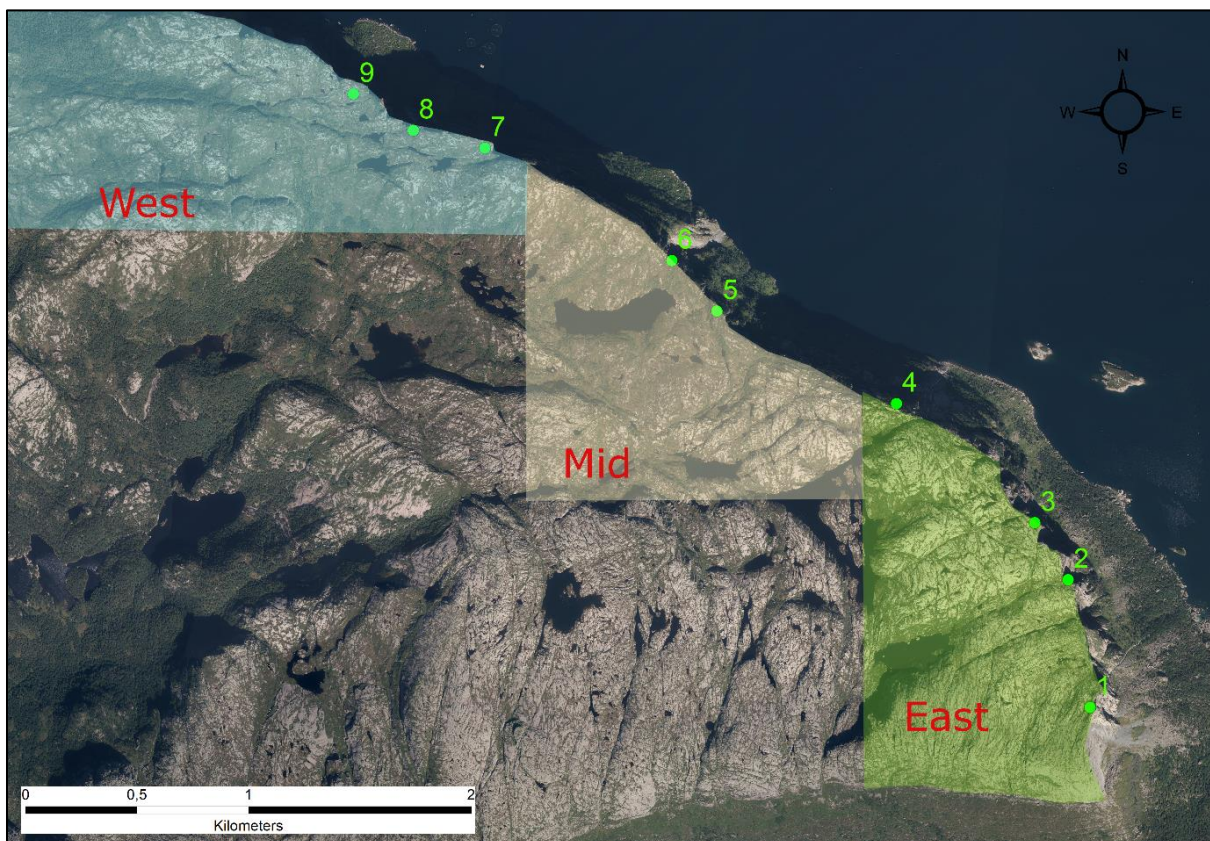


Figure 4.16: Orthophoto showing the locations of detected unstable slopes. The number connected to each unstable slope refers to the location in the further text.

4.4.2 Delimiting structures

This chapter focuses on the delimiting structures of the detected unstable slopes. The assessment has been carried out following the recommendations in Hermanns, *et al.* (2012b), describing the assessment of evaluating the criteria needed for a hazard classification. In this chapter, unstable slopes will be mentioned as locations, and detachments of the same slope with differing structural controls will be presented as scenarios. The locations will be numbered, and the scenarios marked with letters. The scenarios have different interpreted toe lines, where the depth to the toe line is mentioned with distance in meters.

Location 1

Location 1 is the largest detected unstable slope along the cliff of Lifjellet. The cliff slope is following an old rockslide scar, which is the source area for the largest prehistoric failure collapsed along the cliff. The back scarp starts at the free northern flank. It extends parallel to the slope orientation along structures with the same orientation as J4. The fracture is open all the way to the southern flank, where the rock mass is strongly fractured. The opening of the back scarp varies between 10-50cm, with boulders in the openings suggesting movement. The southern flank consists of stepwise structures along J2 and J3, two vertical structures.

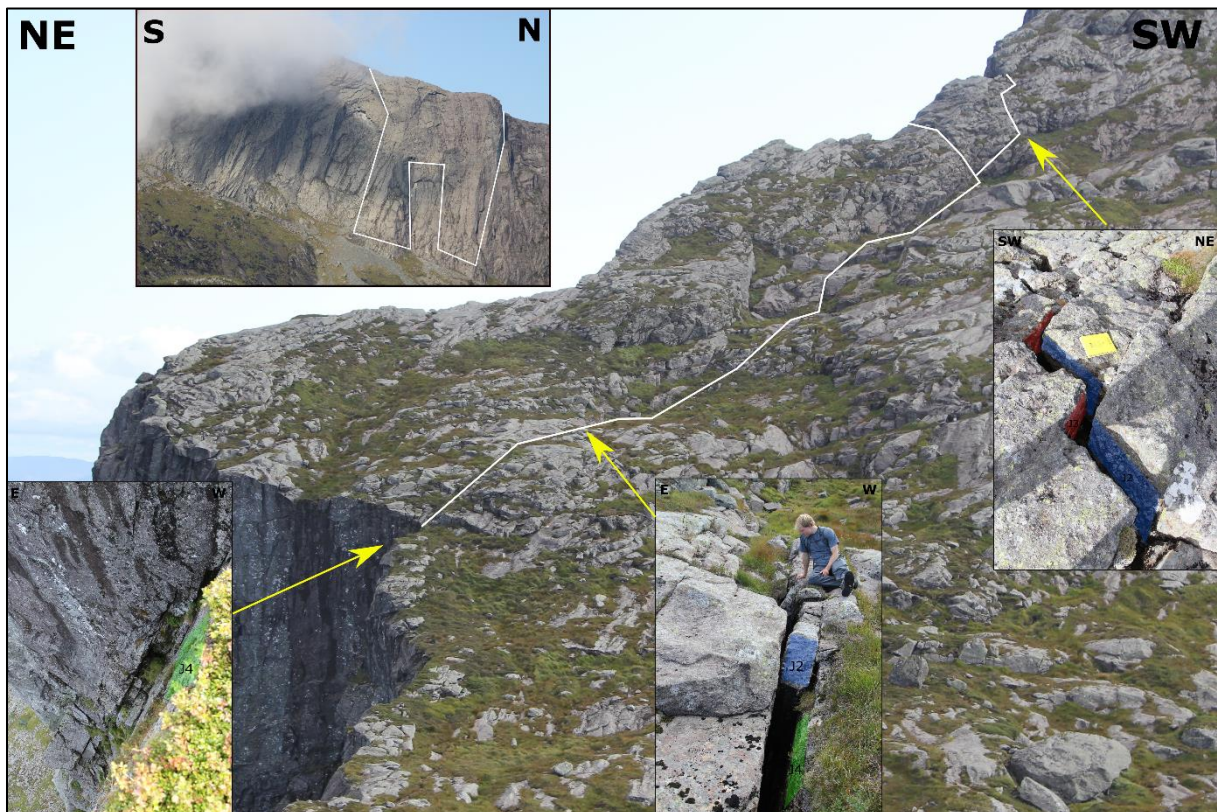


Figure 4.17: The white line follows the open back scarp detaching the unstable slope. Overview picture showing the unstable slope at the cliff face. Inserted pictures showing open structures along the back scarp and the southern flank.

The kinematics suggests a failure mechanism of planar failure, with breaking of rock bridges at the toe. The toe is placed at the lowest point of the cliff, where the thickness of the rock mass above the interpreted J4 is lowest. At this point, the scenario is delimited into two spatial columns of rock mass.

The volume calculation at this slope is based on the DEM of the area, because of lack of point cloud data from the photogrammetric model. This gives a less detailed calculation but should be sufficient for the volume size that is assessed. The scenario is calculated to a volume of 600 000m³ of rock mass.

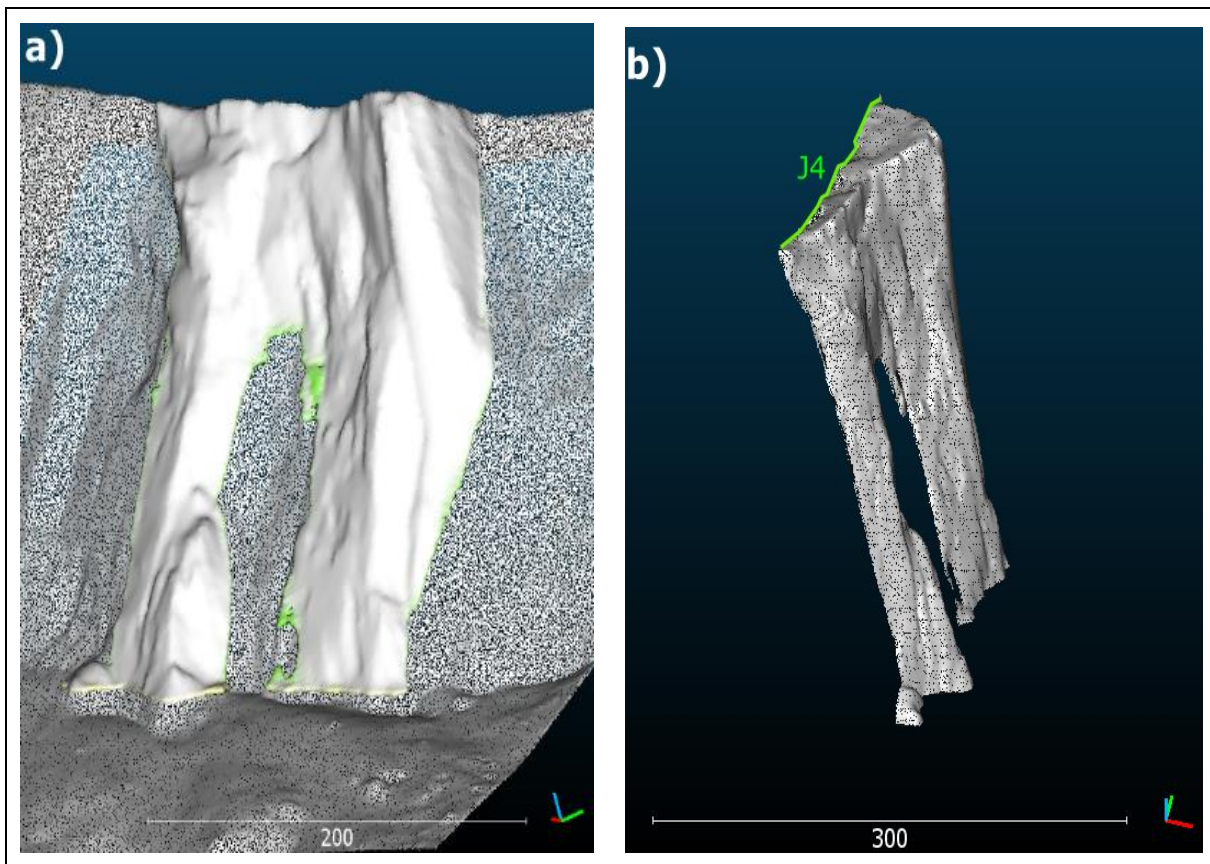


Figure 4.18: a) Scenario delimited by J4, with a toe line at 250m depth. The scenario consists of two columns separated at a depth of 120m. b) The rock mass of the scenario delimited by J4.

Location 2

The block is located 510 meters above sea level. A depression crossing over a rounded face of the cliff delimits this unstable slope. At the intersection between the depression and the free eastern flank, an open crack is seen approximately 50m deep. At the free northern flank, the depression is not so clear, but the orientation of the depression suggests a coherence with a clear structure following the same dip as the southern crack, interpreted in the 3D-model. The toe line of the possible scenario is not well defined, but there is an area of slightly more blocky rock mass. The interpreted toe lies 100m below the cliff top.



Figure 4.19: Main picture shows the depression intersecting the east flank with an open crack. Inserted figures show the fracture continuing down the cliff face, and that the depression follows a significant structure in the eastern domain, J4.

Based on the kinematic analysis of the domain, planar sliding along J4 is possible. This assumes that J4 is daylighting, which is not the situation for this scenario. The failure of the scenario is dependent on rupture of rock bridges at the toe or a stepwise failure between planes to create a failure surface. The volume of the block in Figure 4.20 is calculated to 150 000m³.

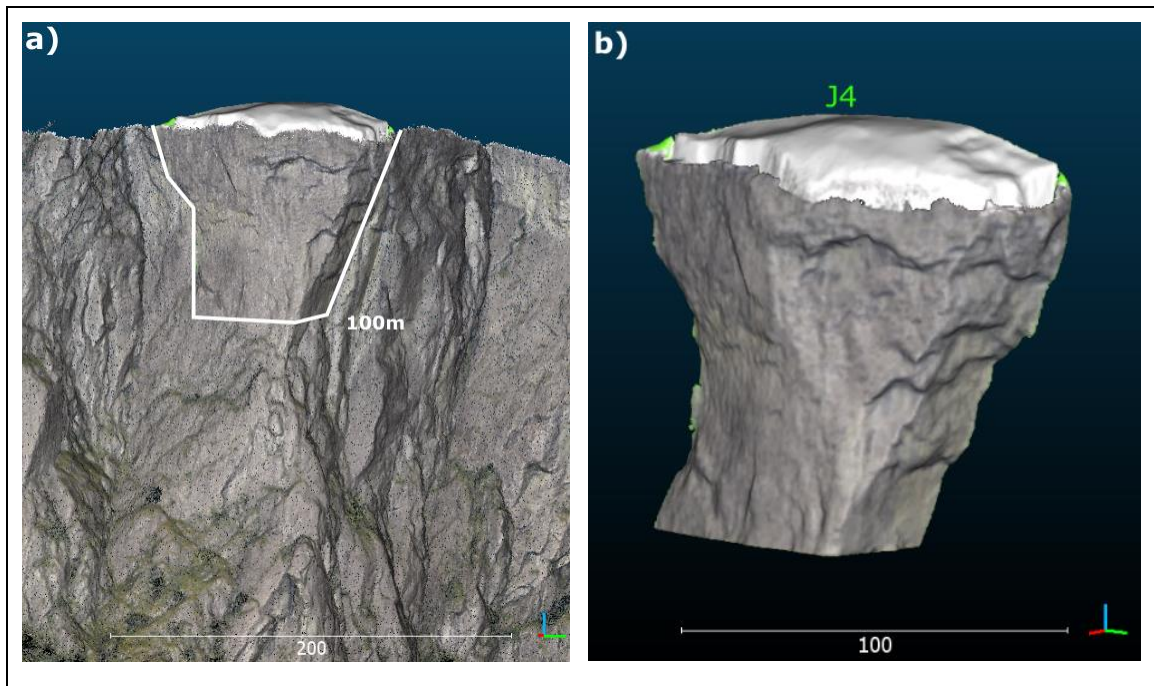


Figure 4.20: a) Picture from the 3D-model showing an overview of the block's position at the cliff face, with toe line at 100m depth. b) The rock mass of the unstable block delimited by J4.

Location 3

Location 3 is a complex slope hanging 480m above the fjord. It consists of two divided blocks, controlled by different structures. The total volume is presented as scenario A. The eastern scenario (scenario C) is detected in the field, while the western part was detected through the interpretation phase of the photogrammetric model. Scenario C has an open back scarp stretching 45m, with an opening of 20cm (Figure 4.21). The crack is infilled and only 1m deep. The back scarp intersects with a free flank to the east. At the western flank, a clear structure controls the block. This structure follows the orientation of J5, which is not a significant joint set in this domain. The structure has 20cm opening and is water-bearing. The orientation of this structure gives the scenario an inclined western flank.

This flank is the eastern limit of scenario B. The back scarp of the scenario shows an offset of several meters, interpreted by the photogrammetric model. The western flank is following the orientation of J4. The toe of the interpreted block is set to a blocky rock mass showing evidence of rockfall activity. This area is lying 200m below the cliff top.

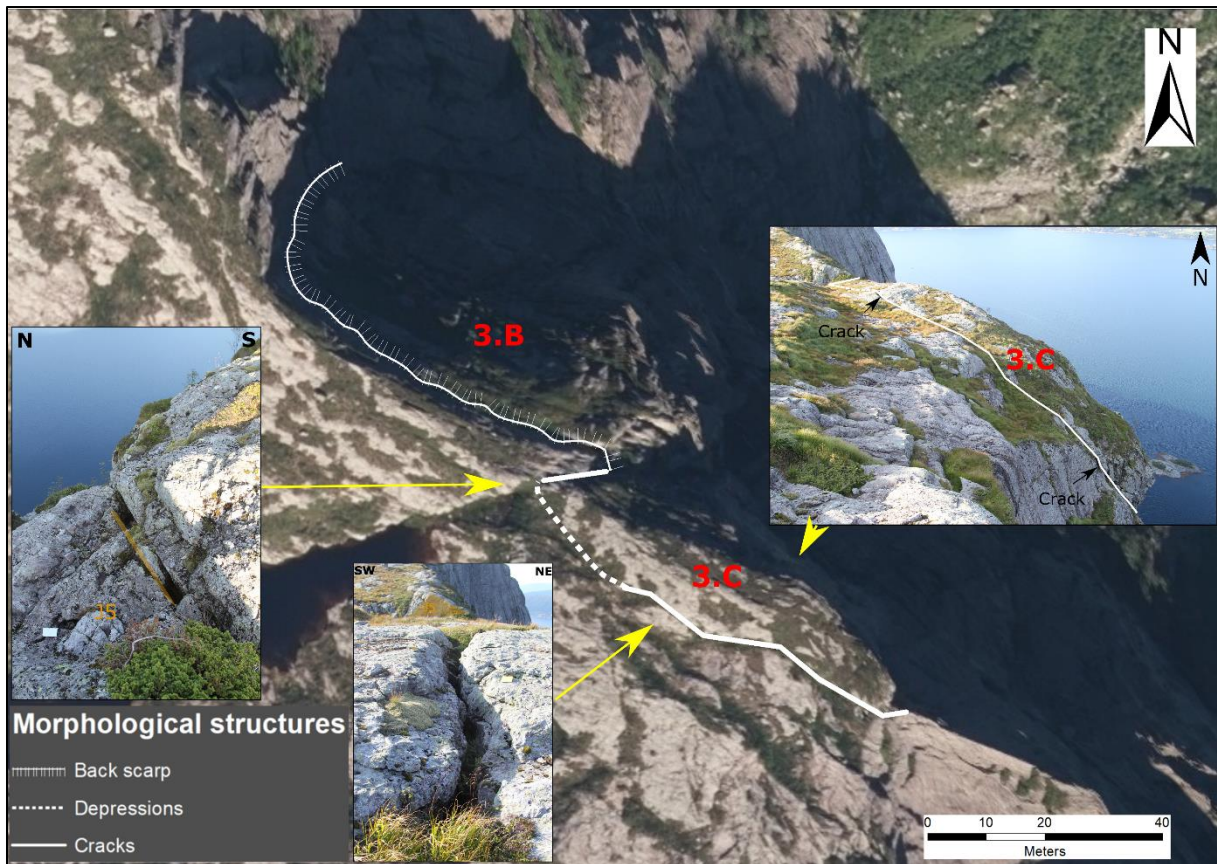


Figure 4.21: Orthophoto of location 3 showing the mapped morphological structures delimiting the two separate blocks of scenario B and scenario C. Inserted pictures show structures mapped on the orthophoto.

Based on the kinematic feasibility of the domain, wedge failure along J2 and J4 is possible. The back scarp of the unstable slope is following the orientation of J2, but not along penetrative structures. Also, planar sliding along variations of J2 is possible, a feasible failure mechanism for scenario C. A collapse of both blocks at the same time (scenario A), removing the inclined flank of the eastern scenario, will give a total volume of 150 000m³. Another possibility is scenario B collapsing without failure of the eastern scenario. This will release a volume of 130 000 m³. The eastern scenario has the smallest volume, a volume of 20 000m³.

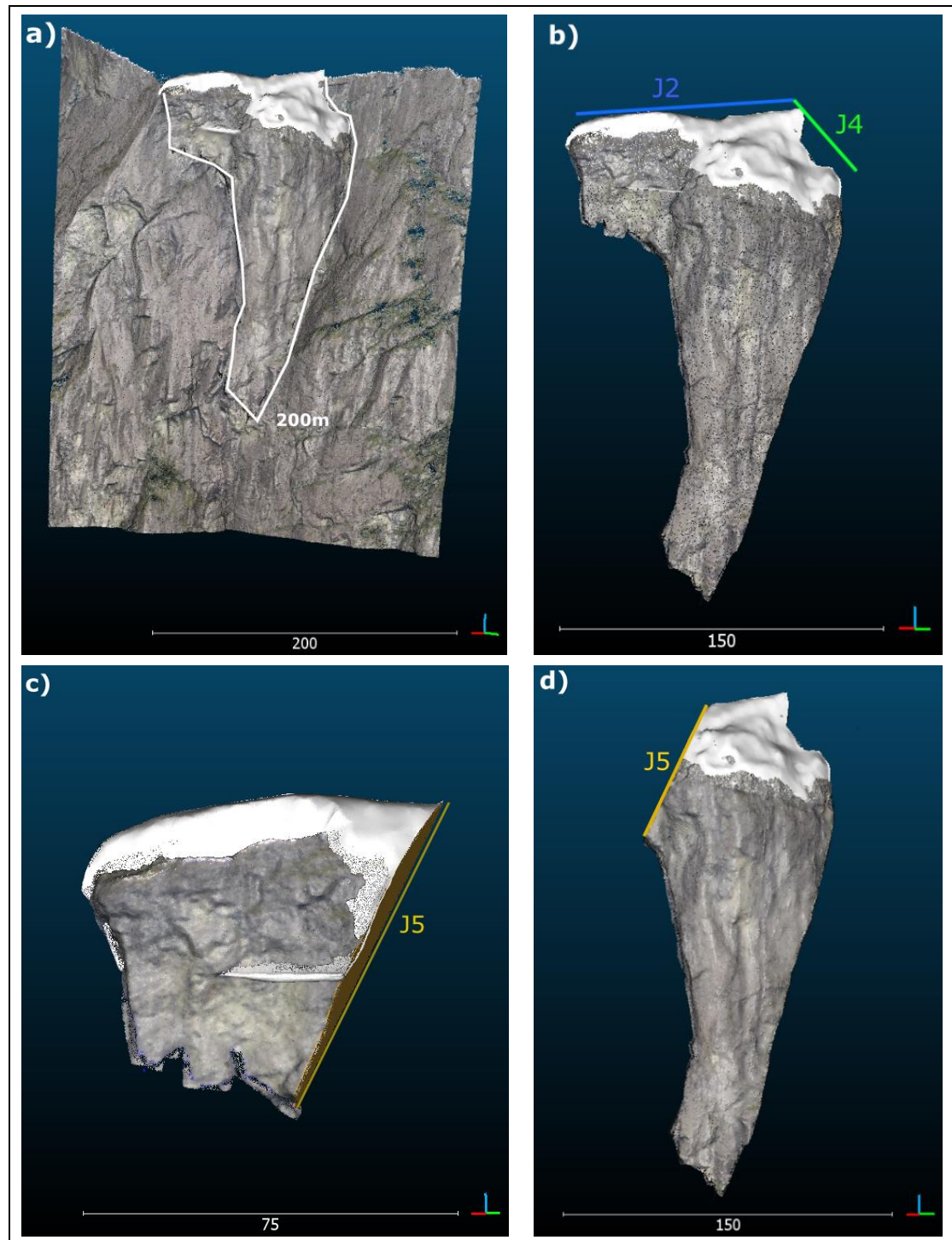


Figure 4.22: a) Location 3 shown in the 3D-model. b) Scenario A delimited by orientations of J2 and the western flank following J4. The possible failure mechanism is wedge failure. c) Scenario C delimited by J2 and J5. Possible failure mechanism is planar sliding along a variation of J2. d) Scenario B delimited by J2, with flanks following J4 and J5.

Location 4

Location 4 is detected at a height of 444 meters above the fjord. An unstable block is completely detached by a 2m wide back scarp filled with loose blocks. From the west side of the block, the depth of blocky rock mass was estimated to at least 20 meters (Figure 4.23). The block has a free western flank. The interpreted eastern flank is following a depression. The toe of the block is not visible in the photogrammetric model. The block has a short horizontal distance to the fjord, only 200m.

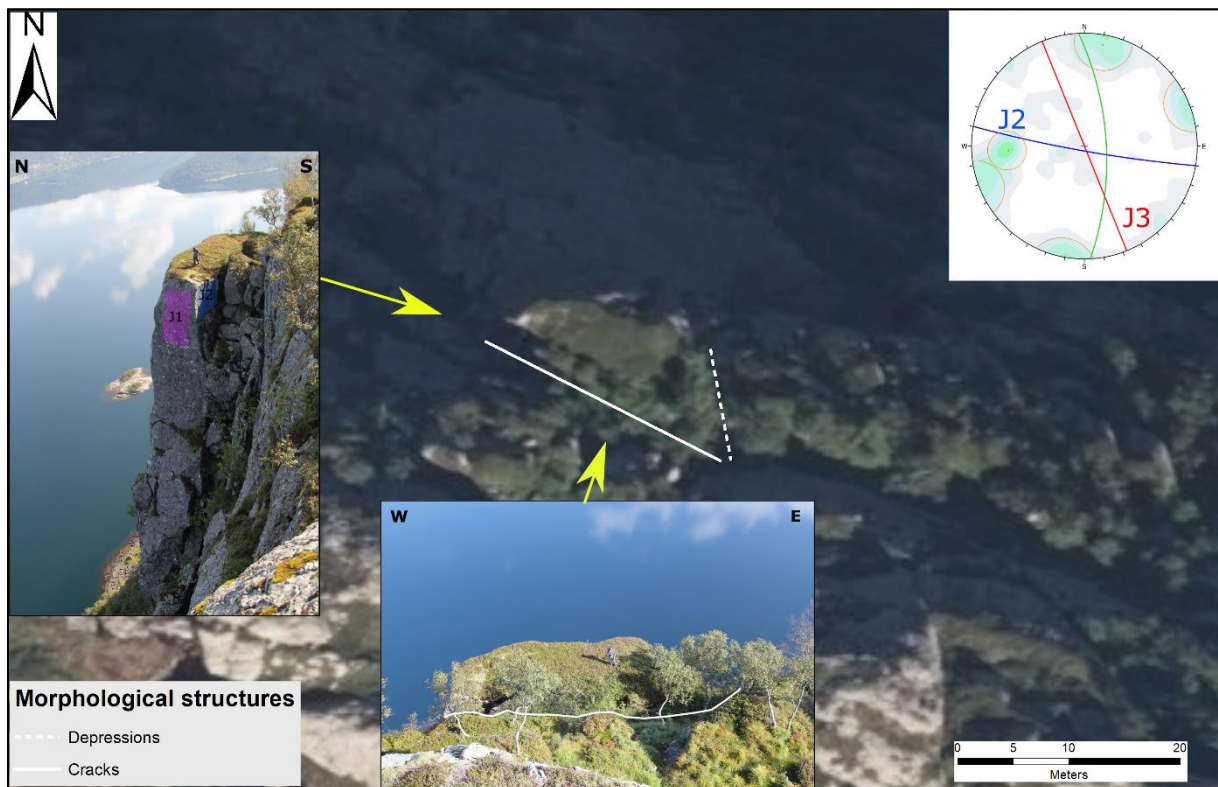


Figure 4.23: Orthophoto of location 4 showing the back scarp and the position of the depression along the orientation of J3. The inserted pictures show the back scarp from the side and from a birdview, as seen in the field. The stereoplot shows the significant structures of the domain surrounding location 4.

The back scarp of the unstable slope is following the orientation of J2. The eastern flank is following J3, which is a very visual structure in the eastern domain. Possible failure mechanisms in the eastern domain are both planar sliding and toppling along structures of J2. The type of failure is controlled by the dip of J2.

With an interpreted toe line at 50m from the top, the block is almost completely detached. The volume of the block is calculated to 5500m³.

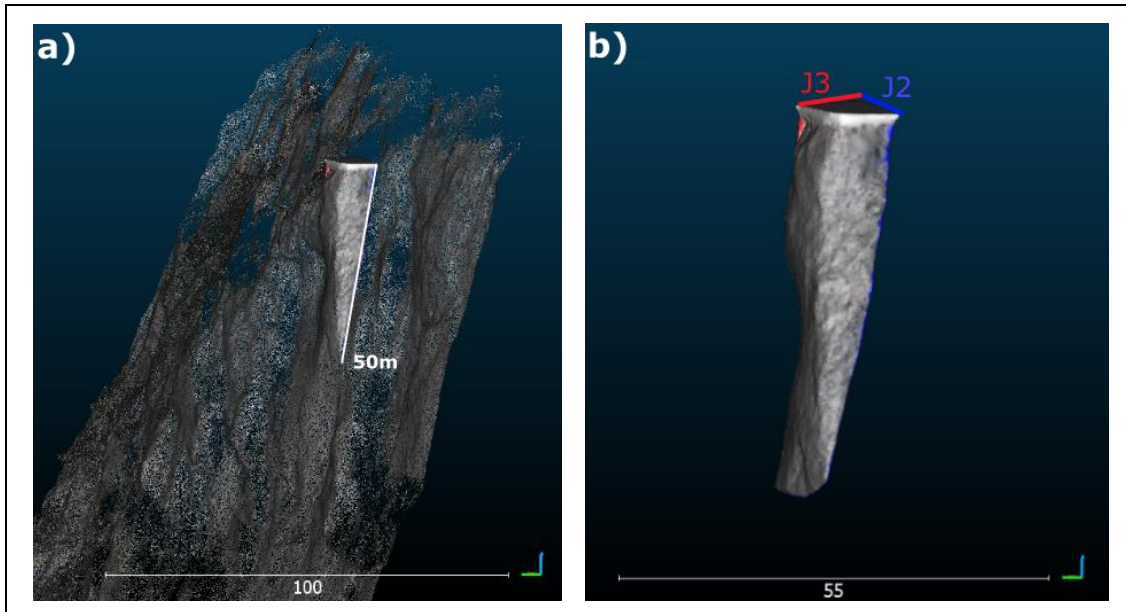


Figure 4.24: a) The unstable block is seen highlighted in the 3D-model. The toe is set to 50m below the top of the block. b) The block is controlled by structures following the orientation of J2 and J3.

Location 5

Location 5 is a large block with its highest point 440m above the fjord. The back scarp is at the eastern side of the block an open crack infilled with blocks. The open crack persists for 75m down in the rock mass, seen at the free eastern flank (Figure 4.25). The back scarp continues as a depression over the width of the block, with some sporadic openings of cracks. The western flank is set to an intersection with the slope where the rock mass is highly fractured with a close spacing for a 5m wide zone. The flank is free at the outer point of the block, while it follows a depression with the same width against the intersection with the back scarp. The flank detaching scenario 5.B is intersecting the slope as an open crack and continues as a depression.

The toe of the two scenarios is set to depths of 75 and 140 meters. This is based on structures seen at the eastern flank of the block, highlighted in the inserted picture in Figure 4.25. These structures are dipping to the north-west creating a sliding plane, but not within the lateral tolerance of 30 degrees from the orientation of the slope. The morphology of the cliff face shows a more fractured character of the eastern part of the block, where open fractures are seen expressing possible rupture surfaces of scenario 5.B.

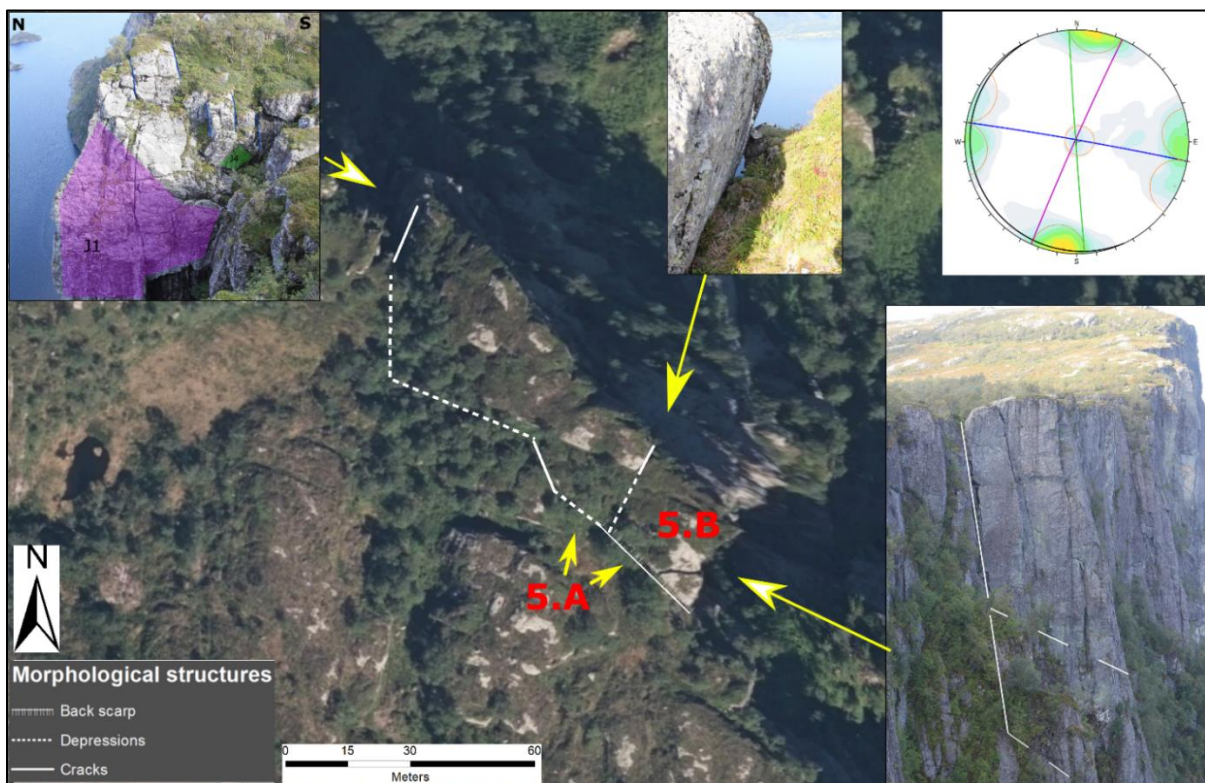


Figure 4.25: Orthophoto of location 5 with morphological structures drawn with white lines. Pictures are showing delimiting structures where upper pictures show lateral limits and the lower picture shows the interpreted toe lines of the scenarios at the eastern flank. The stereonet shows the significant structures for the mid domain.

The delimiting structures of the block fit well with the significant structures of the mid domain. The back scarp is following the orientation of J2 where the crack is open, while sporadically openings of the back scarp show orientations along J4. The flanks are following the orientation of J1. The structure delimiting scenario 5.B follows the orientation of J1 but dips to the west within the variability of the joint set.

The failure mechanism feasible for scenario A is a complex biplanar sliding along J2 and an outgoing structure. For scenario B, a toppling failure to the east, controlled by the slacker dipping J1 is possible. The volume of the largest scenario, scenario A, with a toe at 140m is calculated to 520 000m³. Scenario A with a toe line at 75m is calculated to 250 000m³. The smaller scenario, scenario B, delimited by the structure following J1 is calculated to a largest volume of 240 000m³ and a smaller volume of 90 000m³.

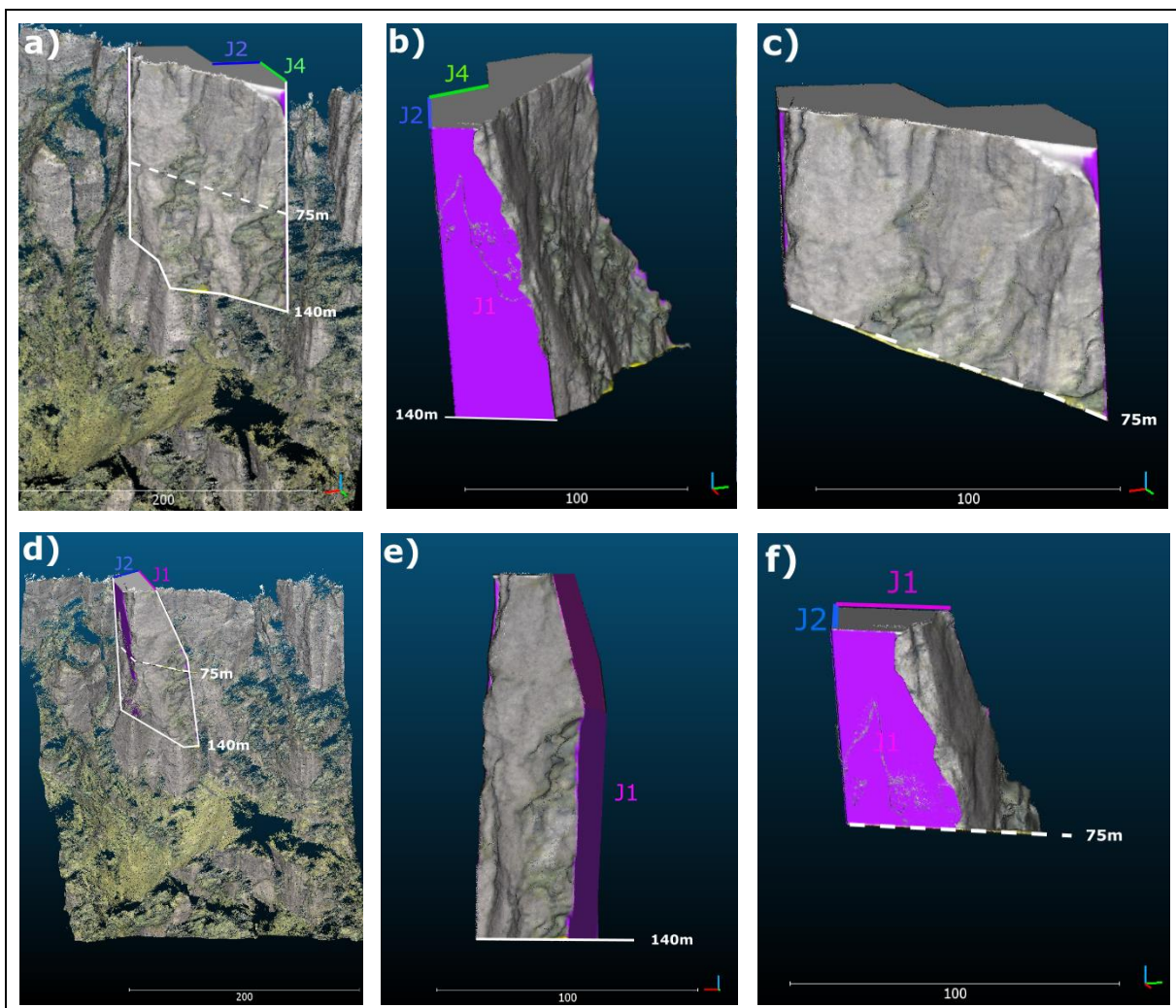


Figure 4.26: Figures exported from the 3D-model showing the unstable blocks calculated in the volume assessment. a) Overview of the position of scenario A at the cliff of Lifjellet. b) The rock mass of scenario A with toe line at 140m seen from the east. c) Scenario A with toe line at 75m. d) Overview of the position of scenario B. e) Volume calculated for scenario B with toe line of 140m. f) Scenario B with toe line at 75m.

Location 6

Location 6 is a monitored slope as part of the national database of unstable rock slopes (NGU, 2017). The slope is also assessed in the report of Böhme, *et al.* (2011) as the location Lifjellet East, and a historic collapse from the same site is investigated by Harbitz (1999). The slope hangs 440m above the fjord. The back scarp of the slope is a 30m long open crack with an opening of 30cm. It is measured to a depth of 30 meters. The crack has a smooth and persistent surface following one distinct plane. Cracks following the same orientation as the back scarp are delimiting the slope into several blocks. The western flank is an open crack with a persistence of 35m, an opening of 30-40cm and depth of 5m. The eastern flank is seen as a depression continuing with a persistence of 130m until it meets a lake. The depression is a 10m wide zone depressed by several meters. Toe lines are set due to structures visible at the cliff face detected in the photogrammetric model. The structures are detected at a depth of 80 and 125 meters from the top of the cliff.



Figure 4.27: Orthophoto of location 6 with drawn morphological structures detected in the field. Pictures are showing delimiting structures, both back scarps following the orientation of J2 and flanks following the orientation of J1 and J4. The stereonet shows that the structures at the orthophoto coincide with the significant structures of the mid domain.

The area is controlled by the structures assessed in the structural analysis. The back scarp follows the orientation of J2, while the western flank follows J4 and the eastern flank follows J1. The failure mechanism feasible for scenarios delimited by such structures is a toppling failure. Scenario 6.B is assessed due to distinct structural controls of the block. The back scarp is seen in the picture in Figure 4.27. It has 50 cm opening and is 50m deep. It is open until it meets the eastern flank, seen as the mid depression in the orthophoto of Figure 4.27.

Displacement measurements have been obtained both with dGNSS-measuring and extensometer-measurements. With the dGNSS-technique, displacement rates for scenario 6.B have been measured once a year since 2007. Results show significant displacement of 4mm directed to the north and no significant displacement in the vertical direction.

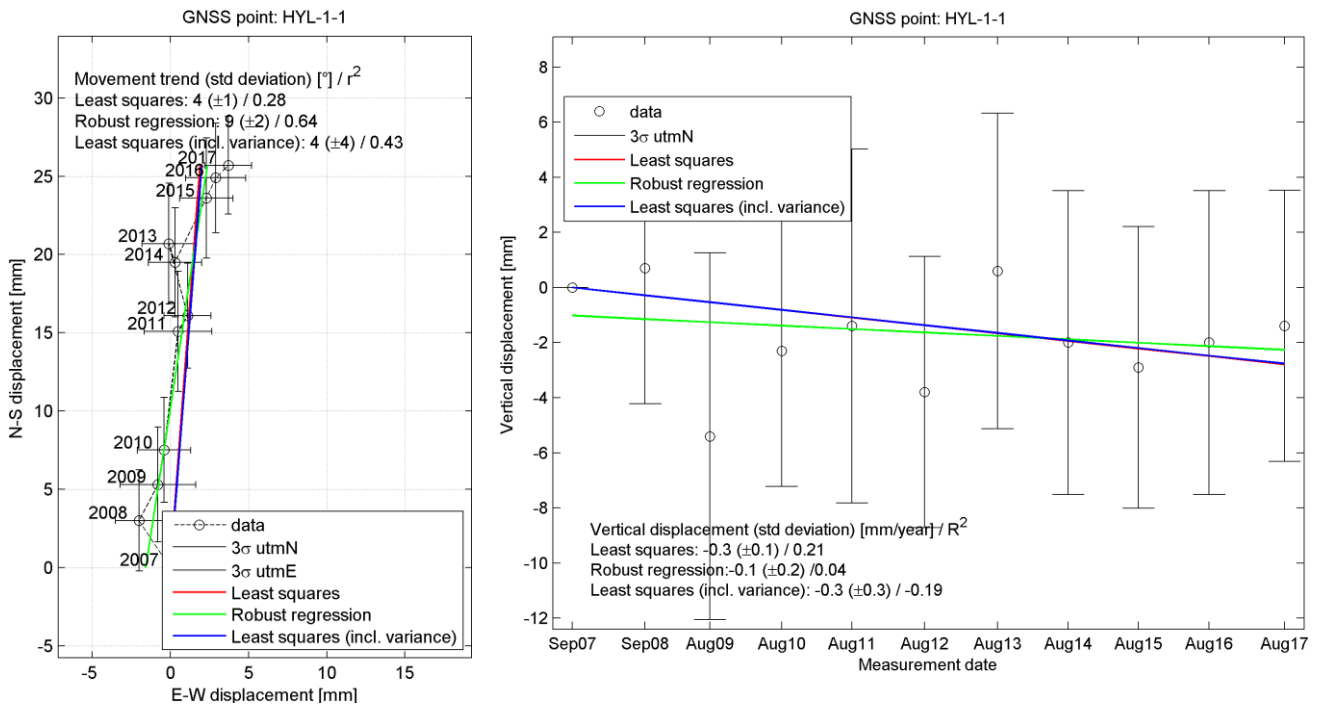


Figure 4.28: Analysis of the dGNSS-measurements of cumulative displacement of scenario 6.B in both horizontal and vertical direction.

Extensometer-measurements have been collected for the period from 2012-2017, at five different measuring points around scenario 6.B. The placing of the measuring stations is shown in Figure 4.29. The point showing the largest yearly rate is placed at the back scarp of scenario 6.B, with displacement directed to the north. Displacement rates are calculated to 2,41mm/year.

Table 4-5: Extensometer-measurements

Station	Total length difference (2012-2017)	Yearly rate (mm/y)
LiEx01	8,67	1,73
LiEx02	2,21	0,44
LiEx03	12,05	2,41
LiEx04	4,16	0,83
LiEx05	1,82	0,36

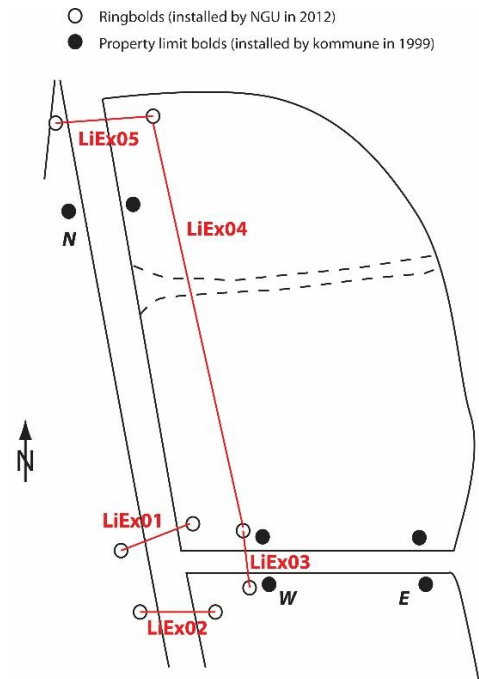


Figure 4.29: Placing of extensometer bolts, and the gaps measured at scenario 6.B.

Volumes of the two scenarios have been calculated with toe lines at 80m and 125m, as seen in Figure 4.30. For scenario A the maximum calculated volume is 223 000m³ and the smaller volume is calculated to 130 000m³. For scenario B the calculated volumes are 42 000m³ for the largest, and 25 000m³ for the smaller volume.

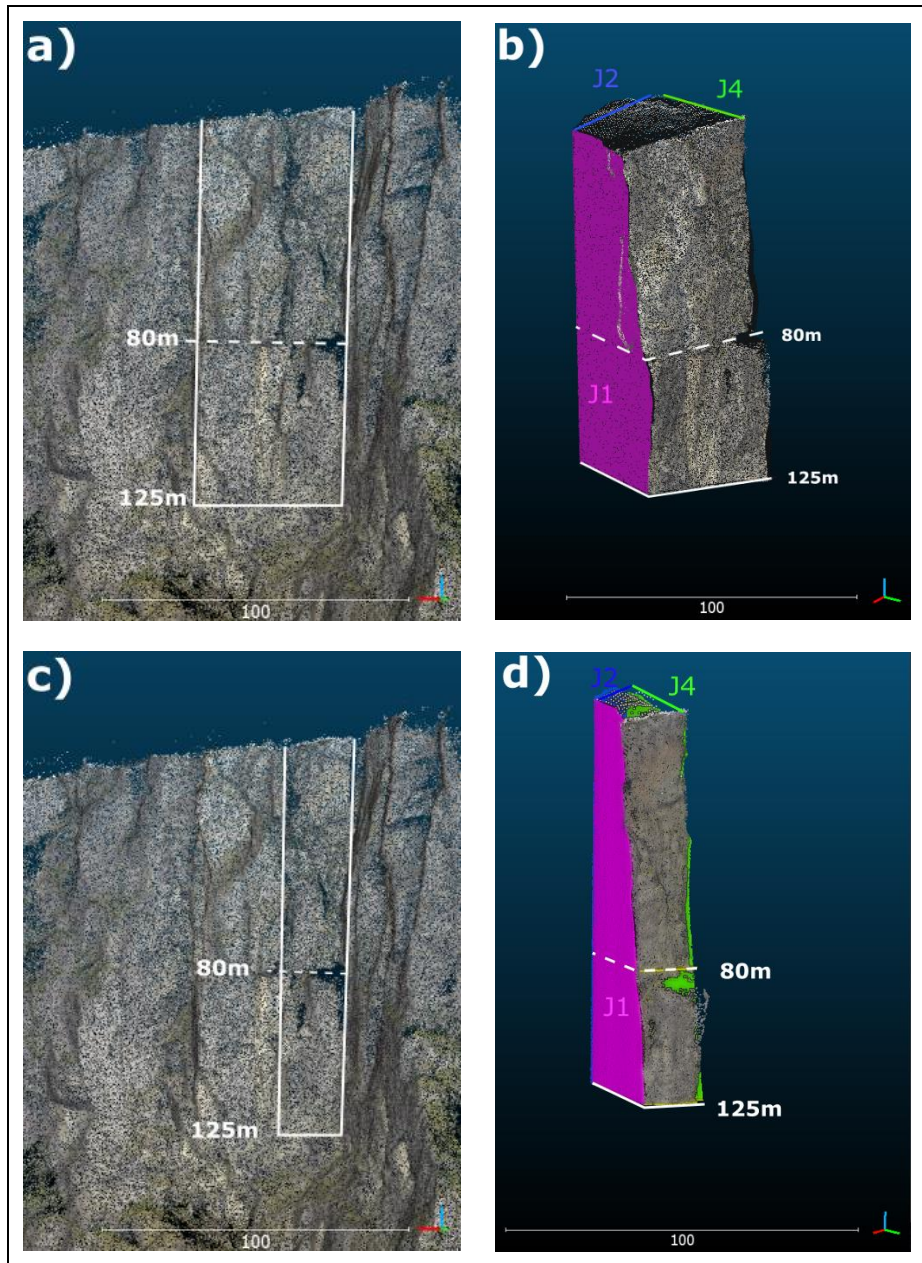


Figure 4.30: Figures from the 3D-model showing the unstable blocks of location 6. a) Overview of scenario A, with toe lines at 80m and 125m. b) Calculated volume of scenario A, with delimiting structures. c) Overview of scenario B. d) Calculated volume of scenario B with controlling structures marked.

Location 7

Location 7 is also a monitored slope as part of the national database of unstable rock slopes (NGU, 2017), and described as Lifjellet Vest in the report of Böhme, *et al.* (2011). The unstable block hangs 495m above the fjord. It is detached by a fully developed back scarp. Estimated depth is 100meters, based on the time a rock is heard falling in the crack. The fracture has an average opening of 50cm. The eastern flank is a free slope, where the back scarp is seen as a fracture along the slope (Figure 4.31). Where the western flank intersects the slope, a small block is detached from the cliff. A daylighting structure is detected in the 3D-model intersecting the block at two different depths. This structure is dipping 35 degrees to the N-W.

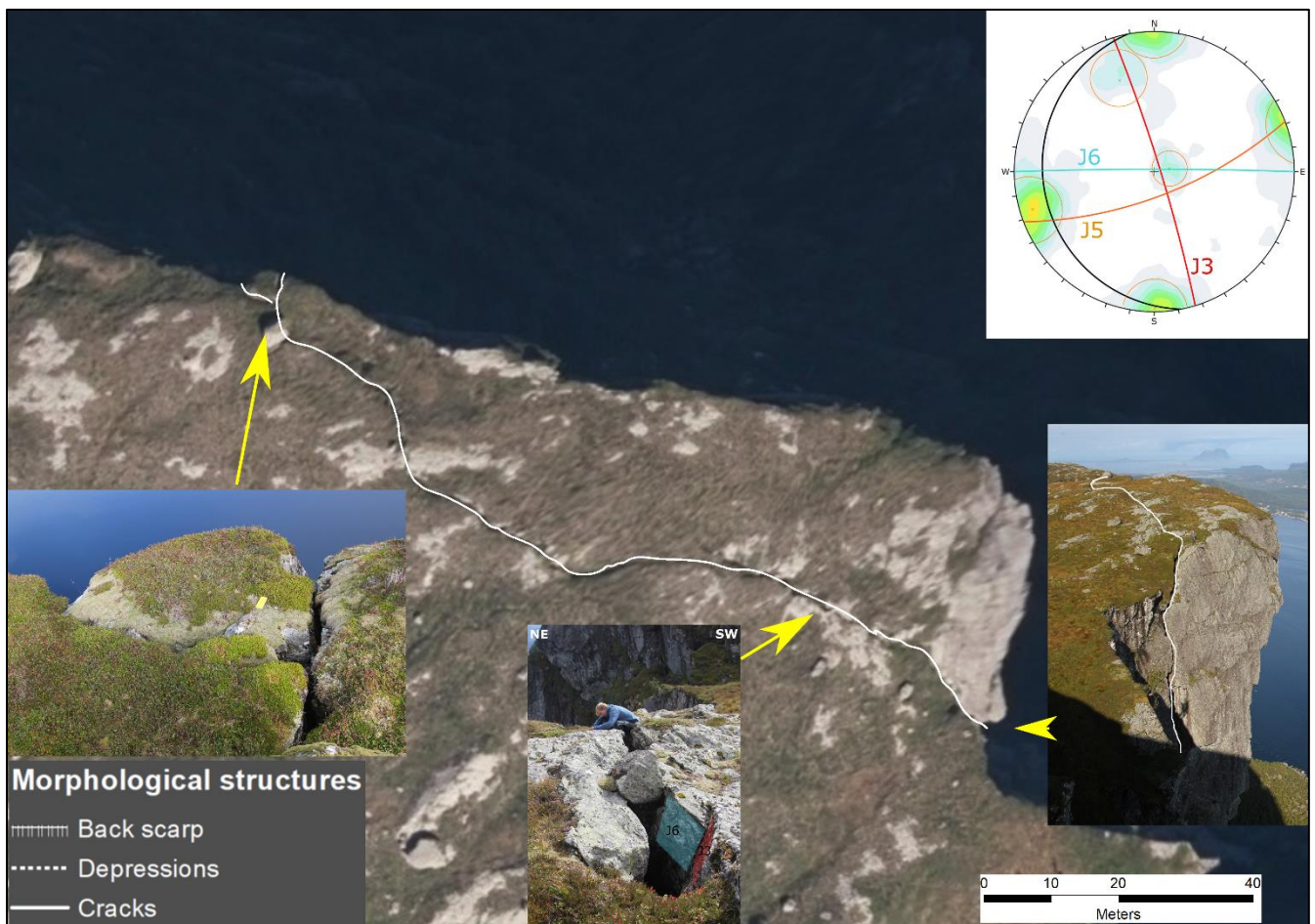


Figure 4.31: Orthophoto showing the morphological structure delimiting the unstable block of location 7. Picture shows an example of the stepwise back scarp controlled by J3 and J6. The stereoplot shows the significant structures found in the domain of the location.

Field measurements of the back scarp suggest a structural control consisting of J3 and J6 (Figure 4.31). These orientations are also delimiting structures for the smaller block at the western flank. Along the vertical structures, a toppling failure is kinematically feasible.

Displacement measurements of location 7 have been collected both with dGNSS-measurements and with extensometer-measurements. For the dGNSS-measurements, data have been processed from 2007-2017. Results show no significant displacement in the horizontal and vertical direction, as shown in Figure 4.32.

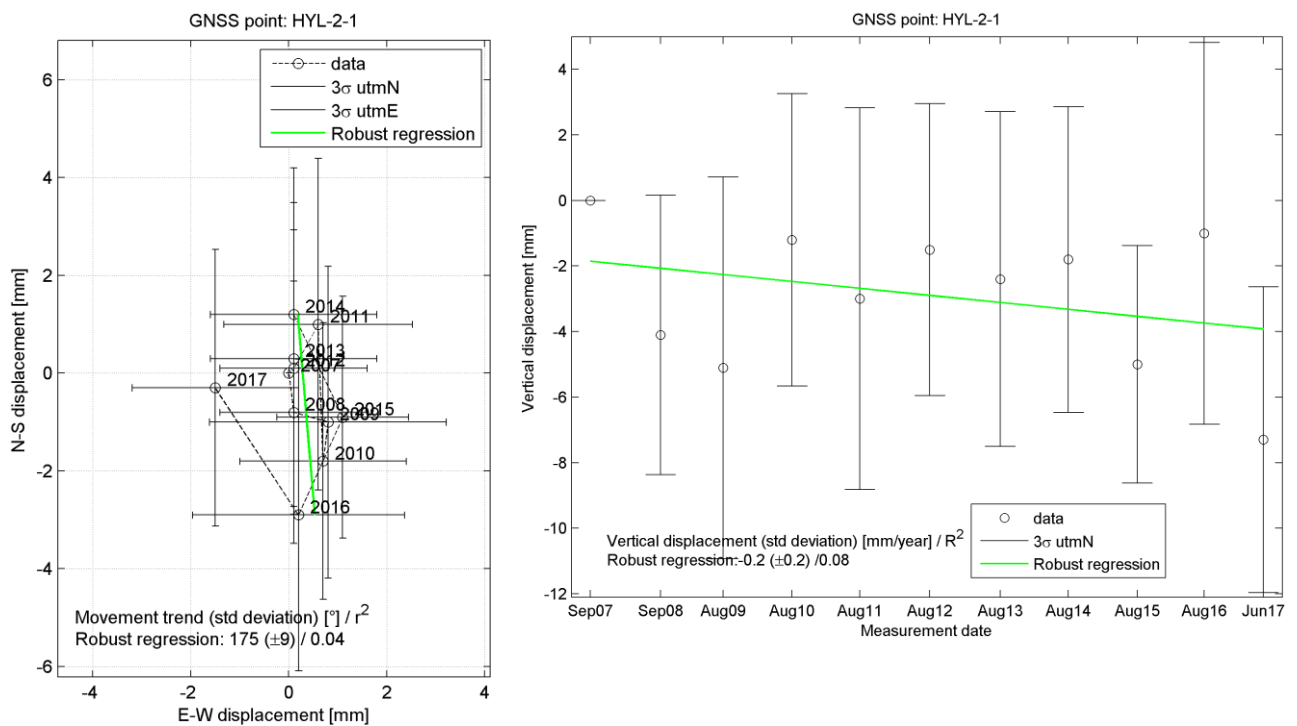


Figure 4.32: Analysis of the dGNSS-measurements of cumulative displacement of location 7 in both horizontal and vertical direction.

Extensometer measurements have been collected for less than two years. The measuring points are crossing the back scarp of the block at two different positions. The largest yearly displacement rate is 0,69 mm/year, which is below the significance level for such measuring.

Table 4-6: Extensometer measurements

Station	Total length difference (mm)	Yearly rate (mm)
LiWEx01	1,20	0,69
LiWEx02	0,52	0,30

Volumes of the unstable block have been calculated based on the structures found along the back scarp and the two toe lines, interpreted at 75m and 130m from the top of the block. Calculations result in a volume of 195 000m³ for the largest interpreted block, and 116 000m³ for the smaller block.

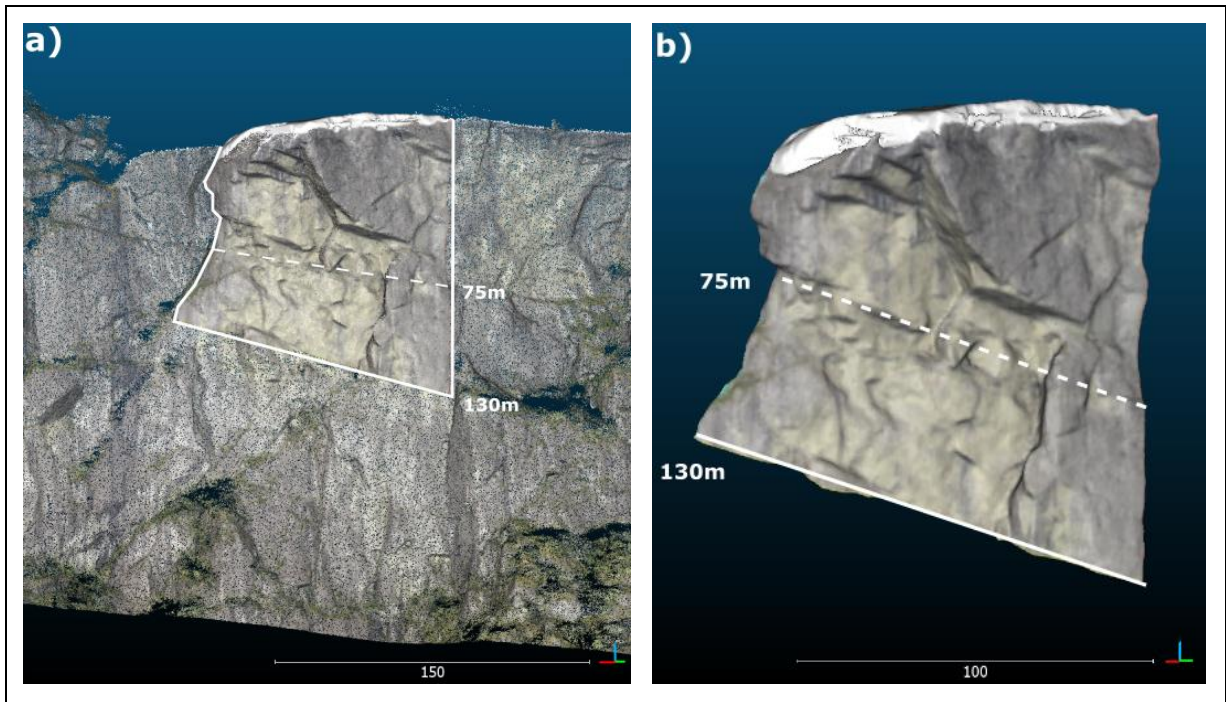


Figure 4.33: a) The unstable block is shown in the 3D-model with flanks and toe lines at depths of 75 and 130 meters delimiting the block. b) The figure showing the calculated volume of the block, the largest volume with a depth of 130m and the smallest volume with a depth of 75m from the top of the cliff.

Location 8

This unstable slope is hanging 470m above the fjord. The back scarp is an open crack, 20cm wide and estimated to be 20-30m deep at the eastern side of the block. Where the back scarp intersects the western flank, it is seen as a vague depression. The western flank intersects the slope along an open structure with an opening of 50cm, but at the intersection with the back scarp, the structure is not visible. The eastern flank is free. A release plane is suggested at the slope, seen as flat-lying rock beds in the cliff face. Interpreted planes are daylighting and dipping 35 degrees towards the N-W.

An internal block is delimited by a structure of another orientation. The back scarp has a 2m wide opening persisting for approximately 30 meters and dipping into the slope. The western flank follows a distinct structure, seen as red planes in Figure 4.34.

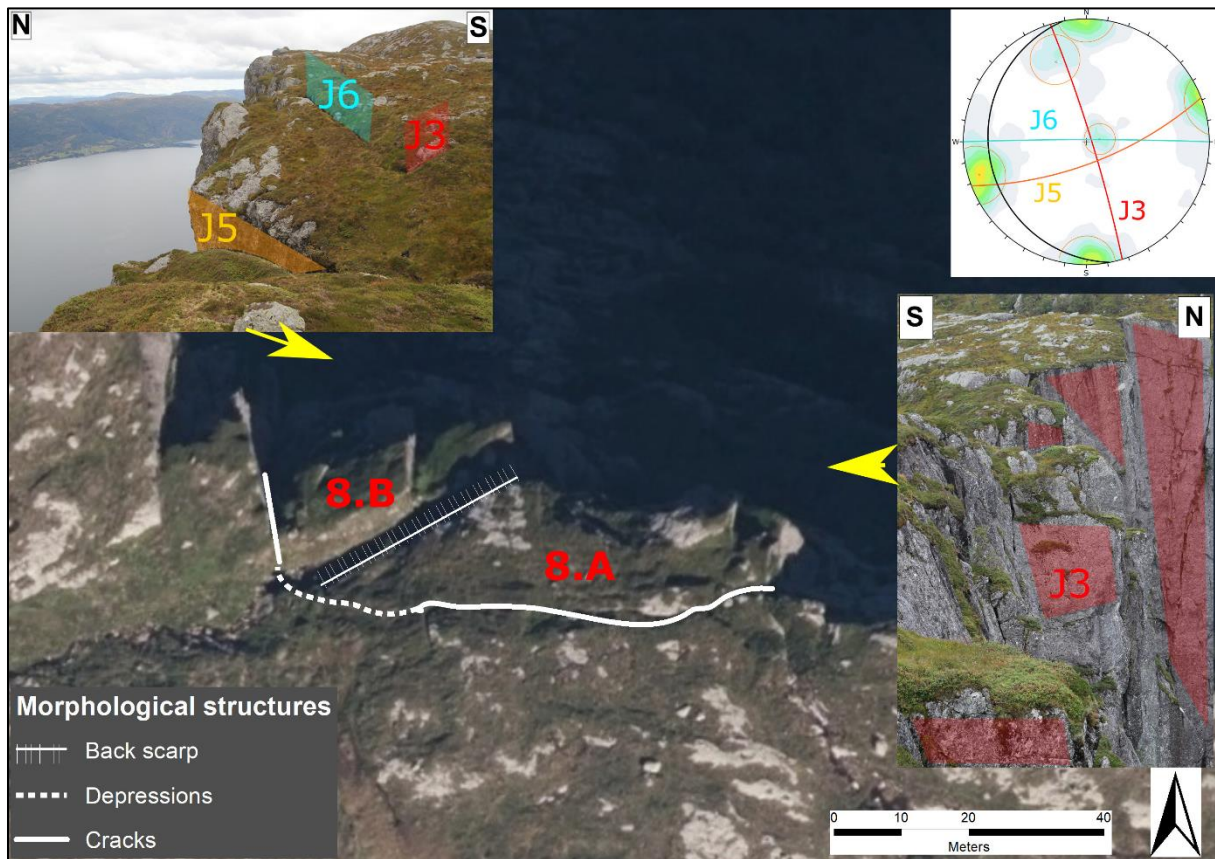


Figure 4.34: Orthophoto of location 8 marked with morphological structures detected in the field. Left picture is showing the morphological structures following the orientation of J3, J5, and J6. Right picture shows the clear structure of J3 intersecting the cliff face with a spacing of 15m. The stereoplot shows the correlation between the delimiting structures and the structural analysis of the western domain.

The largest scenario is suggested delimited by J6 due to the orientation of the structure. The joint set is seen with a rough surface, which can explain the rough expression of the back scarp. The western flank is following the orientation of J3. The back scarp of scenario 8.B follows the orientation and dip of J5, with the same western flank as the largest scenario. The structures delimiting both scenarios show a feasibility for toppling failure.

The two scenarios are calculated with the same toe line, the first visible structure dipping out of the slope. The volume of scenario 8.A is calculated to 75600m³, while scenario 8.B is calculated to a volume of 39 500m³.

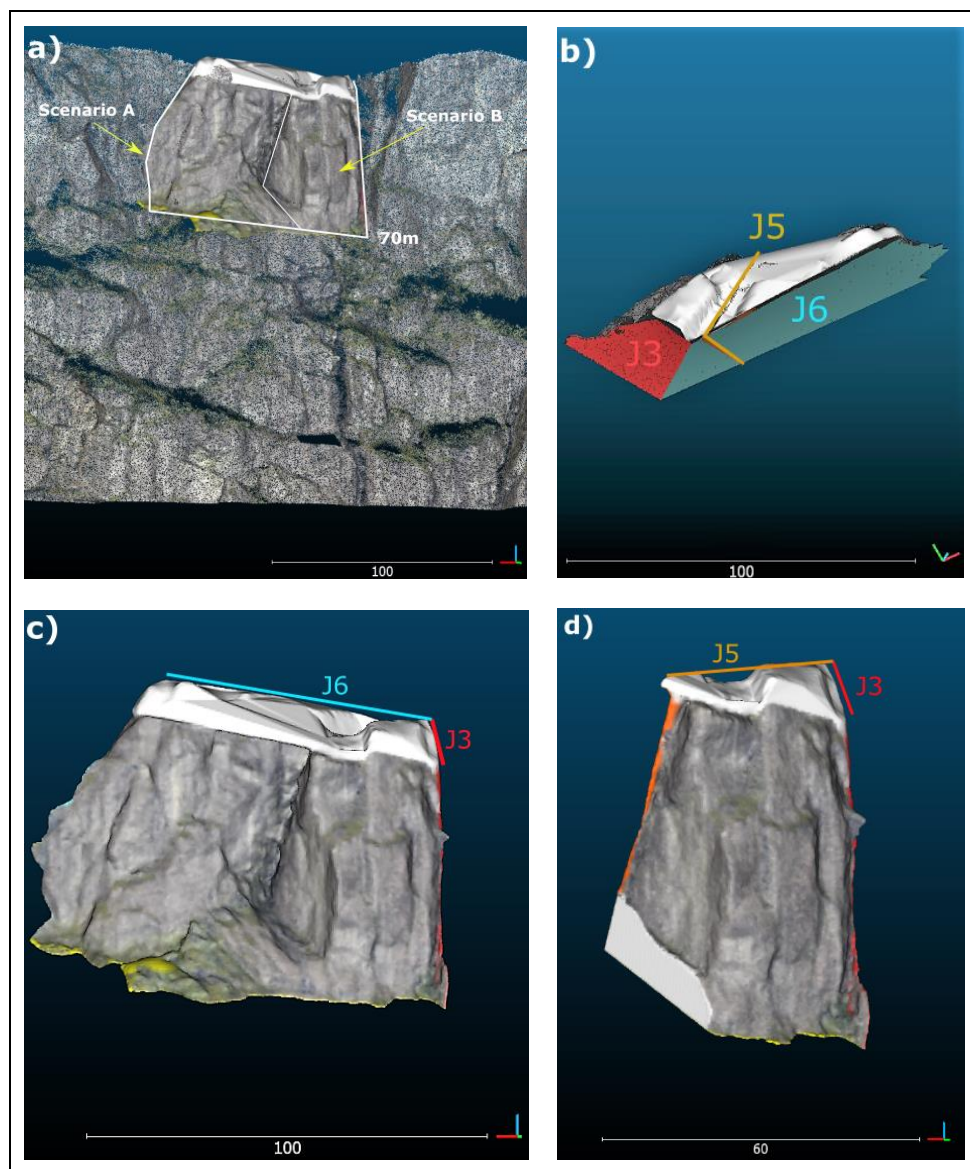


Figure 4.35: The unstable block of location 8 highlighted in the 3D-model. a) Overview of the position of scenario A, and the smaller block of scenario B at the cliff face, with a toe line at 70m depth. b) The block of scenario A seen from behind, with delimiting structures following the orientation of J3 and J6. A crosscutting structure, J5, is delimiting scenario B from the rest of the block. c) Scenario A delimited. d) Scenario B delimited.

Location 9

The highest point of this location is 475 meters above the fjord. This block is defined by lineaments shown in the orthophoto (Figure 4.36). The eastern structure is a 10m wide depression consisting of a march continuing into a small lake. The lake is not drained, which imply that the structure is not fully developed. The western structure is more persistent and is also seen as cracks in the rock mass. These cracks have smooth planes with vertical dip. At the intersection to the free slope, there is a 10m wide zone of fractured blocks following the orientation of this structure.

The toe line of the scenario is interpreted at a depth of 240 meters from the top of the block. The structure daylighting is seen as a fracture in the cliff face fitting very well to the other structures seen with a dip of 35 degrees to the N-W.

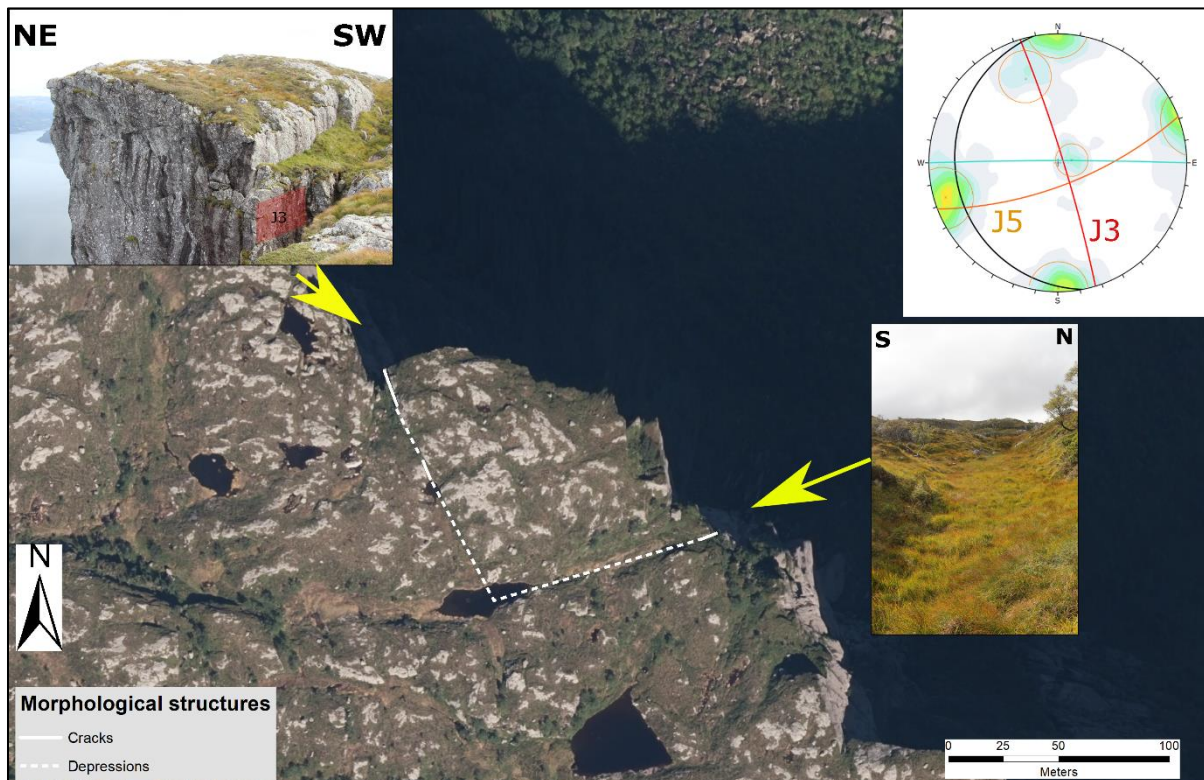


Figure 4.36: Orthophoto of location 9 showing the unstable block delimited by lineaments seen as depressions in the field, following the orientation of J3 and J5. Left picture shows the intersection between the lineament of J3 and the cliff face. Right picture shows the depression following the orientation of J5. The stereonet shows the coherence between the significant structures in the western domain and the lineaments in the orthophoto.

The western lineament is following the orientation of J3, while the eastern lineament is following the orientation of J5. Kinematic feasibility shows that oblique toppling is possible along the structure of J5, with J3 as a lateral limit.

The total volume of the delimited scenario is 2 600 000m³ of rock mass.

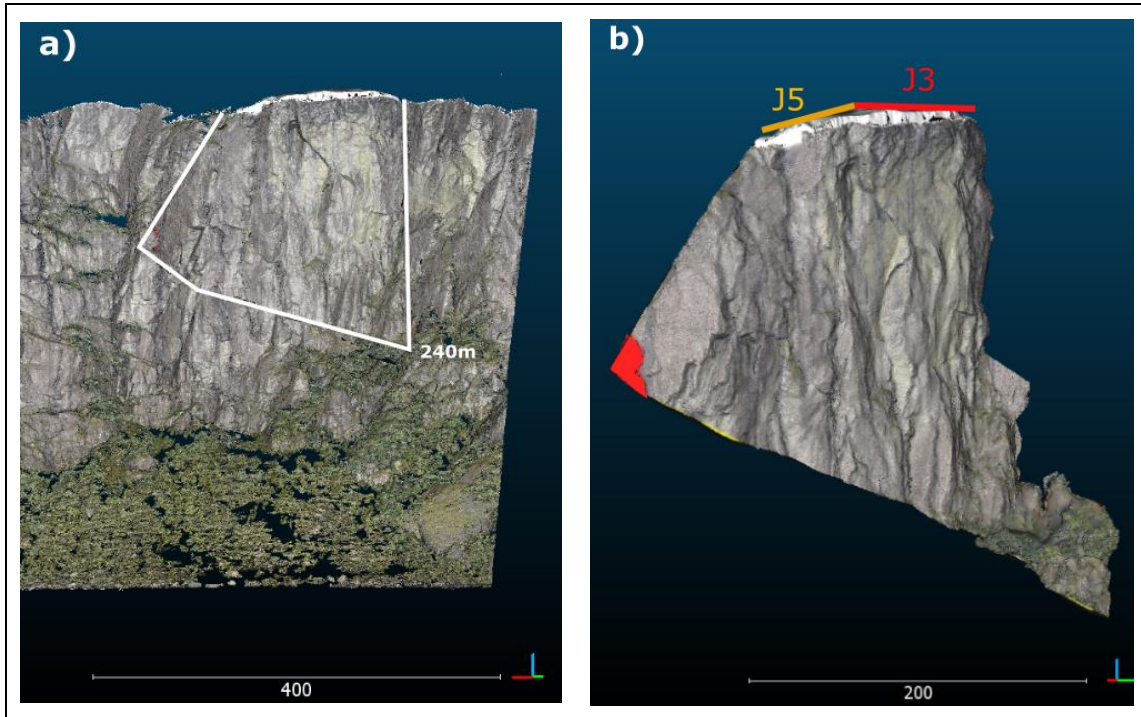


Figure 4.37: a) The scenario of location 9 highlighted in the 3D-model with lateral limits and a toe line at 240m depth. b) The scenario delimited by J3, J5 and a daylighting structure with a dip of 35 degrees.

4.4.3 Calculated volumes

Calculated volumes are obtained by a three-dimensional construction of failure surfaces (Jaboyedoff, *et al.*, 2015). The volumes for each location are calculated for different scenarios of the location and for different depths of failure where various toe lines are interpreted, described for each location in chapter 4.4.2. The variation in depth is not considered as different scenarios but shown as maximum and minimum constructed volumes in the results of the volume calculation highlighted in Table 4-7.

Table 4-7: Results from the volume calculation of all scenarios.

Scenario	Volume	
	Min (Mm3)	Max (Mm3)
1.A		0,597
2.A		0,149
3.A		0,151
3.B		0,129
3.C		0,020
4.A		0.006
5.A	0,249	0,524
5.B	0,090	0,239
6.A	0,130	0,223
6.B	0,025	0,041
7.A	0,116	0,195
8.A		0,076
8.B		0,040
9.A		2,595

Volumes ranging from 0,5-2,6 Mm3 have been calculated of the delimited scenarios. Based on the volume size, a classification of scenarios can be assessed due to expected movement of a failure, described in chapter 2.1.2. Excessive travel length classified as rock avalanches can be expected for the scenarios 1.A, 5.A(maximum volume) and 9.A. The other scenarios are classified as rock slope failures.

4.4.4 Run-out

The empirical runout relationship has been calculated based on the Scheidegger equation for volumes above the Scheidegger cut-off. Scenarios with volumes below the Scheidegger cut-off is set to a standard value due to Corominas (1996), described in chapter 3.4.2. The assessment of whether the potential failures will hit the water body is shown by calculating the angle of reach to the water body. The angle difference between angle to water and angle to run-out toe is considered by the minimum angle of reach due to a conservative approach.

Table 4-8: Estimated angle of reach for each scenario compared with the angle to water.

Scenario	Volume (Mm ³) [min / max]	Angle to water (°)	Angle of reach (°) [min / max]	Difference
1.A	0,597	40	27,5	12,5
2.A	0,149	54,8	31	23,8
3.A	0,151	57,6	31	26,6
3.B	0,129	57,6	31	26,6
3.C	0,020	57,6	31	26,6
4.A	0,006	63,6	31	32,6
5.A	0,249 / 0,524	58,5	31 / 27,9	27,5
5.B	0,090 / 0,239	58,5	31	27,5
6.A	0,130 / 0,223	58,9	31	27,9
6.B	0,025 / 0,042	58,9	31	27,9
7.A	0,116 / 0,195	67,5	31	36,5
8.A	0,076	59,2	31	28,2
8.B	0,040	59,2	31	28,2
9.A	2,595	57,3	22,8	34,5

The results of the runout assessments show that the volumes of all scenarios will hit the water body with a margin of more than 12 degrees. The large margin also indicates that a substantial part of the initiated volume will hit the water body.

4.4.5 Hazard classification

The hazard is classified by a calculation of geomorphological and structural criteria, and signs of activity following Hermanns, *et al.* (2013b), obtained through the NGU mapping approach described in chapter 2.4. Methodology for criteria 4 and 6-7 is described in chapter 3.3, while criteria 9 is evaluated due to historic events described in chapter 1.6. The resulting score is

placed between 0 and 12, where high scores mean high hazard. Uncertainties of the hazard score can be evaluated due to the use of probabilities for each criterion. The final score therefore has a minimum, mean and maximum value, with the size of uncertainties varying with the accuracy of the assessment. The complete hazard assessment for each scenario is attached in Appendix D. The resulting hazard scores are highlighted in Table 4-9.

Table 4-9: List of the investigated scenarios with computed volumes, evaluated hazard criteria and resulting hazard scores.

Scenario	Volume (Mm ³) [max/min]	1. Back scarp	2. Sliding structures	3. Lateral release surface (left/right)	4. Kinematic feasibility	5. Rupture surface	6. Displacement rates (mm/year)	7. Acceleration	8. Increase in rockfall activity	9. Past events	Hazard score mean [min; max]	Hazard class (Low/Medium/High)
1.A	0,597	P	P/f	F/P	pF+	N	U	U	N	Y+	5,7 [4,0; 8,8]	M
2.A	0,149	P	P	F/F	P	N	U	U	N	Y+	5,2 [3,8; 8,3]	M
3.A	0,151	F	N	Pf/F	F	Pf	U	U	Y	Y+	6,5 [4,5; 9,8]	M
3.B	0,129	F	N	P/pF	F	Pf	U	U	Y	Y+	6,4 [4,8; 9,5]	M
3.C	0,020	P	P	pF/F	pF	pF	U	U	nY	Y+	6,4 [4,3; 10,3]	M
4.A	0,006	F	P	F/Pf	F+	Npf	U	U	N	Y+	6,0 [4,0; 10,0]	M
5.A	0,524/0,249	P	P	P/F	N	N	U	U	Ny	Y+	4,6 [2,8; 8,3]	L
5.B	0,239/0,090	F	P	P/F	P+/F	Pf	U	U	Ny	Y+	6,7 [4,8; 10,3]	M
6.A	0,223/0,130	F	P	F/P	F+	Npf	n(1)	Ny	N	Y+	5,1 [4,3; 6,3]	M
6.B	0,042/0,025	F	P	F/Pf	F+	Npf	(1)	Ny	N	Y+	5,8 [5,3; 6,5]	M
7.A	0,195/0,116	F	P	pF/F	Pf+	Npf	N	Ny	nY	Y+	5,8 [4,3; 7,5]	M
8.A	0,076	P	N	P/F	F	Npf	U	U	N	Y+	4,9 [3,3; 8,3]	M
8.B	0,040	F	N	F/F	F+	Npf	U	U	N	Y+	5,7 [4,0; 9,0]	M
9.A	2,595	N	N	P/F	F+	Npf	U	U	N	Y+	4,2 [2,3; 8,3]	L

Description for the hazard assessment (most probable condition capital letter/other possibility small letter)

N/n not existing (criteria 1-5,7-9), not significant (criteria 6)

P/p partly developed (criteria 1-3, 5), partly possible (criteria 4)

F/f fully developed (criteria 1-3, 5), fully possible (criteria 4)

Y/y yes (criteria 7-9)

U unknown (standard value used in criteria 6-7)

(1) 0,2-0,5cm/year movement (criteria 6)

+ on persistent discontinuities (criteria 4), younger than 5000 years (criteria 9)

The resulting hazard classification highlights 12 scenarios within the medium hazard class. A comparison of scenarios within the same location highlights the scenario most likely to fail. The uncertainties of each assessment are closely connected to the detail of its evaluation and are mainly related to missing displacement measurements. Scenario 6.B has the lowest total uncertainties due to its low uncertainty connected to displacement rates.

Based on the quantitative thresholds set within the qualitative hazard classification system described in chapter 2.5.1, 9 of the scenarios have an annual probability exceeding the quantitative threshold for safety class 3. The other scenarios do not require further follow-up based on the thresholds set in TEK17.

4.5 Assessment of past events

The assessment of past events is considering the distribution of fjord deposits, volume estimations of detected deposits and a volume-frequency estimation of differing volume classes.

4.5.1 Distribution

Deposits of historic rock slope failures cluster along the slope into three clusters, which I choose to call the eastern, mid, and western cluster. These clusters fit well with the defined domains assessed in chapter 4.4.1. Bathymetric data are not shown in the results due to restrictions from the Norwegian Ministry of Defense. The deposits are shown in the order of stratigraphic position, based on characteristics described in chapter 2.1.4.

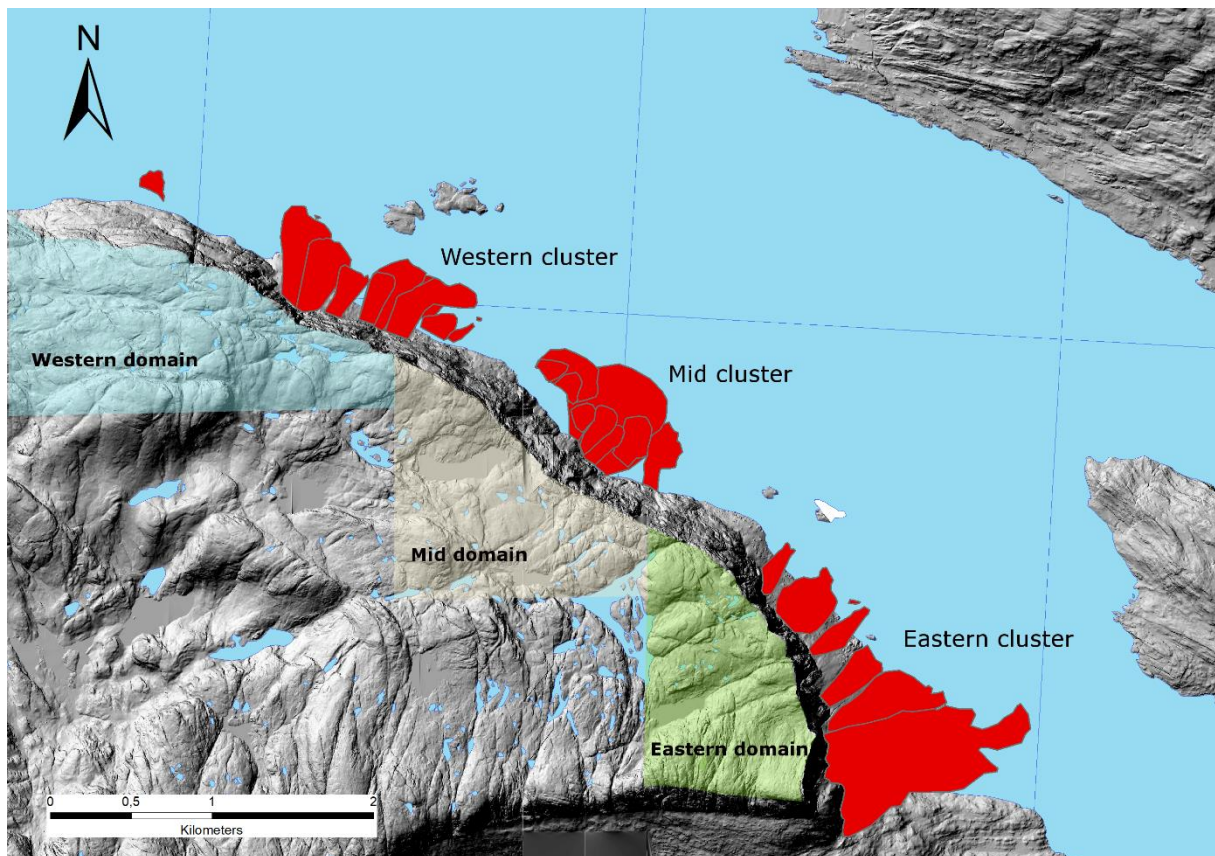


Figure 4.38: Overview of deposits detected in Aafjorden along the cliff of Lifjellet. The deposits cluster into three clusters called the eastern, mid, and western cluster.

There are in total 25 deposits detected and highlighted in Figure 4.38. The volumes calculated ranges from 6000m³ to 2Mm³. The difference between clusters shows larger deposits in the eastern cluster, while the mid cluster has the densest concentration of slides. The degree of depositing in the water body is also changing between the clusters. This is a matter of the topography of the slope. At the eastern cluster, most of the mass is deposited on land because

of both the distance of the rock face towards the fjord and because of the low slope angle in the run-out zone. At the mid cluster, the short horizontal length to the fjord results in a larger percentage of mass reaching the fjord.

Eastern cluster

Deposit	Volume (Mm³)
1	1,919
2	0,222
3	0,140
4	0,071
5	0,312
6	0,041

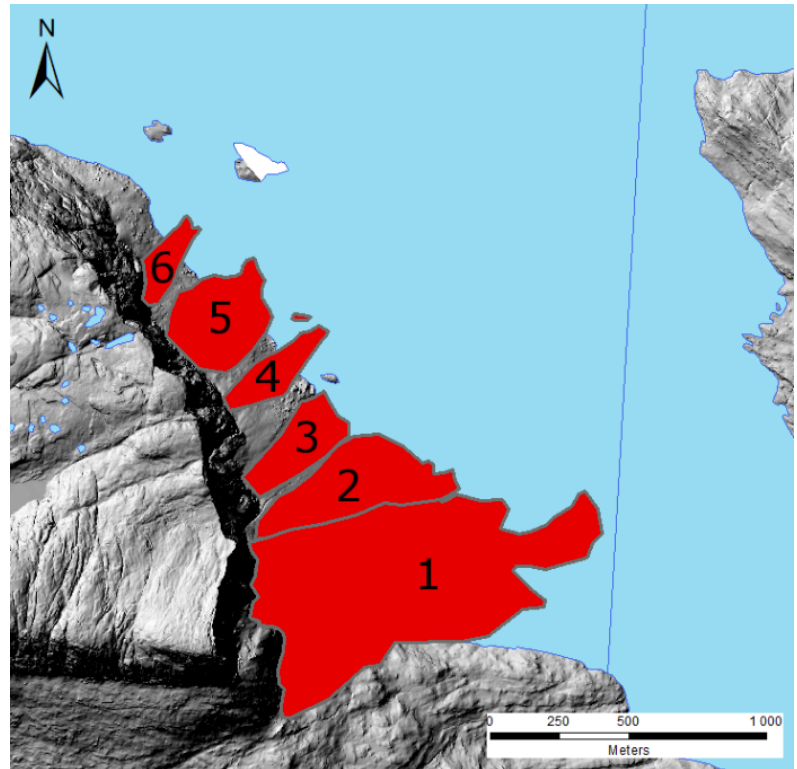


Figure 4.39: Mapped deposits based on the theory of depositing explained in chapter 2.1.4.

In the eastern cluster, there is seen an even distribution of deposits, where no deposits are positioned stratigraphically on top of each other. Deposit 1 is the largest rock slope failure detected in the fjord, with a volume of 1,9 Mm³. The source area of this event is interpreted along the slope of location 1 (chapter 4.4.2). Deposit 1 and 2 is the deposits with estimated largest volumes deposited in the fjord, despite the longest distance to the fjord. Deposit 5 is the deposit in the cluster with the largest estimated average thickness. Two of the deposits are estimated to volumes associated with excessive travel lengths. This is deposit 1 and deposit 5. The only deposit showing excessive travel lengths is deposit 1.

Mid cluster

Deposit	Volume (Mm ³)
7	0,066
8	0,066
9	0,077
10	0,041
11	0,037
12	0,372
13	0,051
14	0,043
15	0,296

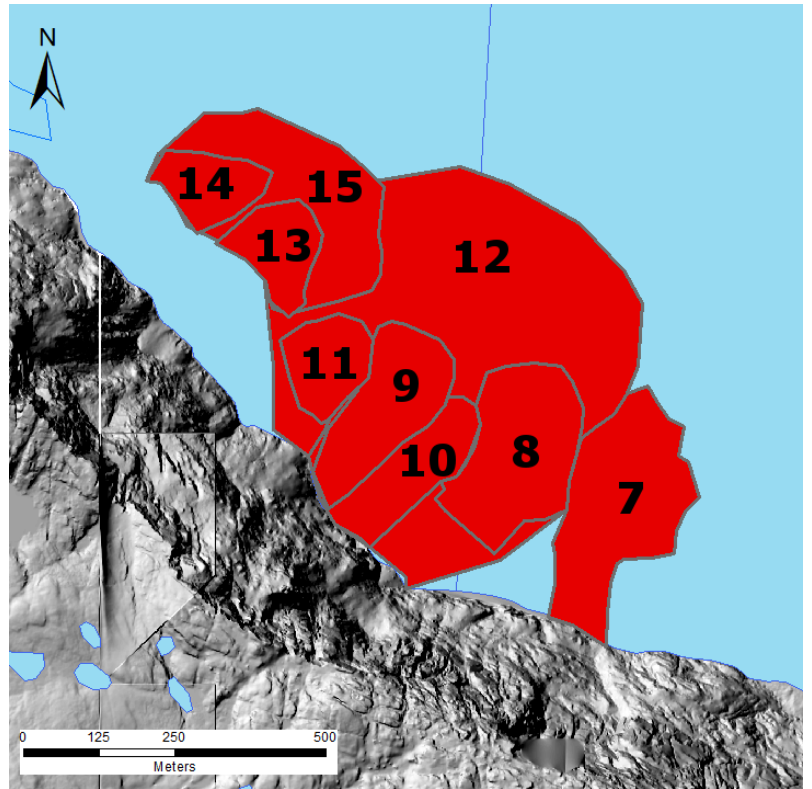


Figure 4.40: Mapped deposits based on the theory of deposition. The overlapping deposits have numbers based on their stratigraphic position.

In the mid cluster, there is seen a more frequent stratigraphic positioning of deposits. Another important discovery is that deposit 12 and deposit 15, the two largest deposits both in volume and travel length is stratigraphically positioned lowest.

There is seen a trend that similar volumes express the same travel lengths. An example, deposit 13 and 14 is estimated to close to the same volume and shows exactly the same run-out. Deposits not showing the same trend is the two largest deposits in the cluster. The area affected by deposit 12 is many times larger than the area affected by deposit 15, even though the difference in volume is quite small.

Western cluster

Deposit	Volume (Mm ³)
16	0,007
17	0,078
18	0,221
19	0,131
20	0,053
21	0,090
22	0,044
23	0,186
24	0,116
25	0,008

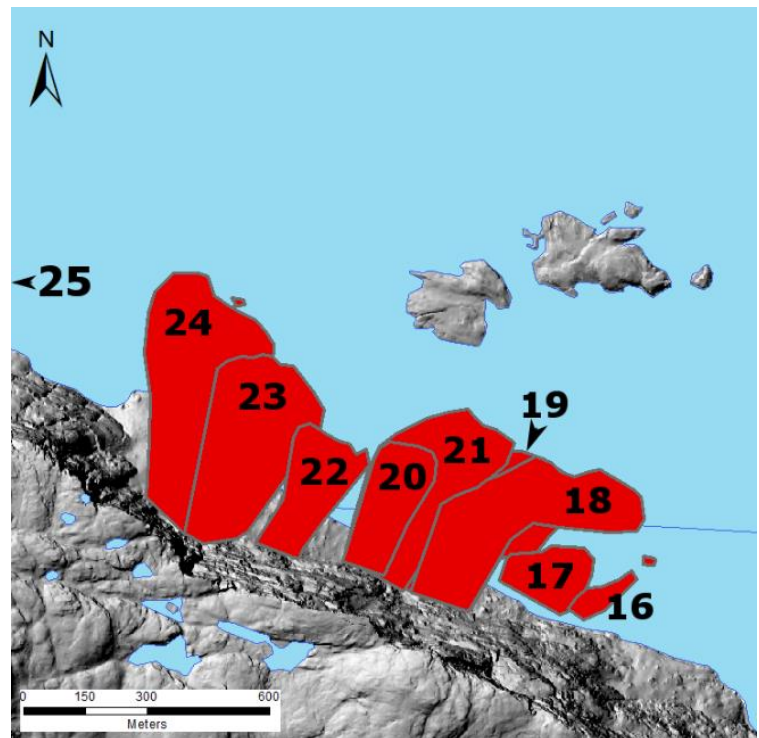


Figure 4.41: Mapped deposits shows a clustering of past events in the eastern domain.

In the western cluster, there are many deposits stratigraphically positioned on top of each other. The interpretation of the stratigraphic positioning of deposits is possible due to the defined lobes seen on top of other deposits. Also, differences in thickness can set limits for an overlying deposit. In this cluster, the smallest estimated volume of a deposit is detected. This is deposit 16, with a volume of 0,007 Mm³. Smaller failure volumes have most likely deposited multiple times, but due to the resolution of the bathymetric data, smaller deposit volumes cannot be detected.

Deposit 19 is almost covered by the overlying deposit 18 and deposit 21. Lobes have been detected between the two deposits suggesting another deposit. Due to the large travel length, an estimated volume has been set manually. Deposit 25 is not seen as part of the western cluster but is marked in the overview map in Figure 4.38.

Deposits are mostly showing the same trend as in the mid cluster, with relative travel lengths connected to their volume size. The deposits not following this trend is deposit 23 and deposit 24 distributed side by side. The volume estimated for the deposit with largest travel length is 0,70 Mm³ smaller than the other deposit showing a clearly shorter travel length.

4.5.2 Volume estimation

Volumes of the 25 detected deposits have been estimated using the SLBL-method developed by NGU. The estimation has followed the method described in chapter 3.4.1. The calculation of the deposit's initial volumes before failure have been assessed due to the volume-frequency analysis in chapter 4.5.3. The fragmentation rate used to estimate initial volume is described in chapter 2.1.4.

Table 4-10: The resulting deposit volumes estimated by the SLBL-method, and the calculated initial volumes before failure considering the fragmentation rate of large rock slope failures.

Deposit	Deposited volume (Mm ³)	Initial volume Mm ³ (fragmentation rate of 0,25)
1	1,919	1,439
2	0,222	0,166
3	0,140	0,105
4	0,071	0,053
5	0,312	0,234
6	0,041	0,030
7	0,066	0,050
8	0,066	0,050
9	0,077	0,058
10	0,041	0,031
11	0,037	0,028
12	0,372	0,279
13	0,051	0,038
14	0,043	0,032
15	0,296	0,222
16	0,007	0,005
17	0,078	0,059
18	0,221	0,166
19	0,131	0,098
20	0,053	0,040
21	0,090	0,068
22	0,044	0,033
23	0,186	0,140
24	0,116	0,087
25	0,008	0,006

Volume estimations of deposits ranges from 0,007- 1,919 Mm³. The smallest detected deposit is deposit 16. The largest detected deposit is deposit 1. A classification based on volume size has been suggested in chapter 2.1.2. Two deposits have been classified as rock avalanches due to their estimated initial volume above 250 000m³. This is deposit 1 in the western cluster and deposit 12 in the mid cluster.

4.5.3 Frequency analysis

The frequency analysis is following the methodology described in chapter 3.5. The aim for the analysis is to assess a frequency of failures along the cliff of Lifjellet and resulting frequencies of varying volume classes.

Frequency distribution

The period of depositing is obtained through a survey of the historical evolution of the area, presented in chapter 1.5.2. Knowing that the area was deglaciated 11 500 years ago, there is reason to believe that no large-scale erosion of the fjord has occurred after that time and that thus all deposits are preserved.

The number of past events detected in the fjord has been interpreted according to the theory about deposition described in chapter 2.1.4. Results of the assessment have been presented in chapter 4.5.1. The smallest detected deposit has a volume of 0,007 Mm³. This lower limit is due to the resolution of the data; thus, the frequency estimate is assessed with a volume threshold at 0,007 Mm³. In total 25 deposits with volumes $\geq 0,007$ Mm³ have been detected.

In chapter 2.1.5, varying models explaining the evolution of landslide failures after deglaciation have been proposed. Due to the lack of absolute dating of the deposits, a constant frequency model has been used, suggesting a constant distribution of rockslide events from deglaciation to present.

Based on a constant frequency model, 25 detected deposits, and a time span of 11500 years, the annual frequency of failure of volumes $\geq 0,007$ Mm³ is 0,0022, a recurrence rate of 455 years.

Volume-frequency distribution

The volume-frequency distribution is evaluated based on the distribution models suggested in chapter 3.5. The distribution is analyzed in a plot with cumulated number of events and a logarithmic distribution of volume size.

The distribution of volume-frequency of past events is best fit with a power-law model for volumes $\geq 0,020$ Mm³. The equation best fitted with accompanying exponents are seen in Figure 4.42.

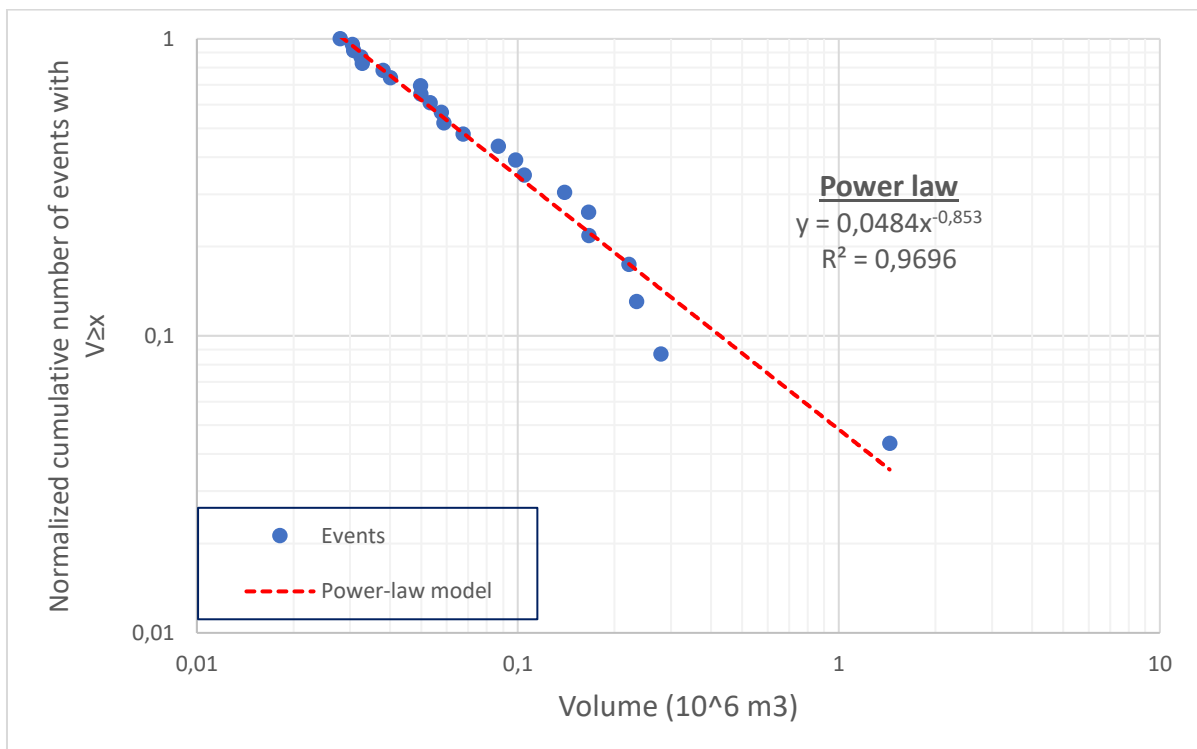


Figure 4.42: Plotted cumulated number of events against their volume size shows the best fit for the power-law model. The power-law equation is shown in the plot with accompanying exponents.

Volume-frequency estimation

A frequency estimation of varying volume classes is assessed based on the power-law equation best fitting the distribution and the annual frequency of failures after the last deglaciation. The estimation is shown in Table 4-11. The lowest volume class is not estimated due to the power-law tails only fitting volumes $\geq 0,02$ Mm³ in the volume-frequency distribution.

Table 4-11: Estimated annual frequency and recurrence rates for volume classes based on the power-law model and the annual frequency of past failures from Lifjellet.

Consequence class	Volume x Mm3	Nr. of deposits	Power law	Annual frequency	Recurrence rate
			$F(V>x) = (ax^{-b})$	$f(V>x,t) = f(V>x) * f(t)$	$1/f(V>x,t)$
1	≥0,005	25	-	-	-
2	≥0,02	23	1,362	$3,00 \times 10^{-3}$	334
3	≥0,250	2	0,158	$3,47 \times 10^{-4}$	2879

The resulting estimated frequencies of rock slope failures with a volume $\geq 0,02$ Mm3 shows a recurrence rate of 334 years. The estimated frequency of rock avalanches from the cliff of Lifjellet, which is defined as a volume above 250 000m3, has a recurrence rate of 2 879 years.

5 Discussion

5.1 Comparing the structural analyses

A validation of the structural analysis of field-measured structures is discussed based on a comparison with the regional lineament analysis obtained in chapter 4.1.2. The most prominent lineaments show the same spatial variation between domains as the resulting analysis of field data. The six lineament orientations detected in the field area is unevenly distributed, and the mid domain is the only domain where all structures could be mapped.

When discussing the significance of field-measured structures, a “rule of thumb” is used in the analysis classifying a structure as significant if the density concentration of a structure is above 4% (Rocscience, 2017b).

5.1.1 Western domain

In the western domain, there are three prominent lineament orientations. Two of them follow the orientation of significant structures in the analysis of field data, J3 and J6. The last prominent lineament is following the orientation of a not significant joint set, J5. A reason for the low significance of J5 can be explained by its rough surface, shown in chapter 4.3.2. Rough surfaces are difficult to detect and measure at a small-scale in the field since the average orientation of a larger area should be measured. This difficulty is connected to the lithology of the conglomeratic rock mass. Structures with a smoother surface are easier to detect and measure in the field, thus an error of the structural measuring might be the reason for the insignificant J5. A validation of the lineaments following the orientation of J5 mapped in the lineament map in Appendix C is assessed based on field observations. Lineaments are connected to steep cliffs with a favorable orientation showing a rough surface, exemplified by Figure 4.14 in chapter 4.3.2.

5.1.2 Mid domain

In the mid domain, the orientation of lineaments most prominent is following the orientation of J2 and J4, which is statistically significant joint sets in the mid domain. Two more prominent lineament orientations are detected following the orientations of J1 and J5, statistically insignificant structures in the mid domain. The largest deviation from the field data is the prominent lineament orientation of J5. J5 is not detected in the field data for the mid domain. Lineaments oriented as J5 can also in the mid domain be connected to steep cliffs with a favorable orientation and a rough surface.

The other prominent lineament insignificant in the analysis of field data is J1. Field observations of lineaments with this orientation indicates that the structure often is shown as depressions. Depressions are detected for the lineament analysis, but difficult to measure for the analysis of field data due to vegetation cover. This might be the reason for the deviation of detected field data compared to lineaments with orientations of J1.

5.1.3 Eastern domain

In the eastern domain, the orientation of the most prominent lineaments is following the orientation of the statistically significant joint sets, J3 and J4. Another prominent lineament is following the orientation of J1, a statistical insignificant structure in the analysis of field data. The deviation of J1 between the two analyses can be explained by the field observation, that of J1 is developed as a depression in the field. Another explanation for the large deviation of J1 is the uneven distribution of lineaments within the eastern domain, revealed in the lineament map in appendix C. Lineaments are mostly found in the southern end of the domain where no field data are collected, thus gives an error for the comparison of the structural analyses.

Another large deviation between compared analyses of the eastern domain is the lack of lineaments following the orientation of the significant joint set of J2. Field observations are verifying the existence of these structures along the cliff, shown in picture *c* in Figure 4.11. The lack of these lineaments suggests a lower persistence of the joint set in the eastern domain. Another finding in the lineament map in Appendix C is that lineaments following J2 are most prominent where the orientation of the lineaments lie parallel with the slope orientation. High numbers of lineaments in these areas might be due to stress release along the cliff opening structures with orientations following J2.

Results from the analysis of field data highlight a spatial variability of dip for J4 between the mid and eastern domain (chapter 4.1.1). By evaluating the results from the lineament analysis, there is seen a similar orientation of lineaments for both domains. The coinciding orientation of lineaments addresses the likelihood of these structures to be of the same joint set with a spatially changing dip towards the east.

5.1.4 Implications for the analyses

The only structure revealed in the structural analysis flatter than 70 degrees is the bedding plane of the sedimentary rock mass. The bedding is an insignificant structure in the analysis of field data. Reasons for the statistical insignificance of the bedding might be connected to

the lithology of the sedimentary conglomerate varying between a massive structure of large clasts to areas where the bedding is visible in small-scale. Quaternary processes like glacial scouring of the landscape is addressed in literature (chapter 1.5.2). The rounded landscape shaped by the glacial processes might be a reason for a lower number of flat structures visible in the field area. An increase in field measurements of flat-lying structures could have been assessed using the software Coltop3D. The software detects structural planes along the cliff face, using the photogrammetric model. This was excluded due to covering by vegetation and scree deposits. Also, the orientation of photos for the photogrammetric model, where all photos were taken from the fjord is reducing the cloud density along flat-lying structures.

The resulting structural analysis of field measurements has been computed using a “rule of thumb” classifying a structure as significant if the density concentration of a structure is above 4% unless the overall quantity of data is high (Rocscience, 2017b). Field investigations highlight insignificant structures as controlling structures of the unstable slopes in half of all locations assessed. Exemplified in location 6, J1 is assessed as structural control for both scenario 6.A and 6.B. In addition, the same structure is following the rock slide scar of the historic event from 1992 (Harbitz, 1999). In location 8, a back scarp with 2 meters opening is following the orientation of the statistically insignificant J5. The structure is clearly controlling the unstable slope. These findings highlight the need for an evaluation of the significance threshold set for the analysis of field data.

5.2 Structures controlling the unstable slopes

Structures controlling the deformation of unstable slopes are discussed based on the findings in chapter 4.4.2. The variability of structural controls between the divided domains is discussed.

5.2.1 Back scarp

There is a distinct correlation between structural domains and the detected orientations of back scarps for the unstable slopes. In the eastern domain, the back scarp is oriented either along J4 or J2. The slopes detached by J4 shows a distinct orientation of back scarps and can detach large slopes. At location 2 the back scarp is interpreted following one structure across the whole back scarp of the block, due to a persistent crack intersecting with the east flank. Orientations of J2 facilitates for a back scarp at location 3 and location 4. A spatial change in controlling structures is seen due to the change in slope orientation favoring orientations of J2. This is validated by detection of J2 as back scarp for all scenarios in the mid domain.

At the western domain, a change of orientation of back scarp is seen. Here, the combination of J3 and J6 creating back scarps are seen in location 7 and in scenario 8.A. At scenario 7.A, the back scarp following these structures is estimated to be 100m deep. Displacement measurements of the block reveal displacement rates below 0,2mm/year. Based on these findings, there is a reason to believe that blocks delimited by these structures will keep stable over a long period of rock bridge breaking after the cracks have been initiated at the surface. Another delimiting structure controlling back scarps in the western domain is J5. In scenario 8.B, the structure is dipping into the slope with an opening of 2 meters. The structure facilitates for toppling failures along the rough surface.

5.2.2 Lateral limits

In the eastern domain, the locations often have free flanks at one or two of the limits. This is seen in location 1,2 and 3. The limits not free is not well developed. Thin structures with stepwise breaking along J2 and J3 is seen, which indicates that the lateral limits are not structural controlled in the eastern domain. The importance of free flanks for the deformation of the slopes is validated by findings in location 3. The back scarp of scenario 3.C is well developed at the side where the flank is free, while the side where the flank is inclined, the back scarp is not developed (chapter 4.4.2).

When the orientation of the slope changes, J3 is seen as an important delimiting structure. Both in location 4 and for all scenarios in the western domain J3 controls the lateral limits of

the slope. In the mid domain, the structure is not detected as a delimiting structure in any of the slopes, coinciding with the results of the structural analyses which shows that the structure is not significant in the analysis of the field data nor prominent in the lineament analysis.

In the mid domain, J1 and J4 is the structures important for the lateral release of blocks. In location 6, J1 releases the eastern flank while J4 releases the western flank. The larger opening of structures along J4 might imply on the control of a slope. J1 is seen only as a depression when delimiting both scenario 6.A, 6.B and 5.A in the mid domain. The depression seen along the structure suggests low deformation and possibly small opening of the cracks. At location 5 field observations of the structure when intersecting the open cliff shows a weakness zone following the orientation with closely spaced cracks and highly fractured rock mass (chapter 4.4.2). The observation of this zone might be the reason for the structure seen as a depression. This also is a liable reason for the insignificant number of field data collected of this structure (chapter 4.1.1).

5.2.3 Toe lines

Toe lines are set along detected structures in the cliff face with large uncertainty. The largest uncertainty is connected to the slopes where the interpreted failure mechanism is toppling. This is due to the failure morphology of such slopes often not showing signs of activity before failure. This is assessed in location 6, where the toe of the scenarios is set considering possible weakness of the rock mass at two distinct structures in the cliff face (Figure 4.30). Such interpretation of toe lines increases the uncertainty of volume calculations of the slopes. For scenarios with failure kinematics showing planar sliding, the toe lines were set at depths where the rock mass had been through visible deformation. This because none of the scenarios were fully daylighting. A cliff face of 400m will show signs of changing lithology and variations in degree of fracturing, and a toe line is thus set with high uncertainty.

The importance of bedding planes as a structural control of the toe is interpreted at numerous locations. The breakage along such bedding planes are seen in small-scale in the field, highlighting the possibility of such failure (Figure 4.27). The importance of the bedding plane is due to the failure mechanism of direct toppling suggested for unstable slopes in all assessed domains. This is the only structure flatter than the frictional cone set for the rock type. Field observations of toe lines for toppling failures also indicate that the bedding plane is the controlling structure. This is due to the lack of rupture surface morphology at the toe. The bedding plane is not seen as a structure in the cliff face other than if failures have occurred along the plane.

5.3 Reduction of uncertainties of the hazard classification

Results from the application of the hazard classification system developed at NGU reveals a moderate hazard score for 12 of the 14 assessed scenarios distributed on 9 unstable slopes. Two of the scenarios obtained a low hazard score (Table 4-9).

A summary of uncertainties of the hazard assessment is shown in Table 5-1, based on the hazard assessment sheets for each scenario attached in Appendix D. A discussion is assessed for the hazard criteria connected to largest uncertainty, and possible improvements to reduce the uncertainties.

Table 5-1: Hazard criteria connected to uncertainties for each scenario is marked with X. The deviation between minimum and maximum hazard score is shown for a comparison with the attached uncertainties of each scenario. Table modified after Table 4-9.

Scenario	1. Back scarp	2. Sliding structures	3. Lateral release surface (left/right)	4. Kinematic feasibility	5. Rupture surface	6. Displacement rates (mm/year)	7. Acceleration	8. Increase in rockfall activity	9. Past events	Hazard score Deviation [min; max]	Hazard class (Low/Medium/High)
1.A				X		X	X			5,7 [4,8]	M
2.A	X			X		X	X			5,2 [4,5]	M
3.A		X	X			X	X			6,5 [5,3]	M
3.B		X	X			X	X			6,4 [4,7]	M
3.C	X	X				X	X			6,4 [6,0]	M
4.A			X		X	X	X			6,0 [6,0]	M
5.A			X		X	X	X	X		4,6 [5,5]	L
5.B				X	X	X	X	X		6,7 [5,5]	M
6.A		X			X					5,1 [2,0]	M
6.B		X			X					5,8 [1,2]	M
7.A			X		X			X		5,8 [3,2]	M
8.A	X				X	X	X			4,9 [5,0]	M
8.B					X	X	X			5,7 [5,0]	M
9.A	X		X		X	X	X			4,2 [6,0]	L

Table 5-1 shows which criteria that is most commonly assessed with uncertainties. Some key findings have been detected. Uncertainty is most commonly connected to criterion 6-7, displacement rates and acceleration. Another common uncertainty factor is criterion 5, the morphologic expression of rupture surface. The only criterion not connected to uncertainty is criterion 9, the presence of post-glacial events along the affected slope and its vicinity due to historic events in the vicinity in the 1990s (Harbitz, 1999). The deviation between minimum and maximum hazard scores for the scenarios express a good fit with the number of criteria attached to uncertainties.

Uncertainties connected to the assessment of displacement rates and acceleration is due to the lack of monitoring of scenarios, except for scenario 6.A, 6.B, and 7.A. For scenarios where displacement measurements are not assessed, standard values are used where a 30% probability is set for the conditions of no movement, movement of 0-0,5cm/year and movement of 0,5-1cm/year. A 10% probability is set to movement of 1-4cm/year. Future measuring of displacement can reduce the uncertainties of the criteria, and this will most likely reduce the hazard scores for scenarios where displacement rates are not measured. This can be validated by the results of the hazard classification for all scenarios where displacement rates were assessed. Exemplified with scenario 7.A, a reduction of the probability connected to displacement was reduced from the standard value to probability of zero due to not significant rates of displacement (appendix D).

The displacement rates obtained in scenario 7.A, insignificant displacement of a block with a certain structural control, reveals important knowledge for scenarios with the same controlling structures. Since scenario 7.A and 8.A is controlled by the same structures, the large-scale deformation along the back scarp of 7.A without significant displacement is likely to be seen for scenario 8.A.

Displacement rates can be assessed by monitoring with either extensometer or by dGNSS-measuring, described in chapter 3.3.2. All scenarios can be monitored by extensometer measuring of back scarps, but due to long measuring distances for scenario 9.A, dGNSS-measuring is here a more reliable method.

The expression of rupture surface is assessed with uncertainty in 9 of the 14 scenarios, due to the use of standard values when toppling is kinematically feasible. This is due to the possibility of no visible rupture surface at the toe before failure. A 50% probability is suggested for no indication of rupture surface, while 25% probability is attached to the

conditions “formation of rupture surface” and “continuous rupture surface”. The suggested higher score for this criterion than field observations reveal, can be validated based on results from the hazard assessment (chapter 4.4.2). Scenario 6.B shows significant displacement, which indicates deformation of the slope but without any visible rupture surface at the toe. In scenario 4.A, the back scarp reveals large deformation with a 20m depth of highly fractured rock mass, but still no visible rupture surface at the toe.

Uncertainties due to structural control of the slope is often connected to the morphologic expression of delimiting structures. Larger uncertainty is connected to structures interpreted along depressions than structures visible as cracks. Due to the interpretation of depressions, probabilities are divided between the conditions “open” and “partly open” in criteria 1 and 3. In general, depressions are connected to a less active deformation than open cracks, which can imply the failure mechanism of the slope. Observations of back scarps at scenario 2.A, 3.C and 8.A shows that open cracks delimit the back scarp at the eastern end of the block, while the back scarp is seen as a depression at the western side of the block. At both scenario 3.C and 8.A, the eastern flanks are open. The observed larger deformation at one flank than the other can be associated with not fully developed back scarps (Hermanns, *et al.*, 2012b). These findings are of interest when placing the instruments measuring displacement.

5.4 Frequency analysis

5.4.1 Applicability of post-glacial distribution model

The temporal distribution of rock slope failures is important for the evaluation of today's potential hazard. Temporal distributions over the Holocene era in Norway also shows a spatial distribution. In Northern Norway, absolute dating of rock avalanches has revealed a clustering of events right after deglaciation (Blikra, *et al.*, 2006b). Data from Storfjorden in Western Norway indicates a higher frequency of failures the last 5000 years, with a possible peak around 3000 years ago. These findings reveal that there is no distribution model best fitting all rock slope failures in general.

The frequency model used in this thesis is based on the constant frequency model due to the lack of absolute dating of rock slide deposits. For further investigations, a need for absolute dating is of importance. Absolute dating will give an exact distribution that will reveal the best fit model for post-glacial frequency in Aafjorden. Results based on the chosen frequency model is discussed against other frequency models and relevant existing literature from Norway (Blikra, *et al.*, 2006b, Böhme, *et al.*, 2015).

Frequency models can be evaluated based on the criteria set for each model. The exhaustion model facilitates slope failures along bedding planes which eliminates future failures of the same slope (Cruden & Hu, 1993)(chapter 2.1.5). Based on observations from Lifjellet, the bedding plane of the conglomeratic rock type is a plane with a shallow dip below the friction angle (chapter 4.3.1). The bedding plane is seen as a structural control on unstable slopes only when the suggested failure mechanism is toppling, and not as a sliding plane. Results of the assessment of past events also show multiple failures originate from the same source area (Figure 4.38). These observations exclude the possibility that the frequency of failures along the cliff of Lifjellet follows an exhaustion model.

The rapid response model suggests that all failures fail in a short period directly after deglaciation, while the frequency of failures after the first centuries are very infrequent (Evans & Clague, 1994). This temporal distribution is seen in Northern Norway, where the temporal distribution is clustering around the deglaciation while only one historic event has occurred in the county of Troms (Blikra, *et al.*, 2006b). Historic events from Aafjorden presented by Harbitz (1999) is showing a frequency of five slope failures within a period of 6 years in the 1990s, where two of the events had volumes above 20 000m³. This frequency of

historic events does not fit the rapid response model suggesting very infrequent failures for the last part of the Holocene era.

The most likely contestant to the constant frequency model is the combined rapid response model with a constant frequency model following the geological norm. This model is based on sediment yields after the last deglaciation (Church & Ryder, 1972). Ballantyne and Stone (2013) point out the removing of confining stresses as the reason for higher frequencies directly after deglaciation. Blikra, *et al.* (2006b) suggests high-magnitude earthquakes or permafrost melting as the main factor for coastal zones in the county of Møre og Romsdal. An implication for the model based on sediment yields is the possibility for a decrease in volumes but not in number of failures. Resulting relative dating of deposits from Aafjorden implies that although smaller deposits underlying larger deposits are not detectable do smaller deposits overlie larger deposits in all the three slope sections (chapter 4.5.1). This is similar to what Hermanns and Longva (2012) find in Storfjorden in Western Norway. It is also feasible that removing of confining stress is just increasing volumes of structural controlled failures, not necessarily inducing a higher frequency.

An argument for the use of the constant frequency model in this thesis is the importance of a conservative estimation of possible failure rates. The constant frequency model is the model with the highest estimated frequency of failures for both present and the future. The use of too low frequencies for the estimation of hazard might cause underestimations of the hazard.

5.4.2 Uncertainties and adjustments done to the used dataset

Uncertainties due to the mapping of deposits assessed in chapter 4.5.1 is connected to the covering of rock fall deposits covering the limits between underlying deposits, especially in the western cluster. Other uncertainties due to depositional characteristics are connected to the subduction of deposits in the fjord. A mix of rock avalanche deposits and valley-fill sediments are seen in trenches at a subducted rock avalanche in Innfjorddalen (Schleier, *et al.*, 2017). This mix suggesting covering of deposits by sediments causes implications for both mapping of fjord deposits and the volume estimation assessed by digital terrain models.

Uncertainties connected to the data available is attached to the evaluation of the “no value” area. The area between the two combined digital terrain models used for the assessment creates large areas where mapping is impossible. The possibility of a new deposit toe lying within this area increasing the frequency of failures must be addressed as an uncertainty for the number of past events. Uncertainty connected to the data assessed is also attached to the

methodology for validating the deposits mapped in the DEM with orthophotos, described in chapter 3.1.1. Orthophotos where the slope direction of the cliff is facing north, shadows from the cliff is covering the depositing area making validation of the deposits found in the digital terrain model impossible.

Limitations for the estimation of deposit volumes are attached to the limited time of access to bathymetric data due to security restrictions. A method for a better adjustment of partly overlapping deposit volumes could be assessed with more time, where an intersection-tool can calculate the area overlapping, and then calculate the volume of this overlapping area by using the SLBL data computed for the overlying deposit. Then, a reduction of the underlying volume can be assessed by reducing the total volume with this estimated value. This method for reducing the volume will be more accurate since an overlying deposit can vary in thickness both in the length and width of the deposit.

An important limitation for the volume estimation is the calculation of the “no value” area. This area is the data in the combined DEM that lies between the subaerial DEM and the bathymetric DEM, an area that is not scanned because of the shallow water. The area stretches at the most 70m in length of the deposit. The size of uncertainties connected to this possible miscalculation is largest for the small deposits since the uncertainty area is as large as the estimated area. Estimation uncertainties are in the range of at least a factor of 2 or possibly of magnitude scale. The method used for the calculation of the “no value” area is based on the average thickness obtained from the bathymetric estimation multiplied by the area of “no value”, as described in chapter 3.4.1. The reason for the use of bathymetric data as input for this calculation is that some events do not deposit any mass within the aerial DEM, such as seen in the eastern cluster (chapter 4.5.1). And if the events deposit only in the aerial DEM, as seen in the eastern cluster, the “no value area” is not calculated. Since the aim for the assessment of deposit volumes are to compare the volumes and divide them into volume classes, a similar method must be used for all deposits.

An adjustment of the volume calculation of overlaying deposits had to be assessed manually based on a non-functional method of dividing stratigraphic deposited events. A regression method was used to calculate the underlying volumes, described in chapter 3.4.1. This method calculates the total volume of all stratigraphic deposited volumes, and then subtracts the overlying deposits. In the calculations of deposit 20 and 22, the resulting estimated volumes were negative, which is an error of the method. In these cases, a qualitative alignment to comparable deposits was done based on deposit thickness and run-out length.

5.5 Quantification of hazard

Due to quantitative thresholds set for the Norwegian regulations on technical requirements for structures (TEK17), quantitative probabilities of the unstable slopes must be assessed. Two methods for quantitative assessment of the unstable slopes are presented in chapter 3.6.

Uncertainties attached to the quantification methods makes for a discussion of the best fit probabilities for the unstable slopes.

5.5.1 Norwegian conversion method

The Norwegian conversion method is based on qualitative hazard scores from 22 unstable slopes in Norway (Hermanns, *et al.*, 2016). Considerations of this dataset are described in chapter 2.5.1. Only the scenario estimated to the highest hazard score from each location in the qualitative hazard assessment is shown in Figure 5.1, represented with their related hazard scores. The quantitative probability thresholds for the safety classes S1, S2 and S3 are drawn following the considerations in Blikra, *et al.* (2016).

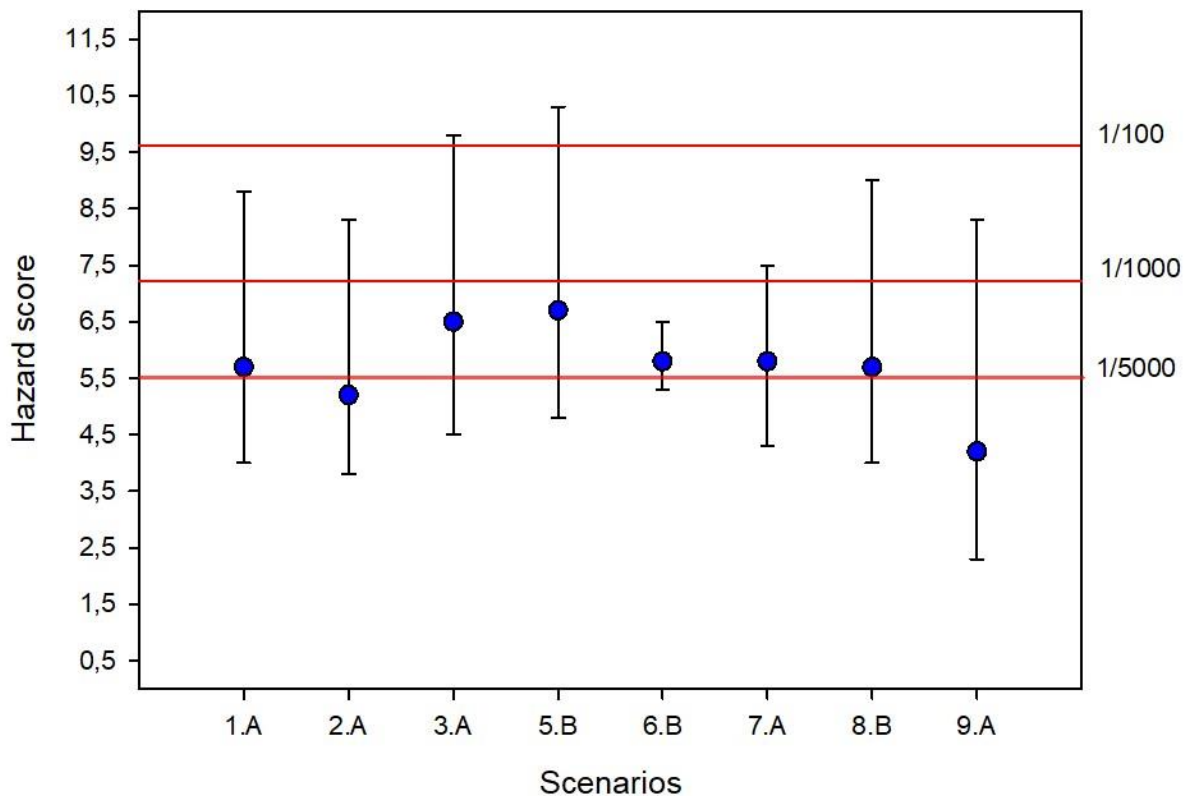


Figure 5.1: The scenarios with estimated highest hazard scores of each location displayed by their mean hazard score, and max and min values as uncertainty limits. Thresholds (red lines) represents an annual probability for the safety classes S1, S2 and S3.

The figure shows that 6 scenarios due to their hazard scores have an annual probability exceeding the threshold for 1/5000.

Both hazard scores and the annual probability follows a logarithmic scale. To define the exact probability for each hazard score, a calculation must be done following the methodology described in chapter 3.6.1. The estimated annual probabilities and recurrence rates for each scenario based on their hazard score is shown in Table 5-2.

Table 5-2: The estimated annual probability for each of the scenarios most likely to fail and for the whole cliff, based on their hazard score and the conversion of Blikra, *et al.* (2016).

Scenario	Hazard score, mean [min; max]	Annual probability, mean [min; max]
1.A	5,7 [4,0; 8,8]	1/4131 [1/20919; 1/215]
2.A	5,2 [3,8; 8,3]	1/6657 [1/25318; 1/346]
3.A	6,5 [4,5; 9,8]	1/1926 [1/12982; 1/83]
5.B	6,7 [4,8; 10,3]	1/1591 [1/9751; 1/51]
6.B	5,8 [5,3; 6,5]	1/3755 [1/6051; 1/1926]
7.A	5,8 [4,3; 7,5]	1/3755 [1/15712; 1/742]
8.B	5,7 [4,0; 9,0]	1/4131 [1/20919; 1/177]
9.A	4,2 [2,3; 8,3]	1/17285 [1/105924; 1/346]
Total		1/421 [1/1808; 1/20]

By adding the annual probability of failure for each unstable slope, an annual probability for the whole cliff is estimated to 1/421 years. The annual probability of unstable slopes is similar to the annual frequency of past events estimated in chapter 4.5.3 which shows 1/455.

5.5.2 Empirical analysis

A quantitative hazard for each of the scenarios with highest hazard score has been estimated based on a relative susceptibility calculated from the qualitative hazard scores, and the annual frequency of past events for each volume class. The calculation of relative susceptibility is described in chapter 3.6.2, while the qualitative hazard scores were defined in chapter 4.4.5. Annual frequencies of past events are calculated in chapter 4.5.3. The method assumes that the inventory of unstable slopes and the inventory of deposits is complete and is described in chapter 3.6.2.

Table 5-3: Estimation of the quantitative annual hazard for each scenario based on the annual frequencies of past events for each volume class, and the relative susceptibility of failure within the volume class.

Volume class (Mm3)	Volume(Mm3) min/max	Scenario	Annual freq. ($x1 < V < x2$)	Hazard score (r_i)	Relative susceptibility	Quantitative annual hazard
	0,006	4.A	-	6	-	-
0,020-0,250	0,040	8.B	1/377	5,7	0,160	1/2361
0,020-0,250	0,025/0,041	6.B	1/377	5,8	0,162	1/2321
0,020-0,250	0,090/0,239	5.B	1/377	6,7	0,188	1/2009
0,020-0,250	0,116/0,195	7.A	1/377	5,8	0,162	1/2321
0,020-0,250	0,149	2.A	1/377	5,2	0,146	1/2588
0,020-0,250	0,151	3.A	1/377	6,5	0,182	1/2071
$\geq 0,250$	0,597	1.A	1/2879	5,7	0,576	1/5000
$\geq 0,250$	2,595	9.A	1/2879	4,2	0,424	1/6786

Scenarios estimated as rock avalanches lie outside the threshold for the hazard class S3. Rock slope failures with an estimated quantitative hazard below 1/5000 do not require further follow-up based on the limits given in TEK17. All six rock slope failures in the volume class 0,020-0,250 show a quantitative hazard above the threshold for S3. Thus, consequences of a failure need to be assessed, followed by hazard zonation of the shores around Aafjorden.

5.5.3 Applicability of the quantification methods

The results of the empirical analyzes assume that the inventory for unstable slopes is complete. Detecting unstable slopes is part of the NGU mapping approach described in chapter 2.4. The detection process used is through remote sensing techniques such as digital elevation models based on airborne LiDAR, aerial orthophotos, and satellite-based radar interferometry. In this thesis, also a photogrammetric model of the cliff face and extensive field work is carried out in order to detect unstable slopes. The methodology for the estimation of quantitative probabilities of instabilities highlights that the analysis is not assessing the full number of scenarios (Chapter 3.6.2). This is because if the largest scenario fails first, the rest of the sub-scenarios cannot fail any longer. Considering this understanding, there is a chance of smaller scenarios failing multiple times from the same location giving an increased number of possible failures within a low volume class, while it creates a decreasing number of scenarios within the larger volume class. This implication alone is subject to large uncertainties for the assessment as the number of sub-scenarios might not be possible to determine today as they might develop over millennia.

The Norwegian conversion method suggested by Blikra, *et al.* (2016) is a quantification based on a dataset of 22 unstable slopes. There are large uncertainties connected to such small datasets. Implications for the dataset pointed out by Hermanns, *et al.* (2016), is that the sites used in the data set are the sites with most public attention. Therefore, it is expected that it will contain a large number of high-risk sites. A re-evaluation of the dataset when all scenarios detected are classified, will reduce the uncertainties attached to the dataset. Other uncertainties of the conversion are the large uncertainties connected to the qualitative hazard scores, discussed in chapter 5.3. The uncertainties of the resulting probabilities for some scenarios is of 3 magnitudes (Table 5-2). Most of these uncertainties are reduced by periodic displacement monitoring as discussed in chapter 5.3, but still, the scenario with monitored displacement, scenario 6.B, shows probabilities varying with 4000 years for the quantitative hazard. The resulting annual probability for the cliff is connected to the same uncertainties considering the completeness of the inventory as the empirical analysis.

5.6 Differing volume sizes of the assessed inventories

An analysis of volume-frequency distributions for unstable slopes compared to the volume-frequency distributions of past events are assessed to consider if the volume calculations of unstable slopes are over- or underestimated.

Normalized cumulated numbers and related volume sizes for the deposits and both largest and smallest calculated volumes of the unstable slopes are shown in a log-log plot (Figure 5.2).

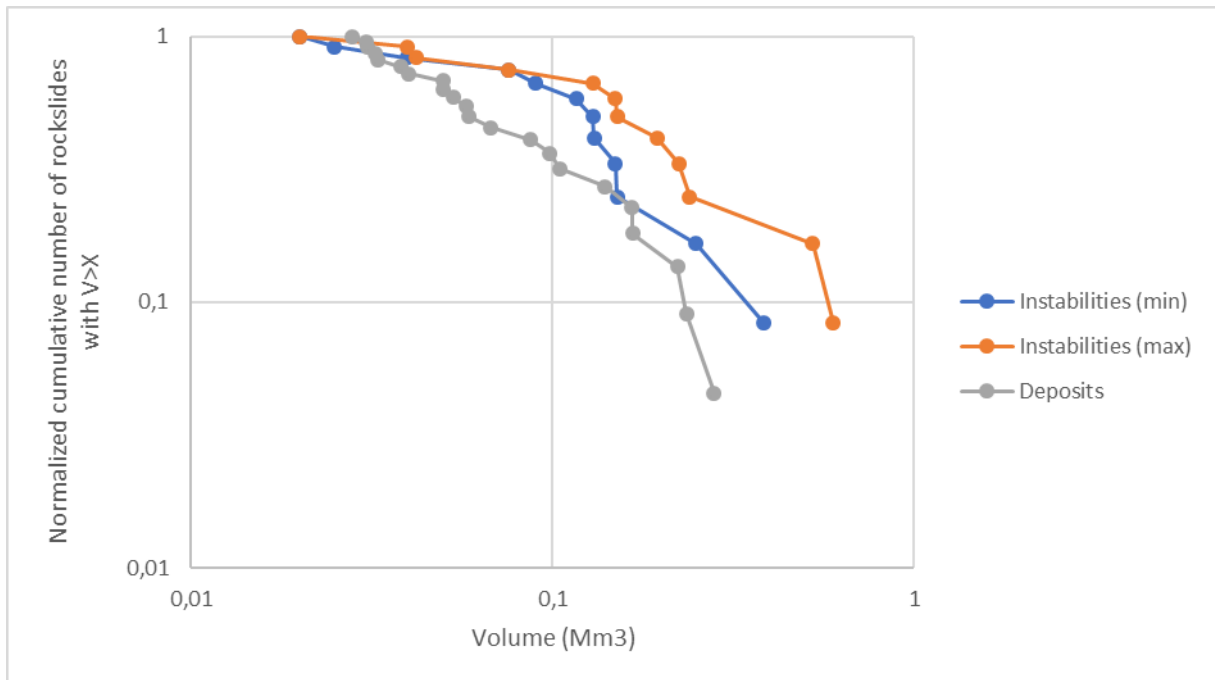


Figure 5.2: Volume-frequency distribution of the cumulated number of past events compared to the minimum and maximum calculated volumes of unstable slopes.

The results show that the volume-normalized cumulative number of rockslides of unstable slopes differ significantly from the analyzed deposit curve. The deviation in the distribution of volumes highlights the possibility of an overestimation of volumes calculated for unstable slopes. This due to at least a factor of volume difference between most cumulative numbers of unstable slopes and deposits (Figure 5.2).

Reasons for a potential overestimation of the volumes might be because unstable slopes will not fail as delimited today but will decompose in smaller departments prior to failure. This deformation of the slope can occur due to the failure of rock bridges between various failure surfaces connecting a more complex surface morphology, as addressed in chapter 2.1.3. The assessment of unstable slopes (chapter 4.4.2) highlights the presence of complex surface morphologies such as:

- bi-planar failure
- active-passive footwall
- multi-planar failure

To consider if the slope is controlled by one of the more complex surface morphologies mentioned, other surveying methods must be introduced. Borehole drilling can be used to detect potential sliding planes at various points on an unstable slope, while displacement measurements of the boreholes can define the active sliding planes (Wyllie, *et al.*, 2004).

6 Conclusion

6.1 Controlling structures and hazard classification

Main conclusions of structural analyses and the inventory assessing unstable slopes are summarized with the following remarks:

- Based on remote sensing using aerial photos and Digital Elevation Models as well as field work, a total of nine unstable slopes were detected along the cliff. Within the nine slopes, fourteen scenarios were established based on varying structural controls and displacement rates, with volumes ranging from 0,006 to 2,595 Mm³.
- Based on an analysis of stereoplots retrieved from 44 spatially distributed measuring stations, the field area has been divided into three domains. Structural analyses of both field-based measurements and regional lineaments extracted from the DEM of each domain was carried out. Joint sets not statistically significant in the analysis of field data, but prominent in the lineament analysis is **highlighted**. Structures represented in each domain are:
 - Western domain: J3 (073/85), **J5 (159/70)**, J6 (360/88)
 - Mid domain: **J1 (294/88)**, J2 (010/88), J4 (266/89)
 - Eastern domain: J2 (190/85), J3 (248/90), J4 (087/68)

The bedding plane of the sedimentary rock is detected in the field, but it is not a structure with a significance level above the “rule of thumb” in the analyzed field data. The mean orientation of the bedding within the highlighted domains is hence (259/13), (245/03) and (048/15), respectively.

- Kinematic analyses of possible failure mechanisms were carried out based on the structures represented within each domain. Findings for each domain are:
 - Western domain: Planar sliding and wedge sliding possible, and oblique toppling possible within variations of the sediment bedding.
 - Mid domain: Planar sliding, wedge sliding, and direct toppling is possible within variations of the significant structures.
 - Eastern domain: Planar sliding, wedge sliding, and oblique toppling is possible.
- Final hazard classifications conclude that 12 of the 14 scenarios obtained mean hazard scores within the medium hazard class. Scenario 5.A and 9.A are placed within the low hazard class. Scenarios with the lowest uncertainties are scenario 6.A, 6.B, and

7.A. These have been monitored by extensometers and dGNSS-measuring reducing uncertainties of the criteria considering displacement rates.

- Due to the Norwegian conversion method, 9 of the scenarios have an annual probability exceeding the quantitative threshold for safety class 3. The other scenarios do not require further follow-up based on the thresholds set in TEK17.
- Run-out estimations conclude that all scenarios detected along the cliff will reach the water body of Aafjorden.

6.2 Inventory of past events and conducted frequencies

Main findings of the mapping of deposits and estimated regional frequencies are summarized with the following remarks:

- Based on the interpretation of bathymetric data and subaerial interpretation of the shore, 25 deposits from rock slope failures were detected. Estimated volumes range from 0,007 to 1,919 Mm³.
- Based on number of events and a constant frequency model for the period after the last deglaciation, rock slope failures $\geq 6000\text{m}^3$ have a recurrence rate of 455 years.
- Volume-frequency distributions of detected deposits were analyzed, best fit to an inverse power-law distribution model. Estimated annual frequencies of deposit volumes above certain volume thresholds are:
 - Rock slope failures ($\geq 0,020\text{Mm}^3$): $1 / 334$ years
 - Rock avalanches ($\geq 0,250\text{Mm}^3$): $1 / 2879$ years
- Quantitative hazard for scenarios based on resulting regional frequencies and the susceptibility of hazard scores within a certain volume class have been discussed. Large uncertainties are connected to the degree of completeness of the assessed inventories of unstable slopes and deposits.

6.3 Further investigations

Recommended further investigations aim to reduce uncertainties of the thesis and carry through final steps of the hazard and consequence assessment of the unstable slopes.

Recommendations are listed as follows:

- Uncertainties due to the hazard classification can be reduced by periodic monitoring of displacement rates. All scenarios can be monitored by extensometer measuring of

back scarps, but due to long measuring distances for scenario 9.A, dGNSS-measuring is here a more reliable method.

- A completion of the hazard and consequence assessment considering the cliff of Lifjellet will need detailed run-out modeling estimating the volume of the potential failures actually reaching the water body. These volumes are used for the subsequent displacement wave analysis considering run-up at the shores along Aafjorden. Based on the run-up, an element at risk analysis can be assessed considering the number of inhabitants affected.

Bibliography

- Aa, A. R. (1985) *Askvoll : beskrivelse til kvartærgeologisk kart 1117 IV - M 1:50 000 (med fargetrykt kart)*. Trondheim: Universitetsforlaget.
- Aarseth, I. and Mangerud, J. (1974) Younger Dryas end moraines between Hardangerfjorden and Sognefjorden, western Norway, *Boreas*, 3(1), pp. 3-22.
- Abele, G. (1974) Bergsturze in den Alpen. Ihre Verbreitung, Morphologie und Folgeerscheinungen, *Wiss. Alpenvereinshefte*, 25. Available at: <https://ci.nii.ac.jp/naid/10027718994/en/>.
- Austrheim, H., Corfu, F., Bryhni, I. and Andersen, T. B. (2003) The Proterozoic Hustad igneous complex: a low strain enclave with a key to the history of the Western Gneiss Region of Norway, *Precambrian Research*, 120(1), pp. 149-175. doi: [https://doi.org/10.1016/S0301-9268\(02\)00167-5](https://doi.org/10.1016/S0301-9268(02)00167-5).
- Ballantyne, C. K. and Stone, J. O. (2013) Timing and periodicity of paraglacial rock-slope failures in the Scottish Highlands, *Geomorphology*, 186, pp. 150-161. doi: <https://doi.org/10.1016/j.geomorph.2012.12.030>.
- Blikra, L., Braathen, A. and Skurtveit, E. (2001) Hazard evaluation of rock avalanches; the Baraldsnes–Oterøya area, *Geological Survey of Norway (NGU), Report*, (2001.108).
- Blikra, L., Majala, G., Anda, E., Berg, H., Eikenæs, O., Helgås, G., Oppikofer, T., Hermanns, R. and Böhme, M. (2016) Fare-og risikoklassifisering av ustabile fjellparti. Faresoner, arealhandtering og tiltak *NVE Report 77/2016, Norwegian Water Resources and Energy Directorate, Oslo*.
- Blikra, L. H., Anda, E., Høst, J. and Longva, O. (2006a) *Åknes/Taffjord-prosjektet: Sannsynlighet og risiko knyttet til fjellskred og flodbølger fra Åknes og Hegguraksla*. (2006.039). Trondheim: NGU.
- Blikra, L. H., Longva, O., Braathen, A., Anda, E., Dehls, J. F. and Stalsberg, K. (2006b) Rock slope failures in Norwegian fjord areas: Examples, spatial distribution and temporal pattern in Evans, S. G., *et al.* (ed.) *Landslides from Massive Rock Slope Failure*. Netherlands: Springer, pp. 475-496.
- Bungum, H., Lindholm, C. and Faleide, J. I. (2005) Postglacial seismicity offshore mid-Norway with emphasis on spatio-temporal–magnitudal variations, *Marine and Petroleum Geology*, 22(1), pp. 137-148. doi: 10.1016/j.marpetgeo.2004.10.007.
- Böhme, M., Saintot, A., Henderson, I. H., Henriksen, H. and Hermanns, R. L. (2011) Rock slope instabilities in Sogn and Fjordane County, Norway: a detailed structural and geomorphological analysis, *Geological Society, London, Special Publications*, 351(1), pp. 97-111.
- Böhme, M., Hermanns, R. L., Oppikofer, T., Fischer, L., Bunkholt, H. S. S., Eiken, T., Pedrazzini, A., Derron, M.-H., Jaboyedoff, M., Blikra, L. H. and Nilsen, B. (2013) Analyzing complex rock slope deformation at Stampa, western Norway, by integrating geomorphology, kinematics and numerical modeling, *Engineering Geology*, 154, pp. 116-130. doi: <https://doi.org/10.1016/j.enggeo.2012.11.016>.
- Böhme, M., Oppikofer, T., Longva, O., Jaboyedoff, M., Hermanns, R. and Derron, M.-H. (2015) Analyses of past and present rock slope instabilities in a fjord valley: Implications for hazard estimations, *Geomorphology*, 248, pp. 464-474.
- Böhme, M., Bunkholt, H., Dehls, J., Oppikofer, T., Hermanns, R., Dalsegg, E., Kristensen, L., Lauknes, T. and Eriksen, H. (2016) Geologisk modell og fare-og risikoklassifisering av det ustabile fjellpartiet Gamanjunni 3 i Manndalen, Troms, *NGU Rapport*, pp. 64.

- Charrière, M., Humair, F., Froese, C., Jaboyedoff, M., Pedrazzini, A. and Longchamp, C. (2015) *From the source area to the deposit: Collapse, fragmentation, and propagation of the Frank Slide*. Geological Society of America Bulletin.
- Church, M. and Ryder, J. M. (1972) Paraglacial Sedimentation; A Consideration of Fluvial Processes Conditioned by Glaciation, *Geological Society of America Bulletin*, 83(10), pp. 3059-3072. doi: 10.1130/0016-7606(1972)83[3059:PSACOF]2.0.CO
- Clague, J. J. (2013) Landslide, in Bobrowsky, P. T. (ed.) *Encyclopedia of Natural Hazards*. Dordrecht: Springer Netherlands, pp. 594-602.
- CloudCompare (2018) CloudCompare (version 2.9.1) [GPL software]. Available at: <http://www.cloudcompare.org/>.
- Corominas, J. (1996) The angle of reach as a mobility index for small and large landslides, *Canadian Geotechnical Journal*, 33(2), pp. 260-271. doi: 10.1139/t96-005.
- Crosta, G., Hermanns, R., Dehls, J., Lari, S. and Sepulveda, S. (2017) Rock avalanches clusters along the northern Chile coastal scarp, *Geomorphology*, 289, pp. 27-43.
- Crosta, G. B., Frattini, P. and Fusi, N. (2007) Fragmentation in the Val Pola rock avalanche, Italian Alps, *Journal of Geophysical Research: Earth Surface*, 112(F1).
- Cruden, D. and Hu, X. (1993) Exhaustion and steady state models for predicting landslide hazards in the Canadian Rocky Mountains, *Geomorphology*, 8(4), pp. 279-285.
- De Blasio, F. V. (2011) Landslides in Peculiar Environments *Introduction to the Physics of Landslides: Lecture notes on the dynamics of mass wasting*. Dordrecht: Springer Netherlands, pp. 223-261.
- ESRI (2017) ArcGIS 10.5. Redlands, California: ESRI. Available at: <https://www.esri.com/en-us/home> (Accessed: 26.09.2017).
- Evans, S. and Gardner, J. (1989) Geological hazards in the Canadian Cordillera, *Quaternary Geology of Canada and Greenland*. (R.J. Fulton, ed.) Geological Survey of Canada, (1), pp. 702-713.
- Evans, S. G. and Clague, J. J. (1994) Recent climatic change and catastrophic geomorphic processes in mountain environments, *Geomorphology*, 10(1), pp. 107-128. doi: [https://doi.org/10.1016/0169-555X\(94\)90011-6](https://doi.org/10.1016/0169-555X(94)90011-6).
- Fell, R., Ho, K., Lacasse, S. and Leroi, E. (2005) *A framework for landslide risk assessment and management*. Proceedings, International Conference on Landslide Risk Management, May 31-Jun 3.
- Fossen, H., Dallman, W., Andresen, A. and Ramberg, I. (2008a) The mountain chain rebounds and founders. The Caledonides are worn down: 405–359 million years, *The Making of a Land. Norwegian Geological Association, Trondheim*, pp. 232-259.
- Fossen, H., Pedersen, R. B., Bergh, S. and Andresen, A. (2008b) Creation of a mountain chain. The building up of the Caledonides: about 500-405 Ma, *The Making of a Land. Norwegian Geological Association, Trondheim*, pp. 178-229.
- Frattini, P., Crosta, G. B. and Agliardi, F. (2012) Rockfall characterization and modeling, *Landslides: types, mechanisms and modeling*, pp. 267.
- Haas, F., Heckmann, T., Wichmann, V. and Becht, M. (2012) Runout analysis of a large rockfall in the Dolomites/Italian Alps using LIDAR derived particle sizes and shapes, *Earth Surface Processes and Landforms*, 37(13), pp. 1444-1455.
- Hacker, B. R., Andersen, T. B., Root, D. B., Mehl, L., Mattinson, J. M. and Wooden, J. L. (2003) Exhumation of high-pressure rocks beneath the Solund Basin, Western Gneiss Region of Norway, *Journal of Metamorphic Geology*, 21(6), pp. 613-629.
- Harbitz, C. B., Pedersen, G. and Gjevik, B. (1993) Numerical Simulations of Large Water Waves due to Landslides, *Journal of Hydraulic Engineering*, 119(12), pp. 1325-1342. doi: 10.1061/(ASCE)0733-9429(1993)119:12(1325).

- Harbitz, C. B. (1999) *Vurdering av skredfare og bølgehøyder i Åfjorden*. (981014-1): Norwegian Geological Institute.
- Harbitz, C. B., Domaas, U. and Varlid, E. (2001) Rock slide generated tsunamis - probability and hazard zoning in Åfjorden, western Norway., *Fjellsprengningsteknikk - bergmekanikk - geoteknikk. Oslo 2001*. Pp. 27.1 - 27.13.
- Harbitz, C. B., Glimsdal, S., Løvholt, F., Kvelde, V., Pedersen, G. K. and Jensen, A. (2014) Rockslide tsunamis in complex fjords: From an unstable rock slope at Åkerneset to tsunami risk in western Norway, *Coastal Engineering*, 88, pp. 101-122.
- Hermanns, R., Hansen, L., Sletten, K., Böhme, M., Bunkholt, H., Dehls, J., Eilertsen, R., Fischer, L., L'Heureux, J. and Høgaas, F. (2012a) Systematic geological mapping for landslide understanding in the Norwegian context, *Landslide and engineered slopes: protecting society through improved understanding*. Taylor & Francis Group, London, pp. 265-271.
- Hermanns, R., Oppikofer, T., Anda, E., Blikra, L., Böhme, M., Bunkholt, H., Crosta, G., Dahle, H., Devoli, G. and Fischer, L. (2012b) Recommended hazard and risk classification system for large unstable rock slopes in Norway, *NGU report*, (2012.029).
- Hermanns, R., Oppikofer, T., Molina, F. X. Y., Dehls, J. F. and Böhme, M. (2014a) *Approach for Systematic Rockslide Mapping of Unstable Rock Slopes in Norway*. Cham. Springer International Publishing.
- Hermanns, R., Oppikofer, T., Roberts, N. and Sandøy, G. (2014b) *Catalogue of Historical Displacement Waves and Landslide-Triggered Tsunamis in Norway*. Cham. Springer International Publishing.
- Hermanns, R., Oppikofer, T., Böhme, M., Dehls, J., Molina, F. and Penna, I. (2016) Rock slope instabilities in Norway: First systematic hazard and risk classification of 22 unstable rock slopes from northern, western and southern Norway, *Proceedings landslides and engineered slopes. Experience, theory and practice: proceedings of the 12th international symposium on landslides, Napoli, Italy*. pp. 12-19.
- Hermanns, R. L. and Longva, O. (2012) Rapid rock-slope failures, in Stead, D. and Clague, J. J. (ed.) *Landslides: types, mechanisms and modeling*. Cambridge: Cambridge University Press, pp. 59-70.
- Hermanns, R. L. (2013) Landslide Dam, in Bobrowsky, P. T. (ed.) *Encyclopedia of Natural Hazards*. Dordrecht: Springer Netherlands, pp. 602-606.
- Hermanns, R. L., L'Heureux, J.-S. and Blikra, L. H. (2013a) Landslide Triggered Tsunami, Displacement Wave, in Bobrowsky, P. T. (ed.) *Encyclopedia of Natural Hazards*. Dordrecht: Springer Netherlands, pp. 611-615.
- Hermanns, R. L., Oppikofer, T., Anda, E., Blikra, L. H., Böhme, M., Bunkholt, H., Crosta, G. B., Dahle, H., Devoli, G. and Fischer, L. (2013b) Hazard and risk classification for large unstable rock slopes in Norway, *Ital J Eng Geol Environ. doi*, 10, pp. 2013-2006.
- Highland, L. and Bobrowsky, P. T. (2008) *The landslide handbook: a guide to understanding landslides*. US Geological Survey Reston.
- Hoek, E. and Bray, J. (1981) *Rock slope engineering*. Rev. 3rd ed. edn. London: The Institution of Mining and Metallurgy.
- Hughes, A. L. C., Gyllencreutz, R., Lohne, Ø. S., Mangerud, J. and Svendsen, J. I. (2016) The last Eurasian Ice Sheets - a chronological database and time-slice reconstruction, *Boreas*, 45(1), pp. 1-45.
- Hungr, D. and Evans, S. G. (2004) Entrainment of debris in rock avalanches: An analysis of a long run-out mechanism *Geol. Soc. Am. Bull.* (vol. 116, pp. 1240-1252).

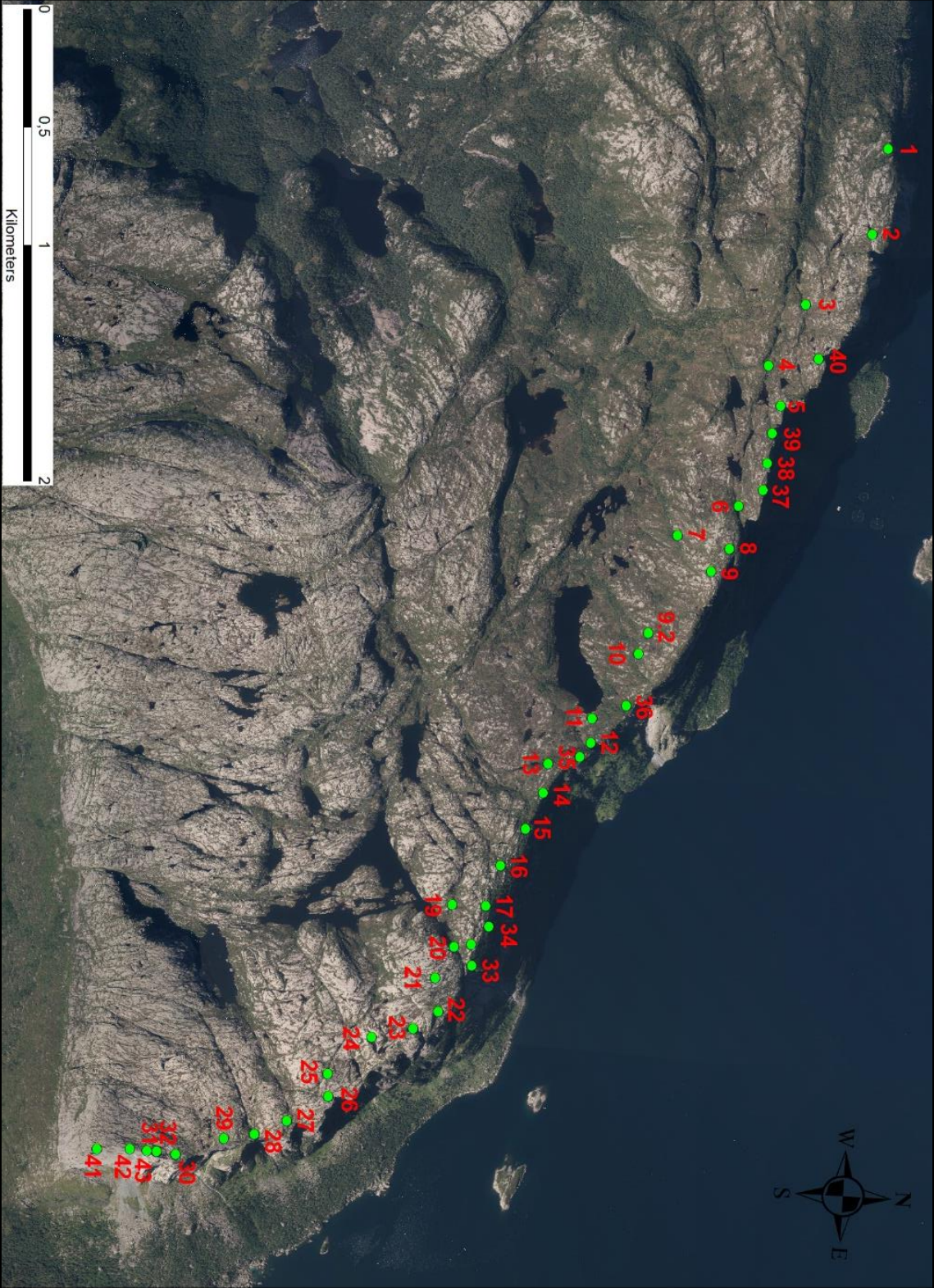
- Hungr, O. and Evans, S. (1989) *Engineering aspects of rockfall hazards in Canada*. Thurber Consultants Limited.
- Hungr, O., Leroueil, S. and Picarelli, L. (2014) The Varnes classification of landslide types, an update *Landslides* (vol. 11, pp. 167-194). doi: 10.1007/s10346-013-0436-y.
- Jaboyedoff, M., Derron, M.-H., Pazzaglia, F. J. and Dramis, F. (2005) A new method to estimate the infilling of alluvial sediment of glacial valleys using a sloping local base level (vol. 28, pp. 37-46). Turin: Turin, Italy: Comitato Glaciologico Italiano.
- Jaboyedoff, M., Oppikofer, T., Abellán, A., Derron, M.-H., Loye, A., Metzger, R. and Pedrazzini, A. (2012) Use of LIDAR in landslide investigations: a review, *Journal of the International Society for the Prevention and Mitigation of Natural Hazards*, 61(1), pp. 5-28. doi: 10.1007/s11069-010-9634-2.
- Jaboyedoff, M., Derron, M., Rudaz, B., Oppikofer, T., Penna, I. and Daicz, S. (2015) A review of geometrical methods for determination of landslide volume and failure surface geometry, *Proceedings of the 68th Canadian Geotechnical Conference GEOQuébec 2015-Challenges from North to South*.
- Keefer, D. K. (1984) Landslides caused by earthquakes, *Geological Society of America Bulletin*, 95(4), pp. 406-421.
- Kveldsvik, V. (1998) *Vurdering av rasfare ved Katlenova og Liffjellet*. Norwegian Geological Institute.
- Li, X. Q., Chen, Z. a., Zhang, L. T. and Jia, D. (2016) Construction and Accuracy Test of a 3D Model of Non-Metric Camera Images Using Agisoft PhotoScan, *Procedia Environmental Sciences*, 36, pp. 184-190. doi: 10.1016/j.proenv.2016.09.031.
- Malamud, B. D., Turcotte, D. L., Guzzetti, F. and Reichenbach, P. (2004) Landslide inventories and their statistical properties, *Earth Surf. Process. Landf.*, 29(6), pp. 687-711. doi: 10.1002/esq.1064.
- Michoud, C., Abellan, A., Derron, M.-H. and Jaboyedoff, M. (2010) *SafeLand deliverable 4.1, 2010. Review of Techniques for Landslide Detection, Fast Characterization, Rapid Mapping and Long-Term Monitoring*. Edited for the SafeLand European project by Michoud C., Abellán A., Derron M.-H. and Jaboyedoff M. Available at <http://www.safeland-fp7.eu>.
- NGU (2017) *Nasjonal database for ustabile fjellparti*. Available at: http://geo.ngu.no/kart/ustabilefjellparti_mobil/ (Accessed: 06.10 2017).
- Norwegian Meteorological Institute (2018) *eKlima*. Available at: http://sharki.oslo.dnmi.no/portal/page?_pageid=73,39035,73_39049&_dad=portal&_schema=PORTAL (Accessed: 30.01.2018).
- NVE (2018) *Skredhendelser*. Available at: <https://temakart.nve.no/link/?link=SkredHendelser> (Accessed: 29.01.2018).
- Oppikofer, T., Saintot, A., Otterå, S., Hermanns, R. L., Anda, E., Dahle, H. and Eiken, T. (2013) Investigations on unstable rock slopes in Møre og Romsdal - status and plans after field surveys in 2012, *Geological Survey of Norway (NGU), Report*, (2013.014).
- Oppikofer, T., Nordahl, B., Bunkholt, H., Nicolaisen, M., Jarna, A., Iversen, S., Hermanns, R. L., Böhme, M. and Yugsi Molina, F. X. (2015) Database and online map service on unstable rock slopes in Norway — From data perpetuation to public information, *Geomorphology*, 249, pp. 69-81. doi: 10.1016/j.geomorph.2015.08.005.
- Oppikofer, T., Böhme, M., Nicolet, P., Penna, I. and Hermanns, R. (2016) Metodikk for konsekvensanalyse av fjellskred, *NGU Report 2016.047*.
- Oppikofer, T., Hermanns, R., Roberts, N. and Böhme, M. (2018) SPLASH: semi-empirical prediction of landslide-generated displacement wave run-up heights, *Geological Society, London, Special Publications*, 477, pp. SP477.471. doi: 10.1144/SP477.1.

- Petley, D., Clague, J. J. and Stead, D. (2012) *Remote sensing techniques and landslides*. Cambridge: Cambridge, United Kingdom: Cambridge University Press.
- Picarelli, L., Leroueil, S., Olivares, L., Pagano, L., Tommasi, P. and Urciuoli, G. (2012) Groundwater in slopes, in Stead, D. and Clague, J. J. (ed.) *Landslides: types, mechanisms and modeling*. Cambridge: Cambridge University Press, pp. 235-251.
- Quinn, R. J., Dix, J. K. and Dean, M. (2008) Chapter 13: Geophysical and remote sensing surveys, in Bowens, A. (ed.) *Archaeology Underwater: The Nautical Archaeology Society Guide to Principles and Practice*. 2nd edn. Oxford.
- Ramberg, I. B., Bryhni, I., Nøttvedt, A. and Norsk geologisk, f. (2006) *Landet blir til : Norges geologi*. Trondheim: Norsk geologisk forening.
- Rocscience (2017a) Dips 7.0. Available at: <https://www.rocscience.com/rocscience/products/dips> (Accessed: 05.10.2017).
- Rocscience (2017b) *Tutorial 4 - Toppling, Planar Sliding, Wedge Sliding*. Rocscience.
- Santana, D., Corominas, J., Mavrouli, O. and Garcia-Sellés, D. (2012) Magnitude–frequency relation for rockfall scars using a Terrestrial Laser Scanner, *Engineering Geology*, 145-146, pp. 50-64. doi: 10.1016/j.enggeo.2012.07.001.
- Scheidegger, A. (1973) On the prediction of the reach and velocity of catastrophic landslides, *Journal of the International Society of Rock Mechanics / Felsmechanik / Mécanique des roches*, 5(4), pp. 231-236. doi: 10.1007/BF01301796.
- Schleier, M., Hermanns, R. L., Gosse, J. C., Oppikofer, T., Rohn, J. and Tønnesen, J. F. (2017) Subaqueous rock-avalanche deposits exposed by post-glacial isostatic rebound, Innfjorddalen, Western Norway, *Geomorphology*, 289, pp. 117-133. doi: <https://doi.org/10.1016/j.geomorph.2016.08.024>.
- Stark, C. P. and Hovius, N. (2001) The characterization of landslide size distributions, *Geophysical Research Letters*, 28(6), pp. 1091-1094. doi: 10.1029/2000GL008527.
- Statens Kartverk, Statens Vegvesen, NIBIO and Geodata AS (2017) *Norge i bilder*. Available at: <http://norgebilder.no/> (Accessed: 21.09.2017).
- Stead, D. and Eberhardt, E. (2013) Understanding the mechanics of large landslides, *Italian Journal of Engineering Geology and Environment*.
- Ten Brink, U. S., Barkan, R., Andrews, B. D. and Chaytor, J. D. (2009) Size distributions and failure initiation of submarine and subaerial landslides, *Earth and Planetary Science Letters*, 287(1), pp. 31-42. doi: 10.1016/j.epsl.2009.07.031.
- Thorn, C. E. and Loewenherz, D. S. (1987) Spatial and temporal trends in alpine periglacial studies: implications for paleo reconstruction, *Periglacial processes and landforms in Britain and Ireland*, pp. 57-65. Available at: <https://www.scopus.com/inward/record.uri?eid=2-s2.0-0023520461&partnerID=40&md5=e3120d937de0922d190eacd721e9b590>.
- Tucker, R. D., Råheim, A., Krogh, T. E. and Corfu, F. (1987) Uranium-lead zircon and titanite ages from the northern portion of the Western Gneiss Region, south-central Norway, *Earth and Planetary Science Letters*, 81(2), pp. 203-211. doi: [https://doi.org/10.1016/0012-821X\(87\)90156-7](https://doi.org/10.1016/0012-821X(87)90156-7).
- Varnes, D. J. (1978) Slope movement types and processes, in Schuster, R. L. and Krizek, R. J. (ed.) *Landslides, analysis and control, special report 176*. Washington, DC: Transportation research board, National Academy of Sciences.
- von Poschinger, A. (2002) Large rockslides in the Alps: A commentary on the contribution of G. Abele (1937-1994) and a review of some recent developments, *Catastrophic Landslides: Effects, Occurrence, and Mechanisms*, 15, pp. 237-255.
- Vorren, T. and Mangerud, J. (2008) Glaciations come and go, *The making of land: geology of Norway*. Geological Society of Norway, Trondheim, pp. 481-533.

- Westley, K., Quinn, R., Forsythe, W., Plets, R., Bell, T., Benetti, S., McGrath, F. and Robinson, R. (2011) Mapping Submerged Landscapes Using Multibeam Bathymetric Data: A case study from the north coast of Ireland, *International Journal of Nautical Archaeology*, 40(1), pp. 99-112. doi: 10.1111/j.1095-9270.2010.00272.x.
- Wieczorek, G. F., Snyder, J. B., Waitt, R. B., Morrissey, M. M., Uhrhammer, R. A., Harp, E. L., Norris, R. D., Bursik, M. I. and Finewood, L. G. (2000) Unusual July 10, 1996, rock fall at Happy Isles, Yosemite National Park, California, *Geological Society of America Bulletin*, 112(1), pp. 75-85.
- Wyllie, D. C., Mah, C. W. and Hoek, E. (2004) *Rock slope engineering : civil and mining*. 4th ed. edn. London: Spon Press.

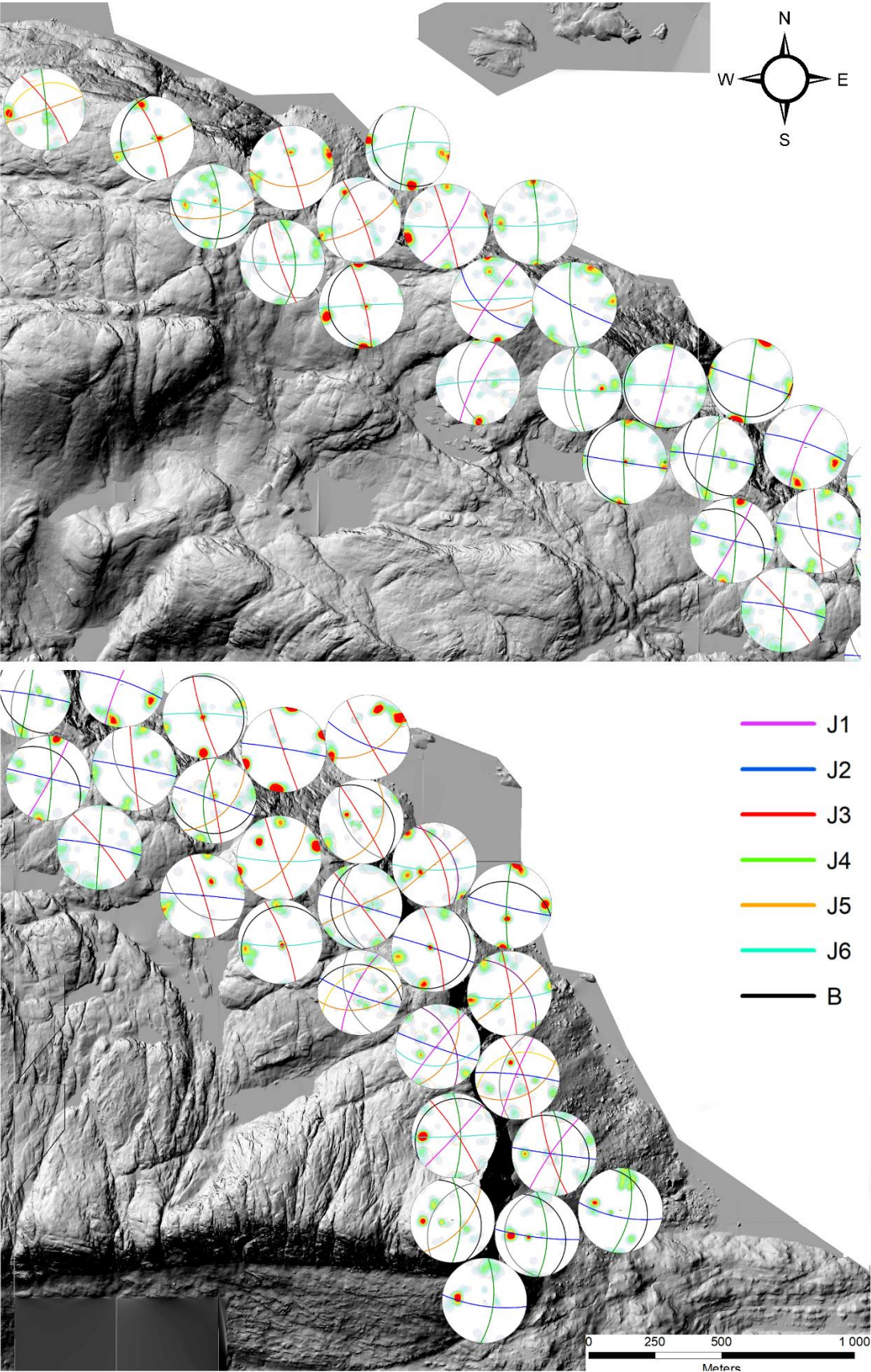
Appendix

Appendix A



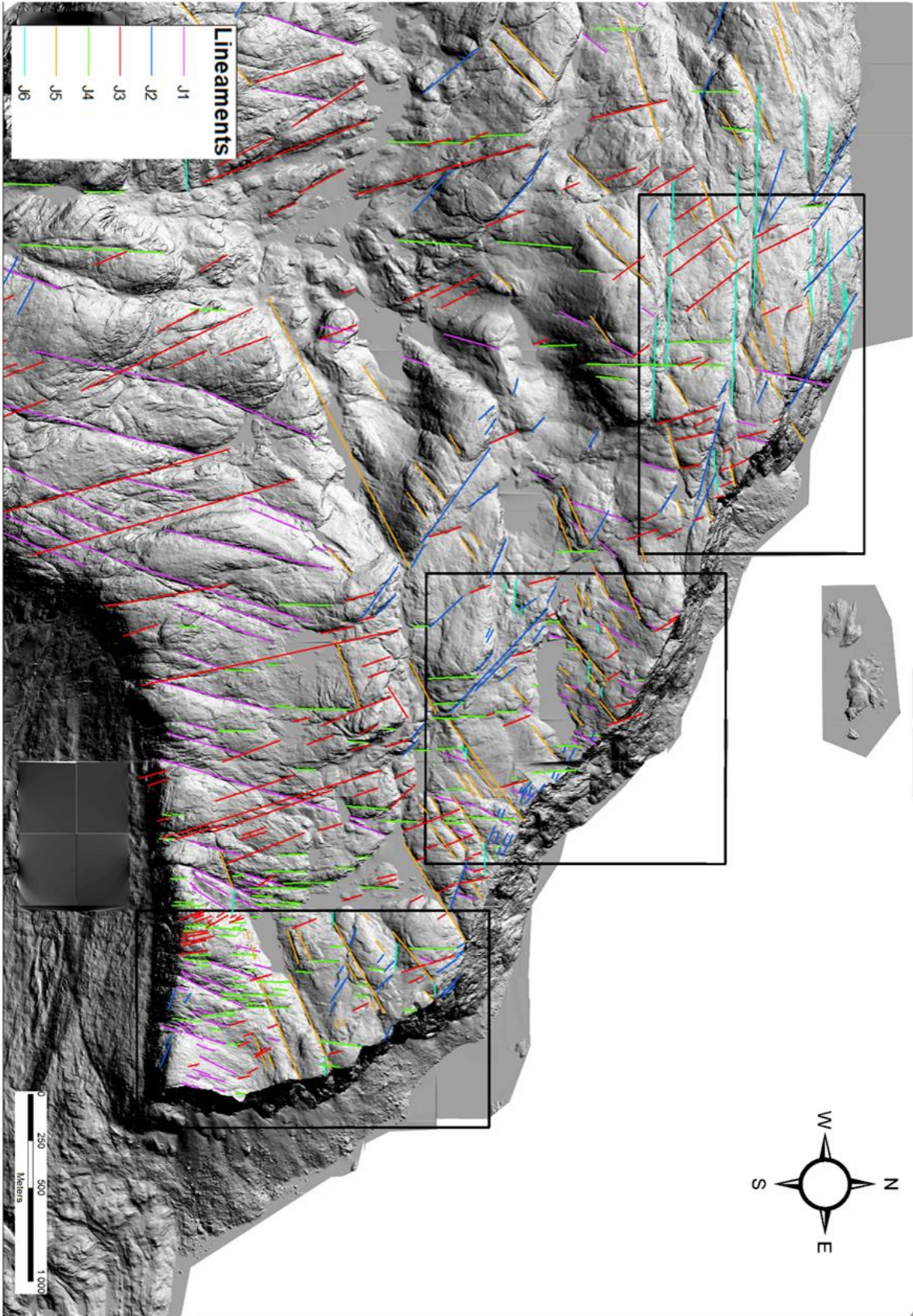
GPS-coordinates showing the position of the measurement stations.

Appendix B



Hilshade of Lifjellet showing the 43 stereoplots distributed at the GPS-location of their measurement stations. Upper picture is the western part of the cliff. Lower is eastern part.

Appendic C



Hillshade map of Lifjellet, showing all lineaments mapped with colors according to orientation. The domains used for the individual lineament analysis for each domain is defined.

Appendix D

Hazard assessment of large unstable rock slopes in Norway

Site name: Location 1 Scenario: A Made by: Vegard Nes Date: 19.05.2018

Hazard classes	Probability	Cumulative prob.
Very low	0,0 %	0,0 %
Low	30,0 %	30,0 %
Medium	57,5 %	87,5 %
High	12,5 %	100,0 %
Very high	0,0 %	100,0 %

Hazard score	
Minimum	4,0
Maximum	8,8
Mode	4,0
Mean	5,7
5% percentile	4,0
95% percentile	7,5

Fitted normal distribution	
Mean μ	5,5
St. dev. σ	1,2
$\mu - 2\sigma$	3,0
$\mu + 2\sigma$	7,9
Corr. Coeff..	0,9992
K-S-test	8,0 %

1. Backscarp	Score	Norm. prob.
Not developed	0	0,0 %
Partly open over width of slide body (few cm to m)	0,5	50,0 %
Fully open over width of slide body (few cm to m)	1	50,0 %
Comment: The backbounding fracture starts at the free northern lateral side. It moves parallel to the cliff along varying structures, but following the same orientation as J4. The fracture is mostly open(10cm-50cm), with some parts seen as depression.		

2. Potential sliding structures	Score	Norm. prob.
No penetrative structures dip out of the slope	0	0,0 %
Penetrative structures dip on average < 20 degree or steeper than the slope	0,5	0,0 %
Penetrative structures dip on average > 20 degree and daylight with the slope	1	100,0 %
Comment: J4 is dipping with the same dip as the slope.		

3. Lateral release surfaces	Score	Norm. prob.
Not developed	0	0,0 %
Partly developed on 1 side	0,25	0,0 %
Fully developed or free slope on 1 side or partly developed on 2 sides	0,5	0,0 %
Fully developed or free slope on 1 side and partly developed on 1 side	0,75	100,0 %
Fully developed or free slope on 2 sides	1	0,0 %
Comment: Free northern, and partly developed southern flank. Southern is a highly fractured area with open cracks following stepwise structures along J2 and J3.		

4. Kinematic feasibility test	Score	Norm. prob.
Kinematic feasibility test does not allow for planar sliding, wedge sliding or toppling	0	0,0 %
Failure is partly kinematically possible (movement direction is more than $\pm 30^\circ$ to slope orientation)	0,5	0,0 %
Failure is kinematically possible (movement direction is less than $\pm 30^\circ$ to slope orientation)	0,75	0,0 %
Failure is partly kinematically possible on persistent discontinuities (movement direction is more than $\pm 30^\circ$ to slope orientation)	0,75	50,0 %
Failure is kinematically possible on persistent discontinuities (movement direction is less than $\pm 30^\circ$ to slope orientation)	1	50,0 %
Comment: Planar sliding is possible along the persistent J4, but held back in the toe. Bi-planar failure possible along J4 and bedding.		

5. Morphologic expression of the rupture surface	Score	Norm. prob.
No indication on slope morphology	0	100,0 %
Slope morphology suggests formation of a rupture surface (bulging, concavity -convexity, springs)	0,5	0,0 %
Continuous rupture surface is suggested by slope morphology and can be mapped out	1	0,0 %
Comment: No indications for morphology along the cliff side, but some layers of deformed rock mass high up in the side.		

6. Displacement rates	Score	Norm. prob.
No significant movement	0	30,0 %
>0 - 0.5 cm/year	1	30,0 %
0.5 - 1 cm/year	2	30,0 %
1 - 4 cm/year	3	10,0 %
4 - 10 cm/year	4	0,0 %
> 10 cm/year	5	0,0 %
Comment: No displacement measurements taken.		

7. Acceleration (if velocity is >0.5 cm/yr and <10 cm/yr)	Score	Norm. prob.
No acceleration or change in displacement rates	0	80,0 %
Increase in displacement rates	1	20,0 %
Comment: Standard value if unknown		

8. Increase of rock fall activity	Score	Norm. prob.
No increase of rock fall activity	0	100,0 %
Increase of rock fall activity	1	0,0 %
Comment: No fresh surfaces at the block		

9. Past events	Score	Norm. prob.
No post-glacial events of similar size	0	0,0 %
One or several events older than 5000 years of similar size	0,5	0,0 %
One or several events younger than 5000 years of similar size	1	100,0 %
Comment: Large post-glacial rockslide-event from this cliffside, and several smaller events in the 1990s.		

Hazard assessment of large unstable rock slopes in Norway

Site name: Location 2 Scenario: A Made by: Vegard Nes Date: 19.05.2018

Hazard classes	Probability	Cumulative prob.
Very low	0,0 %	0,0 %
Low	48,0 %	48,0 %
Medium	44,4 %	92,4 %
High	7,6 %	100,0 %
Very high	0,0 %	100,0 %

Hazard score	
Minimum	3,8
Maximum	8,3
Mode	3,8
Mean	5,2
5% percentile	3,8
95% percentile	7,3

Fitted normal distribution	
Mean μ	5,0
St. dev. σ	1,2
$\mu - 2\sigma$	2,6
$\mu + 2\sigma$	7,5
Corr. Coeff..	0,9982
K-S-test	10,4 %

1. Backscarp	Score	Norm. prob.
Not developed	0	0,0 %
Partly open over width of slide body (few cm to m)	0,5	100,0 %
Fully open over width of slide body (few cm to m)	1	0,0 %
Comment: Backbounding fracture seen at the eastern flank, but only as depression at back scarp, and not very visible at the west side.		

2. Potential sliding structures	Score	Norm. prob.
No penetrative structures dip out of the slope	0	0,0 %
Penetrative structures dip on average < 20 degree or steeper than the slope	0,5	100,0 %
Penetrative structures dip on average > 20 degree and daylight with the slope	1	0,0 %
Comment: J4 is a potential sliding structure, but not fully daylighting at the toe of the block.		

3. Lateral release surfaces	Score	Norm. prob.
Not developed	0	0,0 %
Partly developed on 1 side	0,25	0,0 %
Fully developed or free slope on 1 side or partly developed on 2 sides	0,5	0,0 %
Fully developed or free slope on 1 side and partly developed on 1 side	0,75	0,0 %
Fully developed or free slope on 2 sides	1	100,0 %
Comment: Free flanks on both sides.		

4. Kinematic feasibility test	Score	Norm. prob.
Kinematic feasibility test does not allow for planar sliding, wedge sliding or toppling	0	0,0 %
Failure is partly kinematically possible (movement direction is more than $\pm 30^\circ$ to slope orientation)	0,5	0,0 %
Failure is kinematically possible (movement direction is less than $\pm 30^\circ$ to slope orientation)	0,75	0,0 %
Failure is partly kinematically possible on persistent discontinuities (movement direction is more than $\pm 30^\circ$ to slope orientation)	0,75	100,0 %
Failure is kinematically possible on persistent discontinuities (movement direction is less than $\pm 30^\circ$ to slope orientation)	1	0,0 %
Comment: Planar sliding is possible along the persistent J4, but held back in the toe. Bi-planar failure possible along J4 and bedding.		

5. Morphologic expression of the rupture surface	Score	Norm. prob.
No indication on slope morphology	0	60,0 %
Slope morphology suggests formation of a rupture surface (bulging, concavity -convexity, springs)	0,5	40,0 %
Continuous rupture surface is suggested by slope morphology and can be mapped out	1	0,0 %
Comment: No clear morphological indications, but toe line is interpreted at an area of slightly more fractured rock mass.		

6. Displacement rates	Score	Norm. prob.
No significant movement	0	30,0 %
>0 - 0.5 cm/year	1	30,0 %
0.5 - 1 cm/year	2	30,0 %
1 - 4 cm/year	3	10,0 %
4 - 10 cm/year	4	0,0 %
> 10 cm/year	5	0,0 %
Comment: No displacement measurements taken.		

7. Acceleration (if velocity is >0.5 cm/yr and <10 cm/yr)	Score	Norm. prob.
No acceleration or change in displacement rates	0	80,0 %
Increase in displacement rates	1	20,0 %
Comment: Standard value if unknown.		

8. Increase of rock fall activity	Score	Norm. prob.
No increase of rock fall activity	0	100,0 %
Increase of rock fall activity	1	0,0 %
Comment: No fresh surfaces seen at the cliff face.		

9. Past events	Score	Norm. prob.
No post-glacial events of similar size	0	0,0 %
One or several events older than 5000 years of similar size	0,5	0,0 %
One or several events younger than 5000 years of similar size	1	100,0 %
Comment: Several historic events in the 1990s		

Hazard assessment of large unstable rock slopes in Norway

Site name: Location 3 Scenario: A Made by: Vegard Nes Date: 19.05.2018

Hazard classes	Probability	Cumulative prob.
Very low	0,0 %	0,0 %
Low	4,5 %	4,5 %
Medium	65,1 %	69,6 %
High	30,1 %	99,7 %
Very high	0,3 %	100,0 %

Hazard score	
Minimum	4,5
Maximum	9,8
Mode	5,0
Mean	6,5
5% percentile	4,8
95% percentile	8,4

Fitted normal distribution	
Mean μ	6,5
St. dev. σ	0,0
$\mu - 2\sigma$	6,4
$\mu + 2\sigma$	6,5
Corr. Coeff..	0,9582
K-S-test	49,5 %

1. Backscarp	Score	Norm. prob.
Not developed	0	0,0 %
Partly open over width of slide body (few cm to m)	0,5	30,0 %
Fully open over width of slide body (few cm to m)	1	70,0 %
Comment: Backscarp clearly showing displacement of several meters in one part of scenario, while the other part follows a crack with opening of 20cm for 45m, and the mid part is a depression.		

2. Potential sliding structures	Score	Norm. prob.
No penetrative structures dip out of the slope	0	100,0 %
Penetrative structures dip on average < 20 degree or steeper than the slope	0,5	0,0 %
Penetrative structures dip on average > 20 degree and daylight with the slope	1	0,0 %
Comment: No penetrative structures dip out of the slope, J2 is vertical and J4 is lateral release and dipping 70 degrees out		

3. Lateral release surfaces	Score	Norm. prob.
Not developed	0	0,0 %
Partly developed on 1 side	0,25	0,0 %
Fully developed or free slope on 1 side or partly developed on 2 sides	0,5	0,0 %
Fully developed or free slope on 1 side and partly developed on 1 side	0,75	50,0 %
Fully developed or free slope on 2 sides	1	50,0 %
Comment: Free eastern flank, and a persistent structure (J4) delimiting on the western flank.		

4. Kinematic feasibility test	Score	Norm. prob.
Kinematic feasibility test does not allow for planar sliding, wedge sliding or toppling	0	0,0 %
Failure is partly kinematically possible (movement direction is more than $\pm 30^\circ$ to slope orientation)	0,5	0,0 %
Failure is kinematically possible (movement direction is less than $\pm 30^\circ$ to slope orientation)	0,75	100,0 %
Failure is partly kinematically possible on persistent discontinuities (movement direction is more than $\pm 30^\circ$ to slope orientation)	0,75	0,0 %
Failure is kinematically possible on persistent discontinuities (movement direction is less than $\pm 30^\circ$ to slope orientation)	1	0,0 %
Comment: Wedge failure along J2 and J4 is possible, the intersection line is daylighting.		

5. Morphologic expression of the rupture surface	Score	Norm. prob.
No indication on slope morphology	0	0,0 %
Slope morphology suggests formation of a rupture surface (bulging, concavity -convexity, springs)	0,5	50,0 %
Continuous rupture surface is suggested by slope morphology and can be mapped out	1	50,0 %
Comment: The unstable slope is clearly defined at the cliffside. Can track cracks at both sides of block that looks like it can be a failure surface. But it is massive		

6. Displacement rates	Score	Norm. prob.
No significant movement	0	30,0 %
>0 - 0.5 cm/year	1	30,0 %
0.5 - 1 cm/year	2	30,0 %
1 - 4 cm/year	3	10,0 %
4 - 10 cm/year	4	0,0 %
> 10 cm/year	5	0,0 %
Comment: No displacement measurements taken.		

7. Acceleration (if velocity is >0.5 cm/yr and <10 cm/yr)	Score	Norm. prob.
No acceleration or change in displacement rates	0	80,0 %
Increase in displacement rates	1	20,0 %
Comment: Standard value if unknown		

8. Increase of rock fall activity	Score	Norm. prob.
No increase of rock fall activity	0	0,0 %
Increase of rock fall activity	1	100,0 %
Comment: Fresh surfaces straight under the toe of the block.		

9. Past events	Score	Norm. prob.
No post-glacial events of similar size	0	0,0 %
One or several events older than 5000 years of similar size	0,5	0,0 %
One or several events younger than 5000 years of similar size	1	100,0 %
Comment: Several smaller events in the 1990s.		

Hazard assessment of large unstable rock slopes in Norway

Site name: Location 3 Scenario: B Made by: Vegard Nes Date: 19.05.2018

Hazard classes	Probability	Cumulative prob.
Very low	0,0 %	0,0 %
Low	7,5 %	7,5 %
Medium	64,5 %	72,0 %
High	28,0 %	100,0 %
Very high	0,0 %	100,0 %

Hazard score	
Minimum	4,8
Maximum	9,5
Mode	4,8
Mean	6,4
5% percentile	4,8
95% percentile	8,3

Fitted normal distribution	
Mean μ	6,2
St. dev. σ	1,2
$\mu - 2\sigma$	3,8
$\mu + 2\sigma$	8,6
Corr. Coeff..	0,9992
K-S-test	7,9 %

1. Backscarp	Score	Norm. prob.
Not developed	0	0,0 %
Partly open over width of slide body (few cm to m)	0,5	0,0 %
Fully open over width of slide body (few cm to m)	1	100,0 %
Comment: Backscarp showing displacement of several meters, but not surveyed in the field.		

2. Potential sliding structures	Score	Norm. prob.
No penetrative structures dip out of the slope	0	100,0 %
Penetrative structures dip on average < 20 degree or steeper than the slope	0,5	0,0 %
Penetrative structures dip on average > 20 degree and daylight with the slope	1	0,0 %
Comment: No penetrative structures dip out of the slope. Backscarp is vertical in the significant measurements.		

3. Lateral release surfaces	Score	Norm. prob.
Not developed	0	0,0 %
Partly developed on 1 side	0,25	0,0 %
Fully developed or free slope on 1 side or partly developed on 2 sides	0,5	50,0 %
Fully developed or free slope on 1 side and partly developed on 1 side	0,75	50,0 %
Fully developed or free slope on 2 sides	1	0,0 %
Comment: Persistent structures delimiting the flanks. J5 on the eastern flank has 20cm opening and is water-bearing, J4 at the west flank is not surveyed but is a significant structure.		

4. Kinematic feasibility test	Score	Norm. prob.
Kinematic feasibility test does not allow for planar sliding, wedge sliding or toppling	0	0,0 %
Failure is partly kinematically possible (movement direction is more than $\pm 30^\circ$ to slope orientation)	0,5	0,0 %
Failure is kinematically possible (movement direction is less than $\pm 30^\circ$ to slope orientation)	0,75	100,0 %
Failure is partly kinematically possible on persistent discontinuities (movement direction is more than $\pm 30^\circ$ to slope orientation)	0,75	0,0 %
Failure is kinematically possible on persistent discontinuities (movement direction is less than $\pm 30^\circ$ to slope orientation)	1	0,0 %
Comment: Wedge failure along J2 and J4 is possible, and the intersection line is daylighting.		

5. Morphologic expression of the rupture surface	Score	Norm. prob.
No indication on slope morphology	0	0,0 %
Slope morphology suggests formation of a rupture surface (bulging, concavity -convexity, springs)	0,5	50,0 %
Continuous rupture surface is suggested by slope morphology and can be mapped out	1	50,0 %
Comment: The unstable slope is clearly defined at the cliffside. Can track cracks at both sides of block that looks like a failure surface. But it is massive rock.		

6. Displacement rates	Score	Norm. prob.
No significant movement	0	30,0 %
>0 - 0,5 cm/year	1	30,0 %
0,5 - 1 cm/year	2	30,0 %
1 - 4 cm/year	3	10,0 %
4 - 10 cm/year	4	0,0 %
> 10 cm/year	5	0,0 %
Comment: No displacement measurements taken.		

7. Acceleration (if velocity is >0.5 cm/yr and <10 cm/yr)	Score	Norm. prob.
No acceleration or change in displacement rates	0	80,0 %
Increase in displacement rates	1	20,0 %
Comment: Standard value if unknown		

8. Increase of rock fall activity	Score	Norm. prob.
No increase of rock fall activity	0	0,0 %
Increase of rock fall activity	1	100,0 %
Comment: Fresh surfaces straight under the toe of the block.		

9. Past events	Score	Norm. prob.
No post-glacial events of similar size	0	0,0 %
One or several events older than 5000 years of similar size	0,5	0,0 %
One or several events younger than 5000 years of similar size	1	100,0 %
Comment: Several smaller events in the 1990s. Large deposits straight under the scenario.		

Hazard assessment of large unstable rock slopes in Norway

Site name: Location 3 Scenario: C Made by: Vegard Nes Date: 19.05.2018

Hazard classes	Probability	Cumulative prob.
Very low	0,0 %	0,0 %
Low	12,8 %	12,8 %
Medium	57,9 %	70,7 %
High	29,0 %	99,6 %
Very high	0,4 %	100,0 %

Hazard score	
Minimum	4,3
Maximum	10,3
Mode	5,5
Mean	6,4
5% percentile	4,3
95% percentile	8,4

Fitted normal distribution	
Mean μ	6,4
St. dev. σ	0,0
$\mu - 2\sigma$	6,4
$\mu + 2\sigma$	6,4
Corr. Coeff..	0,9497
K-S-test	50,4 %

1. Backscarp		Score	Norm. prob.
Not developed		0	0,0 %
Partly open over width of slide body (few cm to m)		0,5	80,0 %
Fully open over width of slide body (few cm to m)		1	20,0 %
Comment: Backbounding fracture is open(20cm) almost over the whole body, but a depression follows the last 10m to the west side.			

2. Potential sliding structures		Score	Norm. prob.
No penetrative structures dip out of the slope		0	0,0 %
Penetrative structures dip on average < 20 degree or steeper than the slope		0,5	100,0 %
Penetrative structures dip on average > 20 degree and daylight with the slope		1	0,0 %
Comment: Penetrative structure dips steeper than the slope			

3. Lateral release surfaces		Score	Norm. prob.
Not developed		0	0,0 %
Partly developed on 1 side		0,25	0,0 %
Fully developed or free slope on 1 side or partly developed on 2 sides		0,5	0,0 %
Fully developed or free slope on 1 side and partly developed on 1 side		0,75	50,0 %
Fully developed or free slope on 2 sides		1	50,0 %
Comment: Free eastern flank, and a persistent structure delimiting on the western flank following the orientation of J5, is 20cm open and water-bearing.			

4. Kinematic feasibility test		Score	Norm. prob.
Kinematic feasibility test does not allow for planar sliding, wedge sliding or toppling		0	0,0 %
Failure is partly kinematically possible (movement direction is more than $\pm 30^\circ$ to slope orientation)		0,5	50,0 %
Failure is kinematically possible (movement direction is less than $\pm 30^\circ$ to slope orientation)		0,75	50,0 %
Failure is partly kinematically possible on persistent discontinuities (movement direction is more than $\pm 30^\circ$ to slope orientation)		0,75	0,0 %
Failure is kinematically possible on persistent discontinuities (movement direction is less than $\pm 30^\circ$ to slope orientation)		1	0,0 %
Comment: Planar sliding is partly possible along J2, but is not daylighting along the significantly measured structure.			

5. Morphologic expression of the rupture surface		Score	Norm. prob.
No indication on slope morphology		0	0,0 %
Slope morphology suggests formation of a rupture surface (bulging, concavity -convexity, springs)		0,5	0,0 %
Continuous rupture surface is suggested by slope morphology and can be mapped out		1	100,0 %
Comment: The unstable slope is clearly defined at the cliffside as an overhanging block, with a west lateral limit seen as a crack.			

6. Displacement rates		Score	Norm. prob.
No significant movement		0	30,0 %
>0 - 0.5 cm/year		1	30,0 %
0.5 - 1 cm/year		2	30,0 %
1 - 4 cm/year		3	10,0 %
4 - 10 cm/year		4	0,0 %
> 10 cm/year		5	0,0 %
Comment: No displacement measurements taken.			

7. Acceleration (if velocity is >0.5 cm/yr and <10 cm/yr)		Score	Norm. prob.
No acceleration or change in displacement rates		0	80,0 %
Increase in displacement rates		1	20,0 %
Comment: Standard value if unknown			

8. Increase of rock fall activity		Score	Norm. prob.
No increase of rock fall activity		0	50,0 %
Increase of rock fall activity		1	50,0 %
Comment: Fresh surfaces further down in the cliff face, but no fresh surfaces on this block.			

9. Past events		Score	Norm. prob.
No post-glacial events of similar size		0	0,0 %
One or several events older than 5000 years of similar size		0,5	0,0 %
One or several events younger than 5000 years of similar size		1	100,0 %
Comment: Several smaller events in the 1990s.			

Hazard assessment of large unstable rock slopes in Norway

Site name: Location 4 Scenario: A Made by: Vegard Nes Date: 19.05.2018

Hazard classes	Probability	Cumulative prob.
Very low	0,0 %	0,0 %
Low	18,8 %	18,8 %
Medium	61,0 %	79,7 %
High	20,2 %	99,9 %
Very high	0,1 %	100,0 %

Hazard score	
Minimum	4,0
Maximum	10,0
Mode	5,3
Mean	6,0
5% percentile	4,1
95% percentile	8,0

Fitted normal distribution	
Mean μ	5,8
St. dev. σ	1,3
$\mu - 2\sigma$	3,3
$\mu + 2\sigma$	8,4
Corr. Coeff..	0,9995
K-S-test	5,3 %

1. Backscarp	Score	Norm. prob.
Not developed	0	0,0 %
Partly open over width of slide body (few cm to m)	0,5	0,0 %
Fully open over width of slide body (few cm to m)	1	100,0 %
Comment: Fully open backscarp (2m) along the orientation of J2. Open until a depth of 20meters.		

2. Potential sliding structures	Score	Norm. prob.
No penetrative structures dip out of the slope	0	0,0 %
Penetrative structures dip on average < 20 degree or steeper than the slope	0,5	80,0 %
Penetrative structures dip on average > 20 degree and daylight with the slope	1	20,0 %
Comment: J2 is a vertical structure, which some variations can dip out of the slope.		

3. Lateral release surfaces	Score	Norm. prob.
Not developed	0	0,0 %
Partly developed on 1 side	0,25	0,0 %
Fully developed or free slope on 1 side or partly developed on 2 sides	0,5	0,0 %
Fully developed or free slope on 1 side and partly developed on 1 side	0,75	50,0 %
Fully developed or free slope on 2 sides	1	50,0 %
Comment: Free western flank, and partially open eastern flank seen as depression following the significant J3.		

4. Kinematic feasibility test	Score	Norm. prob.
Kinematic feasibility test does not allow for planar sliding, wedge sliding or toppling	0	0,0 %
Failure is partly kinematically possible (movement direction is more than $\pm 30^\circ$ to slope orientation)	0,5	0,0 %
Failure is kinematically possible (movement direction is less than $\pm 30^\circ$ to slope orientation)	0,75	0,0 %
Failure is partly kinematically possible on persistent discontinuities (movement direction is more than $\pm 30^\circ$ to slope orientation)	0,75	50,0 %
Failure is kinematically possible on persistent discontinuities (movement direction is less than $\pm 30^\circ$ to slope orientation)	1	50,0 %
Comment: Toppling along uncertainties of J2 is possible, and the structure is persistent.		

5. Morphologic expression of the rupture surface	Score	Norm. prob.
No indication on slope morphology	0	50,0 %
Slope morphology suggests formation of a rupture surface (bulging, concavity -convexity, springs)	0,5	25,0 %
Continuous rupture surface is suggested by slope morphology and can be mapped out	1	25,0 %
Comment: Standard value for toppling (morphological rupture not visible in toppling)		

6. Displacement rates	Score	Norm. prob.
No significant movement	0	30,0 %
>0 - 0.5 cm/year	1	30,0 %
0.5 - 1 cm/year	2	30,0 %
1 - 4 cm/year	3	10,0 %
4 - 10 cm/year	4	0,0 %
> 10 cm/year	5	0,0 %
Comment: No displacement measurements taken.		

7. Acceleration (if velocity is >0.5 cm/yr and <10 cm/yr)	Score	Norm. prob.
No acceleration or change in displacement rates	0	80,0 %
Increase in displacement rates	1	20,0 %
Comment: Standard value if unknown		

8. Increase of rock fall activity	Score	Norm. prob.
No increase of rock fall activity	0	100,0 %
Increase of rock fall activity	1	0,0 %
Comment: No fresh surfaces from rock fall activity spotted around the block.		

9. Past events	Score	Norm. prob.
No post-glacial events of similar size	0	0,0 %
One or several events older than 5000 years of similar size	0,5	0,0 %
One or several events younger than 5000 years of similar size	1	100,0 %
Comment: Several events in the 1990s.		

Hazard assessment of large unstable rock slopes in Norway

Site name: Location 5 Scenario: A Made by: Vegard Nes Date: 19.05.2018

Hazard classes	Probability	Cumulative prob.
Very low	0,0 %	0,0 %
Low	66,6 %	66,6 %
Medium	30,8 %	97,4 %
High	2,6 %	100,0 %
Very high	0,0 %	100,0 %

Hazard score	
Minimum	2,8
Maximum	8,3
Mode	3,8
Mean	4,6
5% percentile	2,8
95% percentile	6,8

Fitted normal distribution	
Mean μ	4,6
St. dev. σ	0,0
$\mu - 2\sigma$	4,6
$\mu + 2\sigma$	4,7
Corr. Coeff..	0,9501
K-S-test	45,0 %

1. Backscarp		Score	Norm. prob.
Not developed		0	0,0 %
Partly open over width of slide body (few cm to m)		0,5	100,0 %
Fully open over width of slide body (few cm to m)		1	0,0 %
Comment: Backscarp is clear at eastern side for 40m, following depressions mixed with some open structures to the east. Not easy to define exact limits in field.			

2. Potential sliding structures		Score	Norm. prob.
No penetrative structures dip out of the slope		0	0,0 %
Penetrative structures dip on average < 20 degree or steeper than the slope		0,5	80,0 %
Penetrative structures dip on average > 20 degree and daylight with the slope		1	20,0 %
Comment: Penetrative structure of J2 dip steeper than the slope. Clear penetrative structure seen at cliff face			

3. Lateral release surfaces		Score	Norm. prob.
Not developed		0	0,0 %
Partly developed on 1 side		0,25	0,0 %
Fully developed or free slope on 1 side or partly developed on 2 sides		0,5	0,0 %
Fully developed or free slope on 1 side and partly developed on 1 side		0,75	100,0 %
Fully developed or free slope on 2 sides		1	0,0 %
Comment: Free eastern flank, and partly developed western flank along J1 and J4. The intersection with slope is highly fractured and closely spaced, but difficult to follow further in.			

4. Kinematic feasibility test		Score	Norm. prob.
Kinematic feasibility test does not allow for planar sliding, wedge sliding or toppling		0	100,0 %
Failure is partly kinematically possible (movement direction is more than $\pm 30^\circ$ to slope orientation)		0,5	0,0 %
Failure is kinematically possible (movement direction is less than $\pm 30^\circ$ to slope orientation)		0,75	0,0 %
Failure is partly kinematically possible on persistent discontinuities (movement direction is more than $\pm 30^\circ$ to slope orientation)		0,75	0,0 %
Failure is kinematically possible on persistent discontinuities (movement direction is less than $\pm 30^\circ$ to slope orientation)		1	0,0 %
Comment: Kinematic feasibility test does allow for planar failure and toppling along J2, but this structure is vertical and no significant structures have slacker dip.			

5. Morphologic expression of the rupture surface		Score	Norm. prob.
No indication on slope morphology		0	100,0 %
Slope morphology suggests formation of a rupture surface (bulging, concavity -convexity, springs)		0,5	0,0 %
Continuous rupture surface is suggested by slope morphology and can be mapped out		1	0,0 %
Comment: No morphological expressions			

6. Displacement rates		Score	Norm. prob.
No significant movement		0	30,0 %
>0 - 0.5 cm/year		1	30,0 %
0.5 - 1 cm/year		2	30,0 %
1 - 4 cm/year		3	10,0 %
4 - 10 cm/year		4	0,0 %
> 10 cm/year		5	0,0 %
Comment: No displacement measurements taken.			

7. Acceleration (if velocity is >0.5 cm/yr and <10 cm/yr)		Score	Norm. prob.
No acceleration or change in displacement rates		0	80,0 %
Increase in displacement rates		1	20,0 %
Comment: Standard value if unknown			

8. Increase of rock fall activity		Score	Norm. prob.
No increase of rock fall activity		0	50,0 %
Increase of rock fall activity		1	50,0 %
Comment: Surfaces reminding of rock fall activity, but difficult to define an increase.			

9. Past events		Score	Norm. prob.
No post-glacial events of similar size		0	0,0 %
One or several events older than 5000 years of similar size		0,5	0,0 %
One or several events younger than 5000 years of similar size		1	100,0 %
Comment: Several smaller events in the 1990s.			

Hazard assessment of large unstable rock slopes in Norway

Site name: Location 5 Scenario: B Made by: Vegard Nes Date: 19.05.2018

Hazard classes	Probability	Cumulative prob.
Very low	0,0 %	0,0 %
Low	10,0 %	10,0 %
Medium	53,0 %	63,0 %
High	36,0 %	99,0 %
Very high	1,0 %	100,0 %

Hazard score	
Minimum	4,8
Maximum	10,3
Mode	5,8
Mean	6,7
5% percentile	4,8
95% percentile	8,8

Fitted normal distribution	
Mean μ	6,5
St. dev. σ	1,3
$\mu - 2\sigma$	3,9
$\mu + 2\sigma$	9,1
Corr. Coeff..	0,9985
K-S-test	7,3 %

1. Backscarp	Score	Norm. prob.
Not developed	0	0,0 %
Partly open over width of slide body (few cm to m)	0,5	0,0 %
Fully open over width of slide body (few cm to m)	1	100,0 %
Comment: Backscarp clear with some tilt of block along a variation of J2. Opening of 2m, and clearly penetrative seen along the east flank.		

2. Potential sliding structures	Score	Norm. prob.
No penetrative structures dip out of the slope	0	0,0 %
Penetrative structures dip on average < 20 degree or steeper than the slope	0,5	100,0 %
Penetrative structures dip on average > 20 degree and daylight with the slope	1	0,0 %
Comment: Penetrative structure (J2) dip steeper than the slope.		

3. Lateral release surfaces	Score	Norm. prob.
Not developed	0	0,0 %
Partly developed on 1 side	0,25	0,0 %
Fully developed or free slope on 1 side or partly developed on 2 sides	0,5	0,0 %
Fully developed or free slope on 1 side and partly developed on 1 side	0,75	100,0 %
Fully developed or free slope on 2 sides	1	0,0 %
Comment: Free eastern flank, partly developed western structure along the orientation of J1, but with varying dip, more vertical with depth.		

4. Kinematic feasibility test	Score	Norm. prob.
Kinematic feasibility test does not allow for planar sliding, wedge sliding or toppling	0	0,0 %
Failure is partly kinematically possible (movement direction is more than $\pm 30^\circ$ to slope orientation)	0,5	0,0 %
Failure is kinematically possible (movement direction is less than $\pm 30^\circ$ to slope orientation)	0,75	0,0 %
Failure is partly kinematically possible on persistent discontinuities (movement direction is more than $\pm 30^\circ$ to slope orientation)	0,75	0,0 %
Failure is kinematically possible on persistent discontinuities (movement direction is less than $\pm 30^\circ$ to slope orientation)	1	100,0 %
Comment: Toppling possible along J1 and partly possible along J2. The block can fall in two different directions.		

5. Morphologic expression of the rupture surface	Score	Norm. prob.
No indication on slope morphology	0	0,0 %
Slope morphology suggests formation of a rupture surface (bulging, concavity -convexity, springs)	0,5	66,7 %
Continuous rupture surface is suggested by slope morphology and can be mapped out	1	33,3 %
Comment: Fractures seen at the slope suggests formation of rupture surface and lateral limits. More fractured rock at this scenario than the rest of the location.		

6. Displacement rates	Score	Norm. prob.
No significant movement	0	30,0 %
>0 - 0.5 cm/year	1	30,0 %
0.5 - 1 cm/year	2	30,0 %
1 - 4 cm/year	3	10,0 %
4 - 10 cm/year	4	0,0 %
> 10 cm/year	5	0,0 %
Comment: No displacement measurements taken.		

7. Acceleration (if velocity is >0.5 cm/yr and <10 cm/yr)	Score	Norm. prob.
No acceleration or change in displacement rates	0	80,0 %
Increase in displacement rates	1	20,0 %
Comment: Standard value if unknown		

8. Increase of rock fall activity	Score	Norm. prob.
No increase of rock fall activity	0	50,0 %
Increase of rock fall activity	1	50,0 %
Comment: Surfaces reminding of rock fall activity, but difficult to define an increase.		

9. Past events	Score	Norm. prob.
No post-glacial events of similar size	0	0,0 %
One or several events older than 5000 years of similar size	0,5	0,0 %
One or several events younger than 5000 years of similar size	1	100,0 %
Comment: Several smaller events in the 1990s. Large deposits straight under the scenario.		

Hazard assessment of large unstable rock slopes in Norway

Site name: Location 6 Scenario: A Made by: Vegard Nes Date: 26.04.2018

Hazard classes	Probability	Cumulative prob.
Very low	0,0 %	0,0 %
Low	37,5 %	37,5 %
Medium	62,5 %	100,0 %
High	0,0 %	100,0 %
Very high	0,0 %	100,0 %

Hazard score	
Minimum	4,3
Maximum	6,3
Mode	5,3
Mean	5,1
5% percentile	4,3
95% percentile	6,3

Fitted normal distribution	
Mean μ	5,0
St. dev. σ	0,7
$\mu - 2\sigma$	3,6
$\mu + 2\sigma$	6,4
Corr. Coeff..	0,9975
K-S-test	13,0 %

1. Backscarp	Score	Norm. prob.
Not developed	0	0,0 %
Partly open over width of slide body (few cm to m)	0,5	0,0 %
Fully open over width of slide body (few cm to m)	1	100,0 %
Comment: Continuous, open backbounding fracture with 0,3m opening and 30m depth following the orientation of J2.		

2. Potential sliding structures	Score	Norm. prob.
No penetrative structures dip out of the slope	0	0,0 %
Penetrative structures dip on average < 20 degree or steeper than the slope	0,5	100,0 %
Penetrative structures dip on average > 20 degree and daylight with the slope	1	0,0 %
Comment: J2 dipping vertical, steeper than the slope.		

3. Lateral release surfaces	Score	Norm. prob.
Not developed	0	0,0 %
Partly developed on 1 side	0,25	0,0 %
Fully developed or free slope on 1 side or partly developed on 2 sides	0,5	0,0 %
Fully developed or free slope on 1 side and partly developed on 1 side	0,75	100,0 %
Fully developed or free slope on 2 sides	1	0,0 %
Comment: Western flank fully developed along J4, while eastern limit is following a depression in the orientation of the persistent structure J1.		

4. Kinematic feasibility test	Score	Norm. prob.
Kinematic feasibility test does not allow for planar sliding, wedge sliding or toppling	0	0,0 %
Failure is partly kinematically possible (movement direction is more than $\pm 30^\circ$ to slope orientation)	0,5	0,0 %
Failure is kinematically possible (movement direction is less than $\pm 30^\circ$ to slope orientation)	0,75	0,0 %
Failure is partly kinematically possible on persistent discontinuities (movement direction is more than $\pm 30^\circ$ to slope orientation)	0,75	0,0 %
Failure is kinematically possible on persistent discontinuities (movement direction is less than $\pm 30^\circ$ to slope orientation)	1	100,0 %
Comment: Toppling is possible along the vertical backbounding, penetrative structure of J2.		

5. Morphologic expression of the rupture surface	Score	Norm. prob.
No indication on slope morphology	0	50,0 %
Slope morphology suggests formation of a rupture surface (bulging, concavity -convexity, springs)	0,5	25,0 %
Continuous rupture surface is suggested by slope morphology and can be mapped out	1	25,0 %
Comment: No indications for morphology, but standard value for toppling. (No morphology signs needed)		

6. Displacement rates	Score	Norm. prob.
No significant movement	0	50,0 %
>0 - 0.5 cm/year	1	50,0 %
0.5 - 1 cm/year	2	0,0 %
1 - 4 cm/year	3	0,0 %
4 - 10 cm/year	4	0,0 %
> 10 cm/year	5	0,0 %
Comment: Displacement measurements indicate 2,4mm/year for parts of the scenario, but unsure results for whole scenario.		

7. Acceleration (if velocity is >0.5 cm/yr and <10 cm/yr)	Score	Norm. prob.
No acceleration or change in displacement rates	0	80,0 %
Increase in displacement rates	1	20,0 %
Comment: Standard value if unknown		

8. Increase of rock fall activity	Score	Norm. prob.
No increase of rock fall activity	0	100,0 %
Increase of rock fall activity	1	0,0 %
Comment: No fresh surfaces at the block.		

9. Past events	Score	Norm. prob.
No post-glacial events of similar size	0	0,0 %
One or several events older than 5000 years of similar size	0,5	0,0 %
One or several events younger than 5000 years of similar size	1	100,0 %
Comment: Event from same block in 1992, and many other events visible along the cliff.		

Hazard assessment of large unstable rock slopes in Norway

Site name: Location 6 Scenario: B Made by: Vegard Nes Date: 26.04.2018

Hazard classes	Probability	Cumulative prob.
Very low	0,0 %	0,0 %
Low	0,0 %	0,0 %
Medium	100,0 %	100,0 %
High	0,0 %	100,0 %
Very high	0,0 %	100,0 %

Hazard score	
Minimum	5,3
Maximum	6,5
Mode	5,3
Mean	5,8
5% percentile	5,3
95% percentile	6,5

Fitted normal distribution	
Mean μ	5,6
St. dev. σ	0,5
$\mu - 2\sigma$	4,6
$\mu + 2\sigma$	6,5
Corr. Coeff..	0,9989
K-S-test	10,4 %

1. Backscarp	Score	Norm. prob.
Not developed	0	0,0 %
Partly open over width of slide body (few cm to m)	0,5	0,0 %
Fully open over width of slide body (few cm to m)	1	100,0 %
Comment: Continuous, open backbounding fracture with 0,5m opening and 50m depth, following a very persistent J2.		

2. Potential sliding structures	Score	Norm. prob.
No penetrative structures dip out of the slope	0	0,0 %
Penetrative structures dip on average < 20 degree or steeper than the slope	0,5	100,0 %
Penetrative structures dip on average > 20 degree and daylight with the slope	1	0,0 %
Comment: J2 is a penetrative structure dipping steeper than the slope		

3. Lateral release surfaces	Score	Norm. prob.
Not developed	0	0,0 %
Partly developed on 1 side	0,25	0,0 %
Fully developed or free slope on 1 side or partly developed on 2 sides	0,5	0,0 %
Fully developed or free slope on 1 side and partly developed on 1 side	0,75	50,0 %
Fully developed or free slope on 2 sides	1	50,0 %
Comment: Western flank fully developed along J4 with 30-40cm opening and 5m depth, while eastern limit is following a depression with orientation of J1.		

4. Kinematic feasibility test	Score	Norm. prob.
Kinematic feasibility test does not allow for planar sliding, wedge sliding or toppling	0	0,0 %
Failure is partly kinematically possible (movement direction is more than $\pm 30^\circ$ to slope orientation)	0,5	0,0 %
Failure is kinematically possible (movement direction is less than $\pm 30^\circ$ to slope orientation)	0,75	0,0 %
Failure is partly kinematically possible on persistent discontinuities (movement direction is more than $\pm 30^\circ$ to slope orientation)	0,75	0,0 %
Failure is kinematically possible on persistent discontinuities (movement direction is less than $\pm 30^\circ$ to slope orientation)	1	100,0 %
Comment: Toppling is possible along the vertical backbounding structure of J2.		

5. Morphologic expression of the rupture surface	Score	Norm. prob.
No indication on slope morphology	0	50,0 %
Slope morphology suggests formation of a rupture surface (bulging, concavity -convexity, springs)	0,5	25,0 %
Continuous rupture surface is suggested by slope morphology and can be mapped out	1	25,0 %
Comment: No indications for morphology, but standard value for toppling. (No morphology signs needed)		

6. Displacement rates	Score	Norm. prob.
No significant movement	0	0,0 %
>0 - 0.5 cm/year	1	100,0 %
0.5 - 1 cm/year	2	0,0 %
1 - 4 cm/year	3	0,0 %
4 - 10 cm/year	4	0,0 %
> 10 cm/year	5	0,0 %
Comment: Displacement measurements indicate 2,4mm/year for the scenario.		

7. Acceleration (if velocity is >0.5 cm/yr and <10 cm/yr)	Score	Norm. prob.
No acceleration or change in displacement rates	0	80,0 %
Increase in displacement rates	1	20,0 %
Comment: Standard value if unknown		

8. Increase of rock fall activity	Score	Norm. prob.
No increase of rock fall activity	0	100,0 %
Increase of rock fall activity	1	0,0 %
Comment: No fresh surfaces at the block.		

9. Past events	Score	Norm. prob.
No post-glacial events of similar size	0	0,0 %
One or several events older than 5000 years of similar size	0,5	0,0 %
One or several events younger than 5000 years of similar size	1	100,0 %
Comment: Event from same block in 1992, and many other events visible along the cliff.		

Hazard assessment of large unstable rock slopes in Norway

Site name: Location 7 Scenario: A Made by: Vegard Nes Date: 19.05.2018

Hazard classes	Probability	Cumulative prob.
Very low	0,0 %	0,0 %
Low	13,0 %	13,0 %
Medium	81,5 %	94,4 %
High	5,6 %	100,0 %
Very high	0,0 %	100,0 %

Hazard score	
Minimum	4,3
Maximum	7,5
Mode	5,5
Mean	5,8
5% percentile	4,3
95% percentile	7,1

Fitted normal distribution	
Mean μ	5,7
St. dev. σ	0,8
$\mu - 2\sigma$	4,0
$\mu + 2\sigma$	7,3
Corr. Coeff..	0,9993
K-S-test	7,8 %

1. Backscarp	Score	Norm. prob.
Not developed	0	0,0 %
Partly open over width of slide body (few cm to m)	0,5	0,0 %
Fully open over width of slide body (few cm to m)	1	100,0 %
Comment: Continuous, open backbounding fracture with 0,5m opening and estimated 100m depth. Fracture is following structures of J3 and J6.		

2. Potential sliding structures	Score	Norm. prob.
No penetrative structures dip out of the slope	0	0,0 %
Penetrative structures dip on average < 20 degree or steeper than the slope	0,5	100,0 %
Penetrative structures dip on average > 20 degree and daylight with the slope	1	0,0 %
Comment: Steep structures with orientation of J3 and J6 delimit the block, but is steeper than the slope.		

3. Lateral release surfaces	Score	Norm. prob.
Not developed	0	0,0 %
Partly developed on 1 side	0,25	0,0 %
Fully developed or free slope on 1 side or partly developed on 2 sides	0,5	0,0 %
Fully developed or free slope on 1 side and partly developed on 1 side	0,75	33,3 %
Fully developed or free slope on 2 sides	1	66,7 %
Comment: Free flank on east side, and partly to fully developed on western side.		

4. Kinematic feasibility test	Score	Norm. prob.
Kinematic feasibility test does not allow for planar sliding, wedge sliding or toppling	0	0,0 %
Failure is partly kinematically possible (movement direction is more than $\pm 30^\circ$ to slope orientation)	0,5	0,0 %
Failure is kinematically possible (movement direction is less than $\pm 30^\circ$ to slope orientation)	0,75	0,0 %
Failure is partly kinematically possible on persistent discontinuities (movement direction is more than $\pm 30^\circ$ to slope orientation)	0,75	0,0 %
Failure is kinematically possible on persistent discontinuities (movement direction is less than $\pm 30^\circ$ to slope orientation)	1	100,0 %
Comment: Toppling is possible and partly possible along the two vertical backbounding structures, J3 and J6.		

5. Morphologic expression of the rupture surface	Score	Norm. prob.
No indication on slope morphology	0	50,0 %
Slope morphology suggests formation of a rupture surface (bulging, concavity -convexity, springs)	0,5	25,0 %
Continuous rupture surface is suggested by slope morphology and can be mapped out	1	25,0 %
Comment: No indications for morphology, but standard value for toppling. (No morphology signs needed)		

6. Displacement rates	Score	Norm. prob.
No significant movement	0	66,7 %
>0 - 0.5 cm/year	1	33,3 %
0.5 - 1 cm/year	2	0,0 %
1 - 4 cm/year	3	0,0 %
4 - 10 cm/year	4	0,0 %
> 10 cm/year	5	0,0 %
Comment: No significant displacement in a 10-year period, but displacement is measured.		

7. Acceleration (if velocity is >0.5 cm/yr and <10 cm/yr)	Score	Norm. prob.
No acceleration or change in displacement rates	0	80,0 %
Increase in displacement rates	1	20,0 %
Comment: Standard value if unknown		

8. Increase of rock fall activity	Score	Norm. prob.
No increase of rock fall activity	0	33,3 %
Increase of rock fall activity	1	66,7 %
Comment: Some fresh rock fall from block.		

9. Past events	Score	Norm. prob.
No post-glacial events of similar size	0	0,0 %
One or several events older than 5000 years of similar size	0,5	0,0 %
One or several events younger than 5000 years of similar size	1	100,0 %
Comment: Several events is seen along the cliff, two of them in the 1990's.		

Hazard assessment of large unstable rock slopes in Norway

Site name: Location 8 Scenario: A Made by: Vegard Nes Date: 19.05.2018

Hazard classes	Probability	Cumulative prob.
Very low	0,0 %	0,0 %
Low	52,5 %	52,5 %
Medium	42,0 %	94,5 %
High	5,5 %	100,0 %
Very high	0,0 %	100,0 %

Hazard score	
Minimum	3,3
Maximum	8,3
Mode	4,3
Mean	4,9
5% percentile	3,3
95% percentile	7,0

Fitted normal distribution	
Mean μ	4,7
St. dev. σ	1,3
$\mu - 2\sigma$	2,2
$\mu + 2\sigma$	7,2
Corr. Coeff..	0,9979
K-S-test	9,0 %

1. Backscarp	Score	Norm. prob.
Not developed	0	0,0 %
Partly open over width of slide body (few cm to m)	0,5	100,0 %
Fully open over width of slide body (few cm to m)	1	0,0 %
Comment: Open backbounding fracture , at some points 20m deep at the eastern side followed by a depression the last10m to the west. The crack is not following one spesific structure.		

2. Potential sliding structures	Score	Norm. prob.
No penetrative structures dip out of the slope	0	100,0 %
Penetrative structures dip on average < 20 degree or steeper than the slope	0,5	0,0 %
Penetrative structures dip on average > 20 degree and daylight with the slope	1	0,0 %
Comment: No penetrative structures dip out of the slope.		

3. Lateral release surfaces	Score	Norm. prob.
Not developed	0	0,0 %
Partly developed on 1 side	0,25	0,0 %
Fully developed or free slope on 1 side or partly developed on 2 sides	0,5	0,0 %
Fully developed or free slope on 1 side and partly developed on 1 side	0,75	100,0 %
Fully developed or free slope on 2 sides	1	0,0 %
Comment: Free eastern flank, and partly developed western flank in the orientation of a very persistent structure, J3.		

4. Kinematic feasibility test	Score	Norm. prob.
Kinematic feasibility test does not allow for planar sliding, wedge sliding or toppling	0	0,0 %
Failure is partly kinematically possible (movement direction is more than $\pm 30^\circ$ to slope orientation)	0,5	0,0 %
Failure is kinematically possible (movement direction is less than $\pm 30^\circ$ to slope orientation)	0,75	0,0 %
Failure is partly kinematically possible on persistent discontinuities (movement direction is more than $\pm 30^\circ$ to slope orientation)	0,75	0,0 %
Failure is kinematically possible on persistent discontinuities (movement direction is less than $\pm 30^\circ$ to slope orientation)	1	100,0 %
Comment: Failure is kinematically possible for toppling, along significant joint sets of J6.		

5. Morphologic expression of the rupture surface	Score	Norm. prob.
No indication on slope morphology	0	50,0 %
Slope morphology suggests formation of a rupture surface (bulging, concavity -convexity, springs)	0,5	25,0 %
Continuous rupture surface is suggested by slope morphology and can be mapped out	1	25,0 %
Comment: Standard value for toppling (morphological rupture not visible in toppling)		

6. Displacement rates	Score	Norm. prob.
No significant movement	0	30,0 %
>0 - 0.5 cm/year	1	30,0 %
0.5 - 1 cm/year	2	30,0 %
1 - 4 cm/year	3	10,0 %
4 - 10 cm/year	4	0,0 %
> 10 cm/year	5	0,0 %
Comment: No displacement measurements taken.		

7. Acceleration (if velocity is >0.5 cm/yr and <10 cm/yr)	Score	Norm. prob.
No acceleration or change in displacement rates	0	80,0 %
Increase in displacement rates	1	20,0 %
Comment: Standard value if unknown		

8. Increase of rock fall activity	Score	Norm. prob.
No increase of rock fall activity	0	100,0 %
Increase of rock fall activity	1	0,0 %
Comment: No rockfall activity seen on the block		

9. Past events	Score	Norm. prob.
No post-glacial events of similar size	0	0,0 %
One or several events older than 5000 years of similar size	0,5	0,0 %
One or several events younger than 5000 years of similar size	1	100,0 %
Comment: Several smaller events in the 1990s.		

Hazard assessment of large unstable rock slopes in Norway

Site name: Location 8 Scenario: B Made by: Vegard Nes Date: 19.05.2018

Hazard classes	Probability	Cumulative prob.
Very low	0,0 %	0,0 %
Low	22,5 %	22,5 %
Medium	68,5 %	91,0 %
High	9,0 %	100,0 %
Very high	0,0 %	100,0 %

Hazard score	
Minimum	4,0
Maximum	9,0
Mode	5,0
Mean	5,7
5% percentile	4,0
95% percentile	7,8

Fitted normal distribution	
Mean μ	5,5
St. dev. σ	1,3
$\mu - 2\sigma$	3,0
$\mu + 2\sigma$	8,0
Corr. Coeff..	0,9980
K-S-test	9,3 %

1. Backscarp	Score	Norm. prob.
Not developed	0	0,0 %
Partly open over width of slide body (few cm to m)	0,5	0,0 %
Fully open over width of slide body (few cm to m)	1	100,0 %
Comment: Open backbounding fracture along J5, with 2m opening for a distance of 30m.		

2. Potential sliding structures	Score	Norm. prob.
No penetrative structures dip out of the slope	0	100,0 %
Penetrative structures dip on average < 20 degree or steeper than the slope	0,5	0,0 %
Penetrative structures dip on average > 20 degree and daylight with the slope	1	0,0 %
Comment: No penetrative structures dip out of the slope, but J5 dip into the slope.		

3. Lateral release surfaces	Score	Norm. prob.
Not developed	0	0,0 %
Partly developed on 1 side	0,25	0,0 %
Fully developed or free slope on 1 side or partly developed on 2 sides	0,5	0,0 %
Fully developed or free slope on 1 side and partly developed on 1 side	0,75	0,0 %
Fully developed or free slope on 2 sides	1	100,0 %
Comment: Free eastern flank, and fully developed western flank along the very visible joint set J3.		

4. Kinematic feasibility test	Score	Norm. prob.
Kinematic feasibility test does not allow for planar sliding, wedge sliding or toppling	0	0,0 %
Failure is partly kinematically possible (movement direction is more than $\pm 30^\circ$ to slope orientation)	0,5	0,0 %
Failure is kinematically possible (movement direction is less than $\pm 30^\circ$ to slope orientation)	0,75	0,0 %
Failure is partly kinematically possible on persistent discontinuities (movement direction is more than $\pm 30^\circ$ to slope orientation)	0,75	0,0 %
Failure is kinematically possible on persistent discontinuities (movement direction is less than $\pm 30^\circ$ to slope orientation)	1	100,0 %
Comment: Failure is kinematically possible along J5, which is a persistent structure.		

5. Morphologic expression of the rupture surface	Score	Norm. prob.
No indication on slope morphology	0	50,0 %
Slope morphology suggests formation of a rupture surface (bulging, concavity -convexity, springs)	0,5	25,0 %
Continuous rupture surface is suggested by slope morphology and can be mapped out	1	25,0 %
Comment: Standard value for toppling (morphological rupture not visible in toppling)		

6. Displacement rates	Score	Norm. prob.
No significant movement	0	30,0 %
>0 - 0.5 cm/year	1	30,0 %
0.5 - 1 cm/year	2	30,0 %
1 - 4 cm/year	3	10,0 %
4 - 10 cm/year	4	0,0 %
> 10 cm/year	5	0,0 %
Comment: No displacement measurements taken.		

7. Acceleration (if velocity is >0.5 cm/yr and <10 cm/yr)	Score	Norm. prob.
No acceleration or change in displacement rates	0	80,0 %
Increase in displacement rates	1	20,0 %
Comment: Standard value if unknown		

8. Increase of rock fall activity	Score	Norm. prob.
No increase of rock fall activity	0	100,0 %
Increase of rock fall activity	1	0,0 %
Comment: No rockfall activity seen on the block		

9. Past events	Score	Norm. prob.
No post-glacial events of similar size	0	0,0 %
One or several events older than 5000 years of similar size	0,5	0,0 %
One or several events younger than 5000 years of similar size	1	100,0 %
Comment: Several smaller events in the 1990s.		

Hazard assessment of large unstable rock slopes in Norway

Site name: Location 9 Scenario: A Made by: Vegard Nes Date: 19.05.2018

Hazard classes	Probability	Cumulative prob.
Very low	4,0 %	4,0 %
Low	67,0 %	71,0 %
Medium	28,2 %	99,2 %
High	0,8 %	100,0 %
Very high	0,0 %	100,0 %

Hazard score	
Minimum	2,3
Maximum	8,3
Mode	3,5
Mean	4,2
5% percentile	2,3
95% percentile	6,2

Fitted normal distribution	
Mean μ	4,0
St. dev. σ	1,3
$\mu - 2\sigma$	1,4
$\mu + 2\sigma$	6,6
Corr. Coeff..	0,9995
K-S-test	6,2 %

1. Backscarp	Score	Norm. prob.
Not developed	0	80,0 %
Partly open over width of slide body (few cm to m)	0,5	20,0 %
Fully open over width of slide body (few cm to m)	1	0,0 %
Comment: Backscarp seen as a depression(march) following the orientation of J5.		

2. Potential sliding structures	Score	Norm. prob.
No penetrative structures dip out of the slope	0	100,0 %
Penetrative structures dip on average < 20 degree or steeper than the slope	0,5	0,0 %
Penetrative structures dip on average > 20 degree and daylight with the slope	1	0,0 %
Comment: The penetrative structure of J5 dip into the slope.		

3. Lateral release surfaces	Score	Norm. prob.
Not developed	0	0,0 %
Partly developed on 1 side	0,25	0,0 %
Fully developed or free slope on 1 side or partly developed on 2 sides	0,5	66,7 %
Fully developed or free slope on 1 side and partly developed on 1 side	0,75	33,3 %
Fully developed or free slope on 2 sides	1	0,0 %
Comment: Free eastern flank. Western flank is fractured at the intersection with the cliff face, but only for 10m. Rest is a weak depression.		

4. Kinematic feasibility test	Score	Norm. prob.
Kinematic feasibility test does not allow for planar sliding, wedge sliding or toppling	0	0,0 %
Failure is partly kinematically possible (movement direction is more than $\pm 30^\circ$ to slope orientation)	0,5	0,0 %
Failure is kinematically possible (movement direction is less than $\pm 30^\circ$ to slope orientation)	0,75	0,0 %
Failure is partly kinematically possible on persistent discontinuities (movement direction is more than $\pm 30^\circ$ to slope orientation)	0,75	50,0 %
Failure is kinematically possible on persistent discontinuities (movement direction is less than $\pm 30^\circ$ to slope orientation)	1	50,0 %
Comment: Toppling along J5 is partly possible with a flat plane within the uncertainties of the bedding plane in the domain.		

5. Morphologic expression of the rupture surface	Score	Norm. prob.
No indication on slope morphology	0	50,0 %
Slope morphology suggests formation of a rupture surface (bulging, concavity -convexity, springs)	0,5	25,0 %
Continuous rupture surface is suggested by slope morphology and can be mapped out	1	25,0 %
Comment: Standard value for toppling (morphological rupture not visible in toppling)		

6. Displacement rates	Score	Norm. prob.
No significant movement	0	30,0 %
>0 - 0.5 cm/year	1	30,0 %
0.5 - 1 cm/year	2	30,0 %
1 - 4 cm/year	3	10,0 %
4 - 10 cm/year	4	0,0 %
> 10 cm/year	5	0,0 %
Comment: No displacement measurements taken.		

7. Acceleration (if velocity is >0.5 cm/yr and <10 cm/yr)	Score	Norm. prob.
No acceleration or change in displacement rates	0	80,0 %
Increase in displacement rates	1	20,0 %
Comment: Standard value if unknown		

8. Increase of rock fall activity	Score	Norm. prob.
No increase of rock fall activity	0	100,0 %
Increase of rock fall activity	1	0,0 %
Comment: No fresh surfaces from rock fall activity spotted around the block.		

9. Past events	Score	Norm. prob.
No post-glacial events of similar size	0	0,0 %
One or several events older than 5000 years of similar size	0,5	0,0 %
One or several events younger than 5000 years of similar size	1	100,0 %
Comment: Several events in the 1990s.		